DOCTORAL THESIS

Presented to the Department of Pharmacy

Graduate School of Pharmaceutical Science, XXX Cycle

University of Naples Federico II

DEVELOPMENT OF INNOVATIVE FORMULATIONS BASED ON POLYSACCHARIDES FOR TUMOR TREATMENT

Ph.D. Student

SIMONA GIARRA

Approved by

Ph.D. Supervisor Prof. Laura Mayol

Ph.D. Program Coordinator Prof. Maria Valeria D'Auria

ABSTRACT

The development of a wide spectrum of new strategies based on controlled drug delivery systems for tumor treatment have attracted a great deal of interest thanks to their ability to encapsulate and control the release of a large array of anticancer drugs and to their targeting ability to many tumor sites. In the last years, the use of polysaccharides for the development of innovative formulations for drug delivery and targeting is rapidly growing. This could be probably attributed to their peculiar properties, such as biodegradability, biocompatibility, large availability as natural source, low cost manufacturing process and to the presence of multiple reactive groups in their structures, which make them suitable for an easy chemical functionalization. In this context, the overall aim of this thesis was to design, produce and characterize innovative formulations based on polysaccharides with potential application in tumors treatment. In particular, in the present thesis, two different strategies were envisaged.

The first one is based on the evidence that chemoattraction through the CXCR4-CXCL12 axis has been shown to be an important mechanism to direct circulating tumor cells toward distant sites. Thus, a fake metastatic niche made up of a gel loaded with CXCL12 was realized. This gel was engineered to create a steep concentration gradient of the chemokine in the proximity of the site of administration/injection thus diverting and capturing the circulating $CXCR4^+$ tumor cells. To this aim, different thermo-responsive gels based on methylcellulose or poloxamers, with or without the polysaccharide hyaluronic acid, were designed, loaded with CXCL12 and their mechanical properties correlated with the ability to attract and capture *in vitro* $CXCR4^+$ cells.

The second strategy concerned the use of polysaccharides both as structural and coating component for different types of nano-carriers, prepared with simple and easily up-scalable manufacturing process. In this context, two different polysaccharides were investigated, hyaluronic acid and enoxaparin. These polysaccharides, thanks to their ability to recognize and bind specific receptors and growth factors overexpressed in tumor cells, can favor a greater drug accumulation to target sites, thus promoting and improving the selectivity and effectiveness of the chemotherapy. The nano-carriers here investigated are chitosan-based polyelectrolyte complexes, poly (lactic-co-glycolic acid) polymeric nanoparticles and self-emulsifying drug delivery systems.

TABLE OF CONTENTS

CHAPTER 3

Chitosan-based polyelectrolyte complexes for doxorubicin and zoledronic acid combined therapy to overcome multidrug resistance

CHAPTER 4

Spontaneous arrangement of a tumor targeting hyaluronic acid shell on irinotecan loaded PLGA nanoparticles

CHAPTER 5

***In vitro* evaluation of tumor targeting ability of enoxaparin-coated self-emulsifying drug delivery systems (SEDDS) for parenteral administration**

List of abbreviations

AB	alamar blue
ABC	ATP-binding cassette
ACN	acetonitril
ADME	absorption, distribution, metabolism and excretion
AFM	atomic force microscopy
BSA	bovine serum albumin
Caco-2	human epithelial colorectal adenocarcinoma cell line
Capmul® PG8	propylene glycol monocaprylate
CCRF-CEM	$CXCR4^+$ human T-leukemia cells
CGC	critical gelation concentration
CHI	chitosan
CMC	critical micelle concentration
CO_2	carbon dioxide
Cremophor EL	polyoxyl-35 castor oil
CSCs	cancer stem cells
D_n	average distance between the entanglements of polymer network
DAPI	4,6-Diamidino-2phenylindole
DLS	dynamic light scattering
DMEM	dulbecco's modified eagle's medium
DMSO	dimethyl sulfoxide
Doxo	doxorubicin
DSC	differential scanning calorimetry
E	molar extinction coefficient
E-Pa	enoxaparin-palmitoyl conjugate
ECM	extracellular matrix

EE	entrapment efficiency
Enox	enoxaparin
EO	ethylene oxide
EPCs	endothelial progenitor cells
EPR	enhanced permeation and retention effect
FACS	flow cytometry analysis
FBS	fetal bovine serum
FCS	fetal calf serum
FD	fluorescein diacetate
FDA	food and drug administration
FGF	fibroblast growth factor
G’	elastic modulus
G’’	viscous modulus
GAG	glycosaminoglycan
GlcNAc	N-acetyl-D-glucosamine
GlcUA	D-glucuronic acid
HA	hyaluronic acid
HS578T	breast carcinoma cells CD44 overexpressing
IC50	concentrations inhibiting 50% of cell growth
IRIN	irinotecan
KCl	potassium chloride
KOH	patassium hydroxide
Labrafili® M 1944	oleoyl polyoxyl-6 glycerides
LbL	layer-by-layer
LCST	lower critical solution transition temperature
LMWH	low molecular weight heparin

M_e	average molecular weight of the polymer segments between two entanglements
MC	methylcellulose
MCF7	breast cancer cell line
MDA-MB-231	human breast adenocarcinoma cell line
MDR	multidrug resistance
MDR-1	multidrug resistance protein 1
MEM	minimum essential medium
MSTO-211H	malignant mesothelioma cell line
MW	molecular weight
NaCl	sodium chloride
Na_2HPO_4	dibasic sodium phosphate
NaOH	sodium hydroxide
NPs	nanoparticles
PBS	phosphate buffer saline
PC	palmitoyl chloride
PECs	polyelectrolyte complexes
Peceol™	glyceryl monooleate
PEG	polyethylene glycol
PEO	poly(ethylene oxide)
PG	propylene glycol
P-gp	P-glycoprotein
PI	polydispersity index
PLGA	poly(lactic-co-glycolic acid)
PO	propylene oxide
Polox	poloxamers
Q	flow rate

RES	endoplasmic reticulum
RPMI	roswell park memorial institute medium
SAOS	osteosarcoma cell line
SAOS DX	doxorubicin resistant osteosarcoma cell line
SEC-HPLC	size exclusion ultra-high-performance liquid chromatography
SEDDS	self-emulsifying drug delivery systems
SD	standard deviation
SDF	stromal derived factor
T_c	crystallization temperature
T_g	transition temperature
TEM	transmission electron microscope
THF	tetrahydrofuran
TPP	tripolyphosphate
UFH	unfractionated heparin
UHPLC	ultra-high-performance liquid chromatography
VEGF	vascular endothelial growth factor
Zol	zoledronic acid
ΔH_c	crystallization heat

List of figures

List of tables

CHAPTER 1

General introduction

1.1 Polysaccharides

Polysaccharides are a family of natural polymeric carbohydrate molecules, derived from plant, animal or algal sources in which repeated chains of monosaccharide or oligosaccharide units are linked together through glycosidic bonds. Thanks to some characteristics of their chemical and biochemical composition, there are a large number of polysaccharides with different properties and structures [Liu *et al*., 2008]. The first classification is based on the type of monosaccharide components in the structure; if there is only one type of monosaccharide units, it can be defined homopolysaccharide whereas, if the polysaccharide is composed of two or more different monosaccharides, it is called heteropolysaccharide [Miller *et al*., 2014; Posocco *et al*., 2015]. Depending on their function, they can be classified as storage polysaccharides, an energetic glucose supply for the metabolism of vegetables and animals (e.g. glycogen), structural polysaccharides composing the vegetable tissue structures (e.g. cellulose) and specialized polysaccharides, with physical chemical properties suitable for their adhesion to contact-microenvironments (e.g. heparin sulfate). Moreover, for the presence/absence of superficial charge, they can be divided into non-polyelectrolyte polysaccharides (neutral charge), positively and negatively charged polyelectrolytes. Despite they are available as natural source, the presence of multiple reactive groups in their structures make them suitable for an easy chemical and biochemical modification, resulting in many types of polysaccharide derivatives [Bedini *et al*., 2017; Pawar *et al*., 2015]. Table 1.1 summarizes the chemical structure, source, charge and monosaccharide units composition of some of the most common polysaccharides.

	Structure	Source	Charge	Monosaccharide units
Chitosan	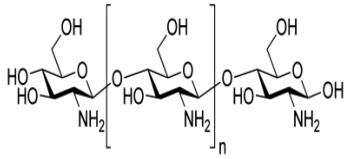	Animal	+	• D-glucosamine • N-acetyl-D-glucosamine
Dextran	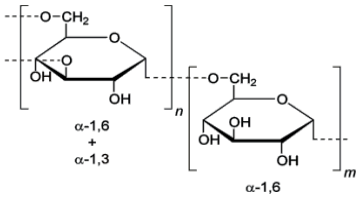	Microbial	+	• Glucose
Alginate	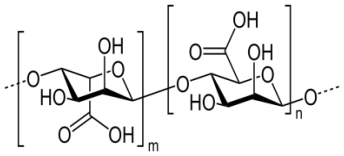	Algal	-	• β-D-mannuronate • α-L-guluronate
Pectin	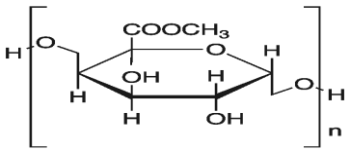	Plant	-	• D-galacturonic acid
Hyaluronic acid	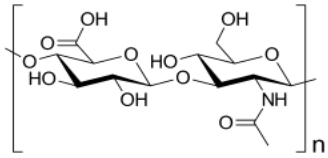	Human	-	• D-glucuronic acid • N-acetyl-D-glucosamine

Table 1.1: chemical structure, source, charge and monosaccharide units of some polysaccharides

1.2 Polysaccharide based formulations in drug delivery

Polysaccharide based formulations for controlled drug delivery and targeting have been examined over the years as strategies to make chemotherapeutic treatments more effective and selective. Indeed, in contrast to conventional- dosage forms, they are able to control the delivery of loaded drug(s) and/or promote its (their) delivery to a specific target. By this way, it is possible to enhance the bioavailability of the active molecule(s), thus decreasing the administration dose, improving the patient's compliance (thus resulting in decrease of the number administration and cost of the therapy) and minimizing the adverse side effects [Aziz, 1996; Mohanraj and Chen, 2006]. During the past decade, thanks to

their advantageous and peculiar properties, the use of polysaccharides for the development of drug delivery systems is rapidly growing [Laurienzo *et al*., 2015; Harshal *et al*., 2015]. It could be probably attributed to their large availability as natural source, low-cost manufacturing process, their biocompatibility and biodegradability; as other biological polymers, after administration, polysaccharides tend to be internalized into the cells, degraded and eliminated rapidly from the body, making their use safe and non-toxic. Moreover, thanks to the presence of several hydrophilic moieties in their structures, they are able to form covalent bonds with biological/mucous membrane, enhancing their mucoadhesion and bioadhesion. By this way, they can be used to extend the bioavailability and the release at specific cells or organs of the drug loaded into formulations. These attractive properties allowed the use of polysaccharides in several biomedical applications such as ophthalmic, infectious diseases, diabetes therapy, diagnostics and cancer [Camponeschi *et al*., 2015; Lemarchand *et al*., 2005; Lemarchand *et al*., 2006; Maltese *et al*., 2006]. In particular, in drug delivery applications, polysaccharides represent attractive candidates both as structural components of drug delivery formulations and/or as coating materials to obtain carriers endowed with hydrophilic surface with targeting ability [Kyung-Oh and Yoon, 2012; Ladaviere *et al*., 2007; Lemarchand *et al*., 2004]. Relying on their mechanism of action and method of administration, current available systems can be divided into two groups [Wolinsky *et al*., 2012]. The first one includes depot-forming formulations such as films, microparticles and gels. These systems are intended for local administration; by this way they can be directly implanted intra-tumorally or close to the target tumor tissue. The second group comprises nano-carrier based formulations, such as polyelectrolyte complexes (PECs), nanoparticles (NPs), and self-emulsifying drug delivery systems (SEDDS); they, thanks to their small size, are predominantly intended for intravenous injection.

1.3 Clinical need for drug delivery systems in cancer therapy

Despite a notable progress in cancer research, tumor remains one of the main causes of death worldwide [Ferlay *et al*., 2010; Bray *et al*., 2012]. The term tumor defines a group of diseases in which the growth of an abnormal mass exceeds that of a normal tissue and it progresses after cessation of the stimuli that have evoked it. In general, the size of organs is normally preserved within optimal values thanks to the action of control tools that regulate

the mitotic cells activity. New cells are produced to restore the oldest and/or damaged ones or to perform new functions. When these complex control mechanisms are altered and the balance between the cell growth and death is disturbed, a tumor may form. Cancer cells are able to reproduce continuously and they have no relation with the specific functions of the tissue with normal growth, from which they originate [Byrne *et al.*, 2008; De Jong and Borm, 2008; Alexis *et al*., 2008]. Whereas the growth of some tumors remains limited to the originated organ (benign tumor), some of them loose contact inhibition, extracellular matrix (ECM) adhesion and penetrate into the bloodstream and/or lymphatic system [Hanahan and Weinberg, 2011]. By this way, they are able to migrate in other organs and tissues where, if it is present a favorable environment for their colonization and proliferation, a second tumor (or metastasis) may form [Arvelo *et al*., 2016]. In the latter case, the tumor becomes cancerous (figure 1.1).

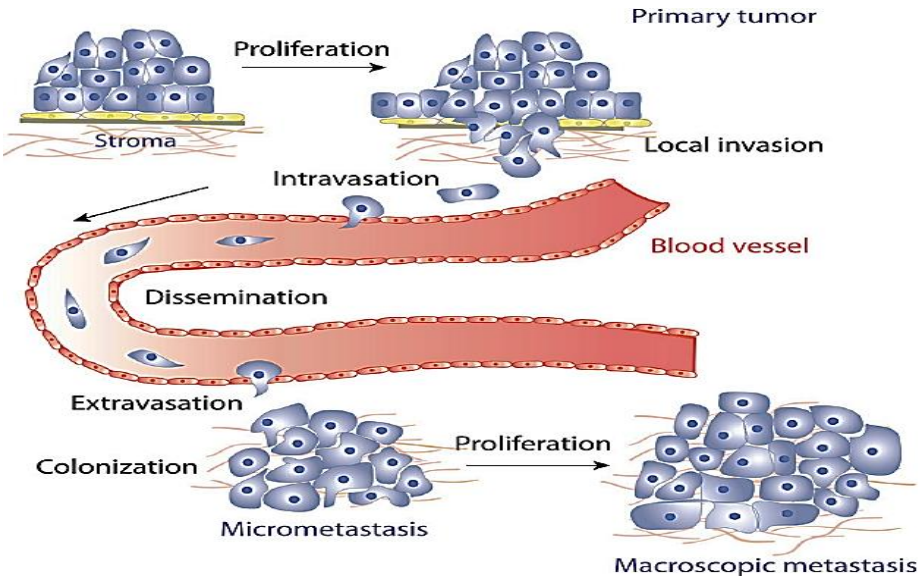

Figure 1.1: schematic representation of the multiple steps for macroscopic metastasis formation from primary tumor (from Saxena and Christofori, 2013)

After the tumor diagnosis, the possibility of survival is one of the main indicators to assess the severity of the disease. The latter is strongly influenced by two tools: early diagnosis and therapy [Smith *et al*., 2015]. In the first case, thanks to the screening programs, the probability of an effectively recovery is higher. The effectiveness of the therapy, as well as the prognosis of the patient, are largely determined by the fact that a tumor remains

localized at the source site. If it metastasizes in other tissues or organs, the survival probability drastically decreases (i.e. the prognosis becomes unfavorable). The available treatment options are rarely able to cure a metastatic tumor. Metastasis management is difficult because cells, survived to the first therapeutic approach, may develop resistance to chemotherapy drugs or radiotherapy treatments. At present, there are no strategies to prevent or control the formation of metastases; usually the treatment has the only purpose of keeping under control the disease or reducing its symptoms. One of the main limitation of the chemotherapy treatments is the development of malignant cell's resistance to one or more anticancer drugs which inevitably leads to a reduction of therapy effectiveness [Gottesman, 2002; Housman *et al*., 2014]. Moreover, most cytotoxic drugs don't show specific action against tumor cells and may affect all patient's cells, especially those with fast proliferation such as bone marrow, lymphoid system, oral and gastrointestinal epithelium, the skin, the germinal epithelium of the gonads and the embryonic structures, causing numerous and serious side effects [Mi Kyung *et al*., 2012; Bae, 2009]. Just for these reasons and for their low therapeutic index the use of chemotherapeutic drugs in clinical approaches is strongly limited. These issues pushed toward the design of formulations for controlled drug delivery and targeting that are able to improve the biopharmaceutical profile of molecules with antitumor activity [Hardman *et al*., 2001; Peer *et al*., 2007; Torchilin, 2007].

1.4 Depot-forming formulations as drug delivery systems

Depot-forming drug delivery systems is one of the most promising strategies to obtain a more effective and specific localized delivery of drugs able to minimize systemic side effect, thus improving the efficacy of the therapy [Kempe and Mäder, 2012; Fakhari and Subramony, 2015]. Despite the large number of potentially useful depot-formulation, most of them lead to irritation and local side effects and, therefore, only few systems based on implants, microparticles and hydrogels have found employment in clinical applications [Couvreur and Vauthier, 2006; Lukyanov and Torchilin, 2004; Tamilvanan, 2004; Thatte *et al*., 2005]. In the case of implants, a surgical procedure for its *in vivo* localization and removal is required. Examples of parenteral implants depot formulations, currently available on the market, are Vantas® (histrelin implant) and Viadur® (leuprolide acetate implant), approved from Food and Drug Administration (FDA) as palliative once-yearly

systems for to relieve the symptoms of the prostate cancer [Fowler *et al*., 2000; Moul and Civitelli, 2001]. Despite these kinds of systems offered a rapid drug administration, they do not obtain a good patient's compliance. On the other hand, the possibility to obtain preformed systems using particles has made possible their administration without requiring any type of surgery. Moreover, the biodegradability of some polymers also avoids their removal after the release of the loaded drug(s) [Lee *et al*., 2010; Wischke and Schwendeman, 2008]. The main examples of these commercially available formulations are Leupron Depot® (leuprolide acetate for depot suspension) and Zoladex® (goserelin acetate), poly (lactic-co-glycolic acid) (PLGA) microspheres for peptide controlled release [Jiang *et al*., 2014; Park *et al*., 2014]. These formulations provide an administration of drug through a two chambers syringe system in which generally lyophilized microparticles are separated from the dispersion medium to prevent their degradation; the depot system will form after injection into the body. Compared with preformed implants systems, the microparticulate depot formulation requires a more complex and expensive manufacturing process. Moreover, the complex administration process could cause the injection of an incomplete dose of drug due to the partial dispersion of microparticles with the medium and/or the clotting of the syringe. To overcome these issues, alternatives *in situ* forming depot systems with low-cost manufacturing process, have been developed [Hatefi and Amsden, 2002; Packhaeuser *et al*., 2004]. The key parameter in this case is the low viscosity of the formulation prior to its injection; this promotes its injection trough syringe with standard diameter. After administrations, a solid or semi-solid depot system will form with body fluids contact and/or pH environment change, thus promoting a prolonged release of the loaded drug(s). By this way, an improved patient's compliance can be achieved by using a less invasive and painful procedure. Currently, two *in situ* forming depots formulations have been approved by FDA for their practical use on market: Atridox® (doxycycline hyclate), a subgingival application for the treatment of chronic periodontitis in adults and Eligard® (leuprolide acetate), an injectable suspension for the palliative treatment of advanced (stage 2) prostate cancer [Javali and Vandana, 2012; Tunn *et al*., 2013]. Furthermore, polymeric hydrogels, such as commercially available belotero®, Juvéderm® and Restylane®, are also used as dermal fillers. Among the systems used as *in situ* depot formulation, thermo-responsive gels have attracted a great attention since they exhibit a drastic change of their physical properties with temperature [Ruel-Gariepy and Leroux, 2004] (figure 1.2). In particular, if the transition temperature is appropriately arranged to be close the physiologic temperature, the matrices can be

administered as a viscous solution at 20 °C and, once at body temperature, are able to form *in situ* a weak gels.

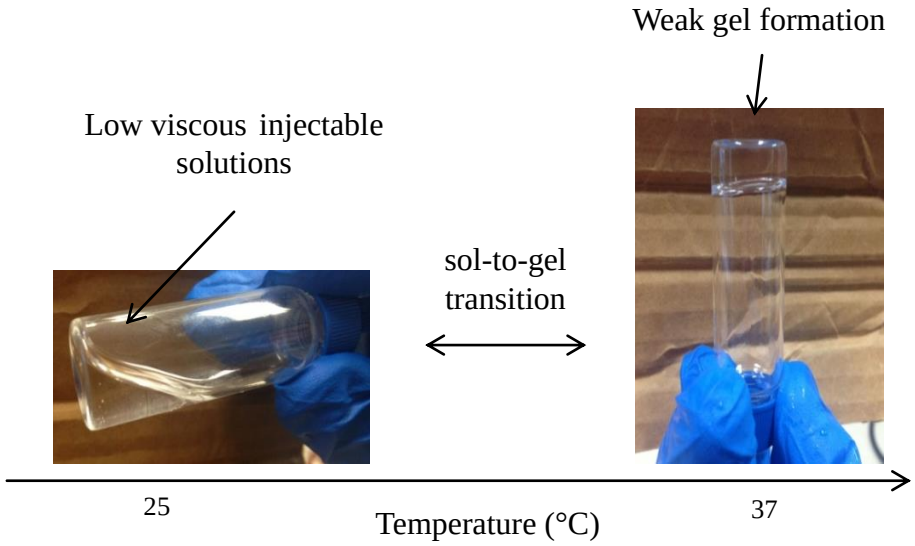

Figure 1.2: example of thermo-responsive gel forming depot formulation

Examples of materials with temperature-dependent phase transition behaviors are represented by poloxamers (Pluronic®), amphiphilic tri-block copolymers with hydrophilic EO (ethylene oxide) units and a central hydrophobic PO (polypropylene oxide) portion (figure 1.3).

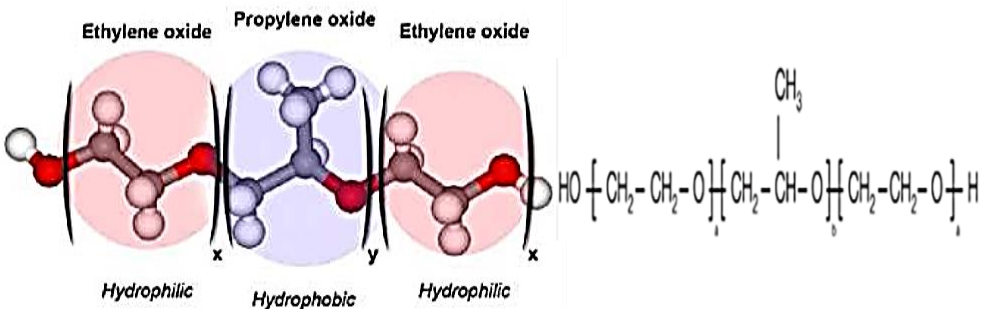

Figure 1.3: poloxamers chemical structure

Poloxamers are frequently used as surfactants in many cosmetics, industrial and pharmaceutical applications since they are able to increase the solubility in water of slightly soluble molecules and the miscibility of molecules that are poorly mixed with each other's [Alexandridis and Hatton, 1995; Santander-Ortega *et al*., 2006]. In water solutions, these amphiphilic tri-block copolymers can self-assemble into micellar structures above the critical micelle concentration (CMC) whereas, above the critical gelation concentration (CGC), are able to produce thermo-sensitive gels [Huynh *et al*., 2011; Pan and Yang, 2011]. Although PEO-PPO-PEO like materials are not biodegradable, molecules with a molecular weight in the range from 10 to 15 kDa are generally filtered from the kidney and eliminated by the urine. As poloxamers, also modified cellulose derivatives can be used as depot formulations since they are able to form *in vivo* thermo-responsive gels. Indeed, if unmodified cellulose results insoluble in aqueous solutions, adding of hydrophilic groups allows their water solubilization and gelling at elevated temperatures (40-50 °C) [Kobayashi *et al*., 1999].

Generally, depot-forming formulations, obtained by using polysaccharide, are preferred compared to systems obtained from other polymers, since they are biodegradable and biocompatible. These peculiar characteristics make them promising candidate for the development of *in vivo* depot forming systems for local drug administration. One of the polysaccharide commonly used as injectable in situ gelling agent is gellan gum. The latter is an anionic heteropolysaccharide, composing of glucose, glucuronic acid and rhamnose monosaccharides, obtained by microbial source. Gelrite, the deacetylated form, is the commercial product of gellan gum, marketed by Merck for glaucoma treatment as controlled release depot formulation (Timoptic). After its administration as low viscous solution to ocular mucosa, Gelrite is able to form a clear gel as result of electrostatic interaction with monovalent and divalent cations composing the tear fluid [Rozier *et al*., 1989; Singh and Harikumar, 2012]. Moreover, polysaccharides can be blended with other polymers to lower their gelation temperature and/or increase the mechanical properties of the formed gel. For example, the addition of hyaluronic acid to methylcellulose aqueous solutions results in blends with typical rheological behavior of a viscous solution at room temperature and of a weak gel at body temperature (37 °C), thus making their use suitable as *in situ* depot forming formulations [Caicco *et al*., 2013].

1.5 Nano-carriers based formulations as drug delivery systems

Over the past two decades, nano-carriers based formulations for drug delivery and targeting have emerged as promising approaches to overcome the limitations of the common chemotherapy. A well-designed nano-system in terms of size and circulation half-life, could promote a controlled release of the loaded drug(s), thus facilitating a better clinical result with reduced aggression compared to classical chemotherapeutics. Moreover, they are able to protect encapsulated drugs from the premature chemical/enzymatic degradation, improving their bioavailability into target sites and thus their therapeutic efficacy. Finally, one of the most challenging tasks in the design of nano-carriers is an efficient drug accumulation into target sites. Indeed, they can passively accumulate into tumours taking advantage of enhanced permeation and retention effect (EPR), associated with increased permeability of blood vessels in the tumour area. This, in principle, increases the chance of drug accumulation in solid tumour tissues (figure 1.4 A). The key parameter in this case will be the particles properties; after administration, size, surface behaviours and composition will be crucial for the solubility and stability of the loaded drug(s), as well as for their interactions with cells [Aktaş *et al*., 2005; Au *et al*., 2001; Ruoslahti *et al*., 2010]. On the other hand, drugs can be selectively delivered to the target site by an active targeting (figure 1.4 B). This strategy provides the functionalization of the carriers surface with specific ligands, such as proteins, antibodies and nucleic acids, able to recognize and bind specific receptors overexpressed by cancer cells, thus allowing a greater accumulation into tumour [Kommareddy *et al*., 2005].

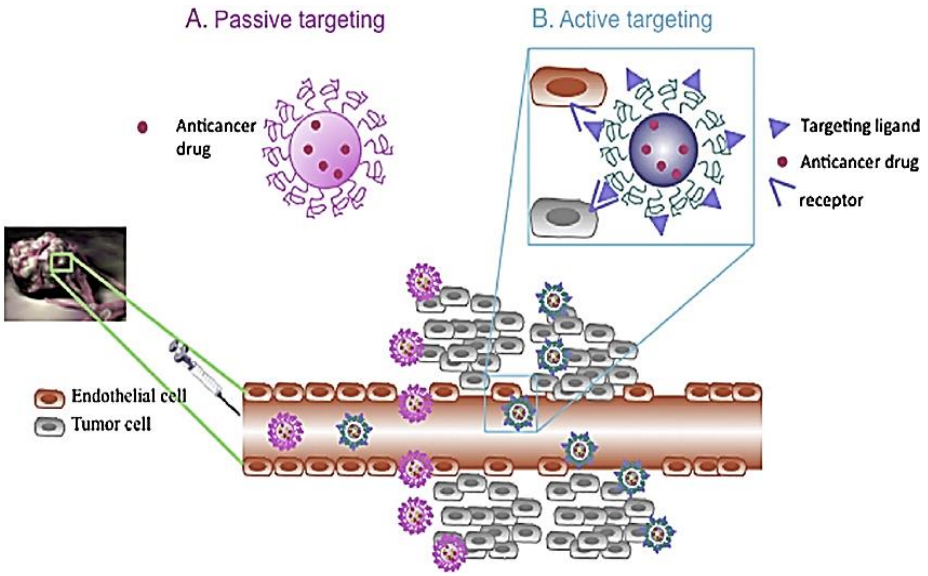

Figure 1.4: carriers can reach tumour target site trough the leaky tumour vasculature by a passive targeting (A), or/and by an active targeting (B), after surface conjugation with ligands for receptors overexpressed by cancer cells (from Duhem *et al*., 2014)

In this context polysaccharides represent a good candidates for the development of drug delivery systems, since they can be used both as structural or coating components of nano-carriers based formulations.

1.6 Polysaccharides as structural component of nano-carriers based formulations

In recent years, an increasing number of research have been directed on the potential application of polysaccharide and their derivatives as structural component of nano-carriers based formulations for drug delivery. Depending on their structural properties, polysaccharides based nano-systems can be obtained by using different methods of production [Debele *et al*., 2016; Mizrahy and Peer, 2012]. Firstly, polysaccharides with negative or positive superficial charge are able to form polyelectrolyte complexes (PECs) after electrostatic interactions with oppositely charged macromolecules, by ionotropic gelation process. One of the main polymers suitable for gelation process is represented by chitosan (CHI), a natural cationic polysaccharide composed of D-glucosamine and N-acetyl-D-glucosamine units with well-known biodegradability, biocompatibility and bioadhesiveness properties. CHI has a pKa value around 6-6.5 and is therefore easily

soluble in the acidic environment by protonation of the functional amine groups of the glucosamine units [Fan *et al*, 2012; Gan *et al*., 2005; Jonassen *et al*., 2012; Ramasamy *et al*., 2014]. The resulting positive charges makes it suitable for the ionotropic gelation process with an anionic counterpart, such as tripolyphosphate and/or hyaluronic acid [Nasti *et al*., 2009]. Commonly, oppositely charged macromolecules aggregate due to their high charge density fluctuation in solutions. Therefore, PECs formation and stability will depend on several parameters such as molecular weight, structure, charge density, mixing ratio of used polyelectrolytes, time of interactions between them as well as on the pH and temperature of the environmental conditions. In this case, the main advantage derived from the simple and easily up-scalable manufacturing process used to obtain PEC based nano-carriers [Boddohi *et al*., 2009; Etrych *et al*., 2005; Hamman, 2010]. Thanks to their amphiphilic nature, some polysaccharides have a propensity to self-assemble in nanoparticulate structures (micelle) as the result of intra and inter-molecular interactions between their hydrophobic and hydrophilic segments in aqueous environment. The derived systems display unique features: they are able to encapsulate lipophilic drugs into hydrophobic core and, simultaneously, they expose hydrophilic moieties on the surface, resulting in increasing accumulation into tumor tissues [Myrick *et al*., 2014; Ozin *et al*., 2009]. In addition, polysaccharide based nano-carriers can be obtained *via* cross-linking reaction, after adding of covalent or ionic cross-linking agents. Despite covalent cross-linking agents allows to obtain more stable formulations thanks to the formation of covalent bonds between polymer chains, their usefulness in drug delivery is often avoided cause their possible undesirable interactions with the active molecule and their toxicity [Alvarez-Lorenzo *et al*., 2013; Janes *et al*., 2001; Jătariu *et al*., 2011].

1.7 Polysaccharides as coating materials of nano-carriers based formulations

After their injection into the body, nano-carriers are quickly eliminated from blood circulation since they are able to recognize and adsorb serum proteins (opsonins) on their surface. Protein adsorption promotes their fast aggregation and makes them easily recognizable by macrophages of endoplasmic reticulum (RES), resulting in their elimination and liver accumulation, where they may cause side effects [Lenaerts *et al*., 1984; Leroux *et al*., 1995; Owens and Peppas, 2006]. The surface behaviours of the systems play a key role in the opsonisation process: carriers with hydrophilic moieties on

the surface, such as polyethylene glycol (PEG), possess stealth properties; they can prevent serum protein adsorption and thus prolong their bloodstream circulation. This, in principle, increases the chances of a preferential nano-devices accumulation in solid tumor tissues taking advantage of the EPR effect [Bhadra *et al*., 2002]. PEG is a biocompatible, biodegradable and non-toxic hydrophilic polymer able to form a protective layer around the carrier inhibiting the adsorption of serum proteins trough repulsion forces [Gref *et al*., 1995; Sun *et al*., 2015]. Despite the physical stability and improved biocompatibility and residence time in blood circulation of the resulting PEGylated systems, this strategy is not suitable to prevent the non-specific interactions between drug delivery systems and proteins. Polysaccharides can be considered a promising alternative as coating materials since, most of them, are able to recognize and bind specific receptors expressed in tumor site, thus making it possible to achieve an active targeting. One of the most investigated polysaccharide as coating material is hyaluronic acid (HA). HA is a glycosaminoglycan (GAG) with a no branched polysaccharide chain, composed of about 2000-2500 disaccharide units of D-glucuronic acid (GlcUA) and N-acetyl-D-glucosamine (GlcNAc), linked through alternating β-1,4 e β-1,3 glycosidic bonds as well as intra-molecular hydrogen bonds, that stabilize its conformation [Almond, 2007]. It is present in all vertebrates and is one of the primary components of the ECM of the mammalian connective tissues, with proteoglycans and collagen fibers. HA has attracted a great deal of interest in the biomedical field for its hygroscopic and viscoelastic properties; the first allows the regulation of tissues hydration, while the latter makes it a good lubricant for the synovial fluid of the joints and for the vitreous humor of the eye [Angelova and Hunkeler, 1999; Kogan *et al*., 2007; Liao *et al*., 2005]. The carboxyl groups of the glucuronic units at physiological pH are ionized giving it a high polarity with high solubility in water. In aqueous solution, thanks to the combination of different interactions, such as intra and inter-molecular hydrogen bonding, HA takes preferred network structures with peculiar properties: they can withstand at short-term deformations, thus exhibiting elastic properties and may flow at long-term deformations, showing viscous properties [Koo *et al*., 2005; Laurent and Fraser, 1992]. HA is also involved in cellular motility, adhesion of cells to the extracellular matrix, cell proliferation and differentiation. Due to its biocompatibility and biodegradability, its chemical-physical properties as well as the ease of chemical functionalization, HA has attracted a great deal of attention and has been extensively used in several biomedical applications, such as regenerative medicine and drug delivery. In recent years, it has been proposed as ligand for an active targeting to cancer cells. Indeed,

it is able to selectively bind CD44 and RHAMM receptors, overexpressed on the surface of some cancer cells, such as prostate, breast or colon cancer cells, and glioblastoma cells [Gotte and Yip, 2006; Ossipov, 2010]. HA, once bound to its receptors, activates an internalization mechanism through receptor-mediated endocytosis; by this way, it is possible to promote cells internalization of bound-HA drugs or drugs loaded in HA-coated systems, thus increasing their concentration into target cells and so their therapeutic efficacy [Ahrens *et al*., 2001; Auzenne *et al*., 2007; Isacke and Yarwood, 2002]. Moreover, recent studies have evidenced the HA targeting ability to tumor cell subpopulations with self-renewal capacity, known as cancer stem cells (CSCs), responsible of invasion, metastasis and therapeutic resistance phenomenon which appears in tumors [Jaggupilli and Elkord, 2012]. In particular, HA-coated systems are able to bind CD44 receptor over-expressed on CSC surface, inhibiting their self-renewal ability and enhancing apoptosis and necrosis, thus resulting in a reduction of tumor growth [Dosio *et al*., 2016].

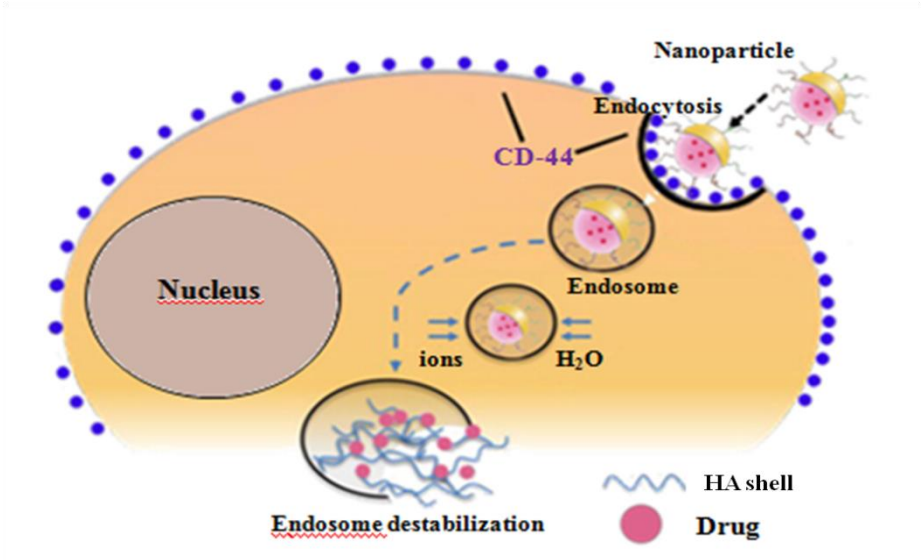

Figure 1.5: example of HA modified NP for targeted drug delivery to CD44 overexpressing cancer cells trough receptor-mediated endocytosis

Another polysaccharide that has recently been evaluated as tumor-active targeting ligand is enoxaparin (Enox). Enox is a kind of low molecular weight heparin (LMWH), obtained by chemical or enzymatic depolymerization of unfractionated heparin (UFH). UFH belongs to GAG's family and it is constituted by repeating disaccharide units of N-acetyl-

glucosamine and L-iduronic acid, with a molecular weight in the range from 3 to 30 kDa [Afratis *et al*., 2012; Francis *et al*., 2006]. The high degree of sulfonylation on different amino and hydroxyl units of disaccharide, make UFH a molecule with a very high negative charge; this is crucial for its electrostatic interaction with some components of ECM, such as growth factors, proteins, cytokines and chemokines [Karamanos *et al*., 1997; Liang and Kiick, 2014; Militsopoulou *et al*., 2002]. Thanks to the proteins-binding ability, it has a key role in ECM organization, contributing to the interactions between cells and ECM, thus promoting cells adhesion and migration [Theocharis *et al*., 2014; Theocharis *et al*., 2015]. For decades, UFH has been used as blood anticoagulant in clinical practice for thromboembolic disorders treatment, as result of its ability to bind antithrombin [De Kort *et al*., 2005]. However, long-term clinical use of UFH is limited, since it can cause several side effects, among which hemolysis and thrombocytopenia [Lapierre *et al*., 1996]. For this reason, several LMWHs with range size between 4000-6000 Da and with low toxicity were produced and their alternative use in therapy were investigated [Belting, 2014; Yang *et al*., 2015]. Various LMWHs have been commercially approved from FDA. In particular, Enox (Lovenox®) was approved for medical use in 1993 and is currently used for the treatment and the prevention of deep vein thrombosis, pulmonary embolism and in patients with heart attacks and acute coronary syndrome [WHO, 2016].

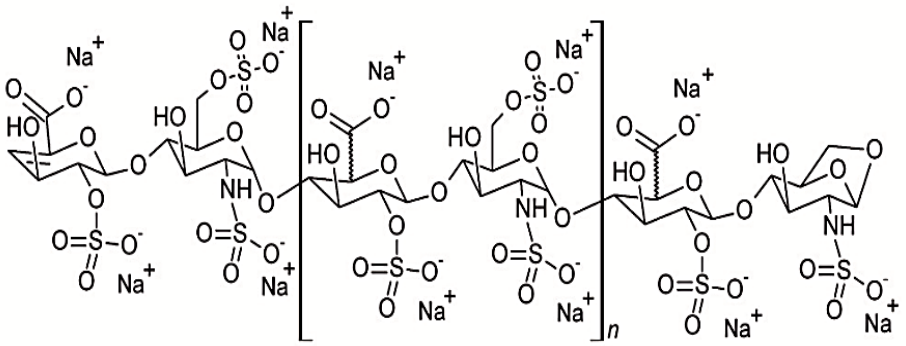

Figure 1.6: Enox chemical structure

Thanks to their UFH similar biological/chemical properties, LMWHs show the same or improved anticoagulant and anti-inflammatory activity compared to UFH. Recent studies demonstrated that UFH, and many of its LMWH derivatives, exhibit anticancer property in

different types of cancers [Gomes *et al*., 2015; Kozlowsky and Pavao, 2011; Niers *et al*., 2007; Nikos *et al*., 2017]. It could be probably related to their ability to bind various molecules involved in the metastasis formation, such as heparinase, over expressed in tumors. The latter is an endoglycosidase that stimulate the degradation of the ECM by cleaving the heparin sulfate chains thus promoting easier tumor cells extravasations [Bouris *et al*., 2015]. They can also inhibit the activity of P and L-selectins, which are involved in cell-cell interactions and of fibroblast growth factor (FGF) and vascular endothelial growth factor (VEGF), involved in angiogenesis process [Läubli and Borsig, 2010]. Moreover, Enox and others LMWHs derivatives are able to selectively bind fibrinogen-derived products and angiogenic growth factors over expressed in the stroma of some tumors and not in normal tissues. These interactions allow enhancing the targeting ability of Enox-coated systems and their internalization into cancer cells.

1.8 Aim of the thesis

The overall aim of this thesis was to design, produce and characterize innovative formulations based on polysaccharides for tumors treatment. To this aim, two different strategies were pursued. The first one concerned the design of *in situ* forming depot systems suitable for local administration into or close to the tumor tissue.

In particular, the first part of the thesis, presented in the chapter 2, deals with the production of thermo-responsive gels acting like a "metastasis traps" for the diversion of $CXCR4^+$ circulating tumor cells. This study is based on the evidence that the CXCL12-CXCR4 axis seems to have a critical role in the metastasis formation since cancer cells that express the receptor CXCR4, are attracted towards tissues that release CXCL12 becoming, therefore, a target for metastasis formation. Thus, the thermo-responsive gels were loaded with CXCL12 in order to create a concentration gradient of the chemokine near the site of administration/injection. By this way the gels can diverge and capture $CXCR4^+$ circulating tumor cells and, in particular, the cells disseminated from primary tumor, thus inhibiting cancer cells migration in other organs and tissues and, consequently, preventing the formation of metastasis. Different thermo-responsive gels were designed, with and without HA, and mechanical optimized to allow the permeation of the $CXCR4^+$ tumor cells into the gels and to capture them for a time frame sufficient to inhibit their migration in other sites.

$CXCR4^+$ human T-Leukemia cells were used to evaluate the biological effectiveness of the formulations by examining the cells migration toward the gels and their presence/permanence into the gels by microscopy and flow cytometry analysis (FACS). The *in vitro* cellular experiments were carried out in collaboration with the National Cancer Institute "G.Pascale" Foundation of Naples.

The second part of this thesis, concerned the use of polysaccharides as structural component and as coating materials for different types of nano-carriers, such as polyelectrolyte complexes (PECs), polymeric nanoparticles (NPs), and self-emulsifying drug delivery systems (SEDDS).

In particular, the second work of the thesis presented in the chapter 3, concerned the use of the polysaccharide CHI as structural component for the development of PECs, for doxorubicin (Doxo) and zoledronic acid (Zol) combined therapy to overcame multidrug resistance against Doxo resistant tumors. PECs were prepared through ionotropic gelation technique, exploiting the electrostatic interactions between opposite charge polymers. By this way, it is possible to direct PECs self-assembly with a simple and easily scale-up method, avoid organic solvents and chemical reactions between polymers. The influence of some experimental parameters was evaluated in order to optimize PECs preparation in terms of size and polydispersity index. Mean diameter, polydispersity index and ζ-potential values were studied over the time, in order to evaluate their stability. Doxo and Zol encapsulation efficiency as well as PECs yield of preparation, were analyzed. Moreover, HA-coated PECs were also developed. Finally, *in vitro* studies were carried out on osteosarcoma, Doxo-resistant osteosarcoma and breast cancer cell lines, to assess the synergism between Doxo and Zol, the restoring of Doxo sensitivity and the targeting of CD44-overexpressing cells by using HA-coated PEC. The *in vitro* cellular experiments were carried out in collaboration with the Department of Biochemistry, Biophysics and General Pathology of the University of Campania "Luigi Vanvitelli".

As far as polymeric NPs are concerned, in the third work of the thesis presented in the chapter 4, we investigated the possibility to direct a spontaneous arrangement of the tumor targeting polysaccharide HA on PLGA NPs loaded with the anticancer drug irinotecan. The basic idea was to bind HA shell on NPs surface by means a lipophilic gradient between the oil and water phases of the emulsions used for the NPs production, using poloxamers as a bridge between the hydrophobic cores made up of PLGA and the

hydrophilic HA shell. By this way, it was possible to obtain spontaneously HA-coated NPs by a single step process easily to scale-up for industrial applications. The obtained NPs were then characterized for their technological properties and a calorimetric study as well as ELISA test were performed, to support the hypothesis of polymer assembly in NPs architecture. *In vitro* biological studies were carried out to verify NPs ability to target CD44 receptor, on CD44-overexpressing breast carcinoma cells. The *in vitro* cellular experiments were carried out in collaboration with the Institute for Polymers, Composites and Biomaterials (IPCB) of the National Research Council (CNR).

As for SEDDS, the aim of the fourth work of the present thesis, presented in the chapter 5, was the *in vitro* evaluation of their tumor targeting ability, once provided them of an Enox coating shell. This work was carried out during my stay abroad in Austria at the Department of Pharmaceutical Technology of Innsbruck under the supervision of Professor Andreas Bernkop Schnürch. These systems are able to spontaneously emulsifying after the exposure with body fluids, producing a transparent and stable nanoemulsion. This makes them easy to manufacture and to scale-up for large-scale production. SEDDS surface were then coated with Enox. This was achieved by firstly preparing an amphiphilic conjugate able to direct the spontaneous exposition of Enox moieties on SEDDS surface. The possibility of Enox coated formulations to be sterilized by filtration and their hemocompatibility needed for administrated by parenteral route, were evaluated. The *in vitro* cell uptake studies of SEDDS decorated with Enox, compared with uncoated formulation, were carried out on both human breast adenocarcinoma and human epithelial colorectal adenocarcinoma cell lines.

REFERENCES

Afratis N, Gialeli C, Nikitovic D, Tsegenidis T, Karousou E, Theocharis A.D., Pavao M.S., Tzanakakis G.N., Karamanos N.K. (2012). Glycosaminoglycans: key players in cancer cell biology and treatment. *Febs J,* 279:1177-1197.

Ahrens T, Assmann V, Fieber C, Termeer C.C., Herrlich P, Hofmann M, Simon J.C. (2001). CD44 is the principal mediator of hyaluronic-acid-induced melanoma cell proliferation. *J invest derm,* 116:93-101.

Aktaş Y, Andrieux K, Alonso M.J., Calvo P, Gürsoy R.N., Couvreur P, Capan Y (2005). Preparation and in vitro evaluation of chitosan nanoparticles containing a caspase inhibitor. *Int J Pharm*, 298:378-383.

Alexandridis P, Hatton T.A. (1995). Poly(ethylene oxide)-poly(propylene oxide)-poly(ethylene oxide) block copolymer surfactants in aqueous solutions and at interfaces: thermodynamics, structure, dynamics, and modeling. *Colloids Surf A Physicochem Eng Asp*, 96:1–46.

Alexis F, Rhee J.W., Richie J.P., Radovic-Moreno A.F., Langer R, Farokhzad O.C. (2008). New frontiers in nanotechnology for cancer treatment. *Urol Oncol*, 26:74-85.

Almond A (2007). Hyaluronan. *Cell Mol Life Sci*, 64: 1591-1596.

Alvarez-Lorenzo C, Blanco-Fernandez B, Puga A.M., Concheiro A (2013). Crosslinked ionic polysaccharides for stimuli-sensitive drug delivery. *Adv Drug Deliv Rev*, 65:1148-1171.

Angelova N, Hunkeler D (1999). Rationalizing the design of polymeric biomaterials. *TIbtech*, 17:409-421.

Arvelo F, Sojo F, Cotte C (2016). Tumor progression and metastasis. *Ecancermedicalscience*, 10:617.

Au J.L., Jang S.H., Zheng J, Chen C.T., Song S, Hu L, Wientjes M.G. (2001). Determinants of drug delivery and transport to solid tumors. *J Contr Rel*, 74:31-46.

Auzenne E, Ghosh S.C., Khodadadian M, Rivera B, Farquhar D, Price R.E. (2007). Hyaluronic acid–paclitaxel: Antitumor efficacy against CD44(+) humanovarian carcinoma xenografts. *Neoplasia*, 9:479–486.

Aziz K.J. (1996). Clinical molecular biology: concepts and applications. *Adv Clin Chem*, 32:39–72.

Bae Y.H. (2009). Drug targeting and tumor heterogeneity. *J Control Release*, 133:2-3.

Bedini E, Laezza A, Parrilli M, Iadonisi A (2017). A review of chemical methods for the selective sulfation and desulfation of polysaccharides. *Carbohydr Polym*, 15:1224-1239.

Belting M (2014). Glycosaminoglycans in cancer treatment. *Thromb Res*, 133:95-101.

Bhadra D, Bhadra S, Jain P, Jain N.K. (2002). Pegnology: a review of PEG-ylated systems. *Pharmazie*, 57:5-29.

Boddohi S, Moore N, Johnson P.A., Kipper M.J. (2009). Polysaccharide-based polyelectrolyte complex nanoparticles from chitosan, heparin, and hyaluronan. *Biomacromol*, 10:1402-1409.

Bouris P, Skandalis S.S., Piperigkou Z, Afratis M, Karamanou K, Aletras A.J., Moustakas A, Theocharis A.D., Karamanos N.K. (2015). Estrogen receptor alpha mediates ephitelial to mesenchymal transition, expression of specific matrix effectors and functional properties of breast cancer cells. *Matrix Biol J Int Soc Matrix Biol*, 43:42-60.

Bray F, Jemal A, Grey N, Ferlay J, Forman D (2012). Global cancer transitions according to the Human Development Index (2008-2030): a population-based study. *Lancet Oncol*, 13:790-801.

Byrne J.D., Betancourt T, Brannon-Peppas L (2008). Active targeting schemes for nanoparticle systems in cancer therapeutics. *Adv Drug Deliv Rev*, 60:1615-1626.

Caicco M.J., Zahir T, Mothe A.J., Ballios B.G., Kihm A.J., Tator C.H., Shoichet M.S. (2013). Characterization of hyaluronan-methylcellulose hydrogels for cell delivery to the injured spinal cord. *J Biomed Mat Research*, 101:1472-1477.

Camponeschi F, Atrei A, Rocchigiani G, Menuccini L, Uva M, Barbucci R (2015). New formulations of polysaccharide-based hydrogels for drug release and tissue engineering. *Gels*, 1:3-23.

Couvreur P, Vauthier C (2006). Nanotechnology: intelligent design to treat complex disease. *Pharm Res*, 231-34.

De Jong W.H., Borm P.J. (2008). Drug delivery and nanoparticles: applications and hazards. *Int J of Nanomed*, 3:133-149.

De Kort M, Buijsman R.C., Van Boeckel C.A. (2005). Synthetic heparin derivatives as new anticoagulant drugs. *Drug discovery today*, 10:769-779.

Debele T.A., Mekuria S.L., Tsai H.C. (2016). Polysaccharides based nanogels in the drug delivery system: application as the carrier of pharmaceutical agents. *Mat Sci Engineering*, 68:964-981.

Dosio F, Arpicco S, Stella B, Fattal E (2016). Hyaluronic acid for anticancer drug and nucleic acid delivery. *Adv Drug Del Rev*, 97:204-236.

Duhem N, Danhier F, Préat V (2014). Vitamin E-based nanomedicines for anti-cancer drug delivery. *J Contr Rel*, 182:33-44.

Etrych T, Leclercq L, Boustta M, Vert M (2005). Polyelectolyte complex formation and stability when mixing polyanions and polycations in salted media: a model study related to the case of body fluids. *Eur J Pharm Sci*, 25:281-288.

Fakhari A, Subramony J.A. (2015). Engineered in-situ depot-forming hydrogels for intratumoral. *J Contr Rel*, 220:465-475.

Fan W, Yan W, Xu Z, Ni H (2012). Formation mechanism of monodisperse, low molecular weight chitosan nanoparticles by ionic gelation technique. *Coll Surf B Bio*, 90:21–27.

Ferlay J, Shin H.R., Bray F, Forman D, Mathers C, Parkin D.M. (2010). Estimates of worldwide burden of cancer in 2008: GLOBOCAN 2008. *Int J Cancer*, 127:2893-2917.

Fowler J.E. Jr, Gottesman J.E., Reid C.F., Andriole G.L. Jr, Soloway M.S. (2000). Safety and efficacy of an implantable leuprolide delivery system in patients with advanced prostate cancer. *J Urol*, 164:730-734.

Francis C.W., Kaplan K.L., In Lichtman M.A., Beutler E, Kipps T.J. (2006). Principles of Antithrombotic Therapy. *Williams Hematology*, Chapter 21:7th ed.

Gan Q, Wang T, Cochrane C, McCarron P (2005). Modulation of surface charge, particle size and morphological properties of chitosan-TPP nanoparticles intended for gene delivery. *Coll Surf B Bioint*, 44:65–73.

Gomes A.M., Kozlowski E.O., Borsig L, Teixeira F.C., Vlodavsky I, Pavao M.S. (2015). Antitumor properties of a new non-anticoagulant heparin analog from the mollusk nodipecten nodosus: effect on P-selectin, heparanase, metastasis and cellular recruitment. *Glycobiology*, 25:386-393.

Gotte M, Yip G.W. (2006). Heparanase, hyaluronan, and CD44 in cancers: a breast carcinoma perspective. *Cancer Res*, 66: 10233-10237.

Gottesman M.M. (2002). Mechanisms of cancer drug resistance. *Annu Rev Med*, 53:615-627.

Gref R, Domb A, Quellec P, Blunk T, Müller R, Vertbavatz J, Langer R (1995). The controlled intravenous delivery of drugs using PEG-coated sterically stabilized nanospheres. *Adv Drug Del Rev*, 16:215-233.

Hamman J.H. (2010). Chitosan based polyelectrolyte complexes as potential carrier materials in drug delivery systems. *Mar Drugs*, 8:1305-1322.

Hanahan D, Weinberg R.A. (2011). Hallmarks of cancer: the next generation. *Cell*, 144: 646–674.

Hardman J.G., Limbird L.E., Goodman G.A. (2001). The pharmacological basis of therapeutics. *McGraw Hill*, 10th edition.

Harshal A.P., Swati R.K., Pritam D.C. (2015). An overview of natural polysaccharides as biological macromolecules: their chemical modifications and pharmaceutical applications. *Biol Med*, 7:1-9.

Hatefi A, Amsden B (2002). Biodegradable injectable in situ forming drug delivery systems. *J Contr Rel*, 80:9-28.

Housman G, Byler S, Heerboth S, Lapinska K, Longacre M, Snyder N, Sarkar S (2014). Drug Resistance in Cancer: An Overview. *Cancers (Basel)*, 6:1769–1792.

Huynh C.T., Nguyen M.K., Lee D.S. (2011). Injectable block copolymer hydrogels: achievements and future challenges for biomedical applications. *Macromol*, 44:6629-6636.

Isacke C.M., Yarwood H (2002). The hyaluronan receptor, CD44. *Int J Biochem Cell Biol*, 34:718-721.

Jaggupilli A, Elkord E (2012). Significance of CD44 and CD24 as cancer stem cell markers: an enduring ambiguity. *Clin Dev Immunol*, 2012:708036.

Janes K, Calvo P, Alonso M (2001). Polysaccharide colloidal particles as delivery systems for macromolecules. *Adv Drug Deliv Rev*, 47:83-97.

Jătariu A.N., Popa M, Curteanu S, Peptu C.A. (2011). Covalent and ionic co-crosslinking-an original way to prepare chitosan-gelatin hydrogels for biomedical applications. *J Biomed Mater Res*, 98:342-350.

Javali M.A., Vandana K.L. (2012). A comparative evaluation of atrigel delivery system (10% doxycycline hyclate) Atridox with scaling and root planing and combination therapy in treatment of periodontitis:a clinical study. *J Indian Soc Periodontol*, 16:43-48.

Jiang H, Wang T, Jiang Z (2014). Goserelin plus endocrine treatments maintained long-term clinical benefit in a male patient with advanced breast cancer. *World J Surg Oncol*, 12:393.

Jonassen H, Kjøniksen A.L., Hiorth M (2012). Stability of chitosan nanoparticles cross-linked with tripolyphosphate. *Biomacromol*,13:3747–3756.

Karamanos N.K., Vanky P, Tzanakakis G.N., Tsegenidis T, Hjerpe A (1997). Ion-pair high-performance liquid chromatography for determining disaccharide composition in heparin and heparin sulphate. *J Chromathogr A*, 765:169-179.

Kempe S, Mäder K (2012). In situ forming implants - an attractive formulation principle for parenteral depot formulations. *J Contr Rel*, 161:668-679.

Kobayashi K, Huang C.I., Lodge T.P. (1999). Thermoreversible gelation of aqueous methylcellulose solutions. *Macromol*, 32:7070-7077.

Kogan G, Soltes L, Stern R, Gemeiner P (2007). Hyaluronic acid: a natural biopolymer with a broad range of biomedical and industrial applications. *Biotechnol Lett*, 29:17-25.

Kommareddy S, Tiwari S.B., Amiji M.M. (2005). Long-circulating polymeric nanovectors for tumor-selective gene delivery. *Technol Cancer Res Treat*, 4:615-625.

Koo O.M., Rubinstein I, Onyuksel H (2005). Role of nanotechnology in targeted drug delivery and imaging: a concise review. *Nanomed*, 1:193-212.

Kozlowsky E.O., Pavao M.S. (2011). Effect of sulfated glycosaminoglycans on tumor invasion and metastasis. *Front Biosci*, 3:1541-1551.

Kyung-Oh D, Yoon Y (2012). Application of polysaccharides for surface modification of nanomedicines. *Ther Deliv*, 3:1447-1456.

Ladaviere C, Averlant-Petit M.C., Fabre O, Durand A, Dellacherie E, Marie E (2007). Preparation of polysaccharide-coated nanoparticles by emulsion polymerization of styrene. *Colloid and Polymer Sci*, 285:621-630.

Lapierre F, Holme K, Lam L, Tressler R.J., Storm N, Wee J, Stack R.J., Castellot J, Tyrrell D.J. (1996). Chemical modifications of heparin that diminish its anticoagulant but preserve its heparanase-inhibitory, angiostatic, anti-tumor and anti-metastatic properties. *Glycobiol*, 6:355-366.

Läubli H, Borsig L (2010). Selectins promote tumor metastasis. *Semin Cancer Biol*, 20:169-177.

Laurent T.C., Fraser J.R.E. (1992). Hyaluronan. *Faseb J*, 6:2397-2404.

Laurienzo P, Fernandes J.C., Colliec-Jouault S, Fitton J.H. (2015). The use of natural polysaccharides as biomaterials. *BioMed res Intern*.

Lee S.S., Hughes P, Ross A.D., Robinson M.R. (2010). Biodegradable implants for sustained drug release in the eye. *Pharm Res*, 27:2043-2053.

Lemarchand C, Gref R, Couvreur P (2004). Polysaccharide-decorated nanoparticles. *Eur J Pharm Biopharm*, 58:327-341.

Lemarchand C, Gref R, Lesieur S, Hommel H, Vacher B, Besheer A, Maeder K, Couvreur P (2005). Physico-chemical characterization of polysaccharide-coated nanoparticles. *J Contr Rel*, 108:97-111.

Lemarchand C, Gref R, Passirani C, Garcion E, Petri B, Muller R, Costantini D, Couvreur P (2006). Influence of polysaccharide coating on the interactions of nanoparticles with biological systems. *Biomat*, 27:108-118.

Lenaerts V, Nagelkerke J.F., Van Berkel T.J., Couvreur P, Grislain L, Roland M, Speiser P (1984). In vivo uptake of polyisobutyl cyanoacrylate nanoparticles by rat liver Kupffer, endothelial, and parenchymal cells. *J Pharm Sci*, 73:980-982.

Leroux J.C., De Jaeghere F, Anner B, Doelker E, Gurny R (1995). An investigation on the role of plasma and serum opsonins on the internalization of biodegradable poly(D,L-lactic acid) nanoparticles by human monocytes. *Life Sci*, 57:695-703.

Liang Y, Kiick K.L. (2014). Heparin-functionalized polymeric biomaterials in tissue engineering and drug delivery applications. *Acta Biomat*, 10:1588-1600.

Liao Y.H., Jones S.A., Forbes B, Martin G.P. (2005). Brown M.B. Hyaluronan: pharmaceutical characterization and drug delivery. *Drug deliv*, 12:327-342.

Liu Z, Jiao Y, Wang Y, Zhou C, Zhang Z (2008). Polysaccharides-based nanoparticles as drug delivery systems. *Adv Drug deliv Rev*, 60:1650-1662.

Lukyanov A.N., Torchilin V.P. (2004). Micelles from lipid derivatives of water-soluble polymers as delivery systems for poorly soluble drugs. *Adv Drug Deliv Rev*, 56:1273-1289.

Maltese A, Borzacchiello A, Mayol L, Bucolo C, Maugeri F, Nicolais L, Ambrosio L (2006). Novel polysaccharides-based viscoelastic formulations for ophtalmic surgery: rheological characterization. *Biomat*, 27:5134-5142.

Mi Kyung Y, Jinho P, Sangyong J (2012). Targeting strategies for multifunctional nanoparticles in cancer imaging and therapy. *Theranostics*, 2:3-44.

Militsopoulou M, Lamari F.N., Hjerpe A, Karamanos N.K. (2002). Determination of twelve heparin- and heparan sulfate-derived disaccharides as 2-aminoacridone derivatives by capillary zone electrophoresis using ultraviolet and laser-induced fluorescence detection. *Electrophoresis*, 23:1104-1109.

Miller T, Goude M.C., McDevitt T.C., Temenoff J.S. (2014). Molecular engineering of glycosaminoglycan chemistry for biomolecule delivery. *Acta Biomater*, 10:1705-1719.

Mizrahy S, Peer D (2012). Polysaccharides as building blocks for nanotherapeutics. *Chem Soc Rev*, 41:2623-2640.

Mohanraj V.J., Chen Y (2006). Nanoparticles – A Review. *Trop J Pharm Res*, 5:561-573.

Moul J.W., Civitelli K (2001). Menaging advanced prostate cancer with Viadur (leuprolide acetate implant). *Urol Nurs*, 21:385-388.

Myrick J.M., Vendra V.K., Krichnan S (2014). Self-assembled polysaccharide nanostructures for controlled-release applications. *Nanotechnol Rev*, 3:319-346.

Nasti A, Zaki N.M., Leonardis P.D., Ungphaiboon S, Sansongsak P, Rimoli M.G., Tirelli N (2009). Chitosan/TPP and chitosan/TPP-hyaluronic acid nanoparticles: systematic optimisation of the preparative process and preliminary biological evaluation. *Pharm Res*, 26:1918–1930.

Niers T.M., Klerk C.P., Di Nisio M, Van Noorden C.J., Buller H.R., Reitsma P.H., Richel P.H., Richel D.J. (2007). Mechanisms of heparin induced anti-cancer activity in experimental cancer models. *Crit Rev Oncol Hematol*, 61:195-207.

Nikos A.A., Konstantina K, Zoi P, Demitrios H.V., Achilleas D.T. (2017). The role of heparins and nano-heparins as therapeutic tool in breast cancer. *Glyconj J*, 34:299-307.

Ossipov D.A. (2010). Nanostructured hyaluronic acid-based materials for active delivery to cancer. *Expert Opin Drug Deliv*, 7: 681-703.

Owens D.E., Peppas N.A. (2006). Opsonization, biodistribution, and pharmacokinetics of polymeric nanoparticles. *Int J Pharm*, 307:93-102.

Ozin G.A., Hou K, Lotsch B.V., Cademartiri L, Puzzo D.P., Scotognella F, Ghadimi A, Thomson J (2009). Nanofabrication by self-assemby. *Mater Today*, 12:12-23.

Packhaeuser C.B., Schnieders J, Oster C.G., Kissel T (2004). In situ forming parenteral drug delivery systems: an overview. *Eur J Pharm Biopharm*, 58:445-455.

Pan W, Yang Z (2011). Thermoreversible Pluronic® F-127-based hydrogel containing liposomes for the controlled delivery of palitaxel: in vitro drug release, cell cytotoxicity, and uptake studies. *Int J Nanomedicine*, 6:151-166.

Park C.Y., Jung S.Y., Lee K.B., Yang S.H. (2014). The feasibility and efficacy of gonadotropin-releasing hormone agonists for prevention of chemotherapy induced ovarian failure in patients with gynecological malignancies. *Obstet Gynecol Sci*, 57:478-483.

Pawar H.A., Kamat S.R., Choudhary P.D. (2015). An overview of natural polysaccharides as biological macromolecules: their chemical modifications and pharmaceutical applications. *Biol Med*, 7:224.

Peer D, Karp J.M., Hong S, Farokhzad O.C., Margalit R, Langer R (2007). Nanocarriers as an emerging platform for cancer therapy. *Nature Nanotec*, 2:751-760.

Posocco B, Dreussi E, De Santa J, Toffoli G, Abrami M, Musiani F, Grassi M, Farra R, Tonon F, Grassi G, Dapas B (2015). Polysaccharides for the delivery of antitumor drugs. *Materials*, 8:2569-2615.

Ramasamy T, Tran T.H., Cho H.J., Kim J.H., Kim Y.I., Jeon J.Y., Choi H.G., Yong C.S., Kim J.O. (2014). Chitosan-Based Polyelectrolyte Complexes as Potential Nanoparticulate Carriers: Physicochemical and Biological Characterization. *Pharm Res*, 31:1302–1314.

Rozier A, Mazuel C, Grove J, Plazonnet B (1989). Gelrite a novel ion activated in-situ gelling polymer for ophtalmic vehicles. Effect on bioavailability of timolol. *Int J Pharm*, 57:163-168.

Ruel-Gariepy E, Leroux J.C. (2004). In situ-forming hydrogels-review of temperaturesensitive systems. *Eur J Pharm Biopharm*, 58:409-426.

Ruoslahti E, Bhatia S.N., Sailor M.J. (2010). Targeting of drugs and nanoparticles to tumors. *J Cell Biol*, 188:759-768.

Santander-Ortega M.J., Jódar-Reyes A.B., Csaba N, Bastos-Gonzáleza D, Ortega-Vinuesa J.L. (2006). Colloidal stability of Pluronic F68-coated PLGA nanoparticles: a variety of stabilisation mechanisms. *J Colloid Interface Sci*, 302:522–529.

Saxena M, Christofori G (2013). Rebuilding cancer metastasis in the mouse. *Molec oncol*, 7:283-296.

Singh K, Harikumar S.L. (2012). Injectable in situ gelling controlled release drug delivery system. *Int J Drug Develop Res*, 4:56-69.

Smith R.A., Manassaram-Baptiste D, Brooks D, Doroshenk M, Fedewa S, Saslow D, Brawley O.W., Wender R (2015). Cancer screening in the United States, 2015: a review of current American cancer society guidelines and current issues in cancer screening. *CA Cancer J Clin*, 65:30-54.

Sun L, Wu Q, Peng F, Liu L, Gong C (2015). Strategies of polymeric nanoparticles for enhanced internalization in cancer therapy. *Coll Surf B Biointerf*, 135:56-72.

Tamilvanan S (2004). Oil-in-water lipid emulsions:implications for parenteral and ocular delivering systems. *Prog Lipid Res*, 43:489-533.

Thatte S, Datar K, Ottenbrite R.M. (2005). Perspectives on: polymeric drugs and drug delivery systems. *J Bioact Compat Polym*, 20:585-601.

Theocharis A.D., Gialeli C, Bouris P, Giannopoulou E, Skandalis S.S., Aletras A.J., Iozzo R.V., Karamanos N.K. (2014). Cell-matrix interactions: focus on proteoglycan-proteinase interplay and pharmacological targeting in cancer. *Febs J*, 281:5023-5042.

Theocharis A.D., Skandalis S.S., Neill T, Multhaupt H.A., Hubo M, Frey H, Gopal S, Gomes A, Afratis N, Lim H.C., Couchman J.R., Filmus J, Sanderson R.D., Schaefer L, Iozzo R.V., Karamanos N.K. (2015). Insights into key roles of proteoglycans in breast cancer biology and translational medicine. *Biochim Biophys Acta*, 1855:276-300.

Torchilin V.P. (2007). Targeted pharmaceutical nanocarriers for cancer therapy and imaging. *The AAPS J*, 11:128-147.

Tunn U.W., Gruca D, Bacher P (2013). Six-month leuprolin acetate depot formulations in advanced prostate cancer: a clinical evaluation. *Clin Interv Aging*, 8:457-464.

Wischke C, Schwendeman S.P. (2008). Principles of encapsulating hydrophobic drugs in PLA/PLGA microparticles. *Int J Pharm*, 364:298-327.

Wolinsky J.B., Colson Y.L., Grinstaff M.W. (2012). Local drug delivery strategies for cancer treatment: gels, nanoparticles, polymeric films, rods, and wafers. *J Control Release*, 159: 14-26.

World Health Organization Model list of essential Medicines (2016), 19th list.

Yang X, Du H, Liu J, Zhai G (2015). Advanced nanocarriers based on heparin and its derivatives for cancer management. *Biomacr*, 16:423-436.

CHAPTER 2

Engineering of thermoresponsive gels as a fake metastatic niche toward the capture of CXCR4$^+$ circulating tumor cells

ABSTRACT

Chemoattraction through the CXCR4-CXCL12 axis has been shown to be an important mechanism to direct circulating tumor cells toward distant sites. In this panorama, a fake metastatic niche made up of a gel loaded with CXCL12 was realized. The gel is able to create a steep concentration gradient of the chemokine in the proximity of the site of administration/injection, aimed to divert and capture the circulating CXCR4$^+$ tumor cells. To this aim, different thermoresponsive gels based on methylcellulose (MC) or poloxamers, with and without HA, were designed, loaded with CXCL12 and their mechanical properties correlated with the ability to attract and capture *in vitro* CXCR4$^+$ cells were evaluated.

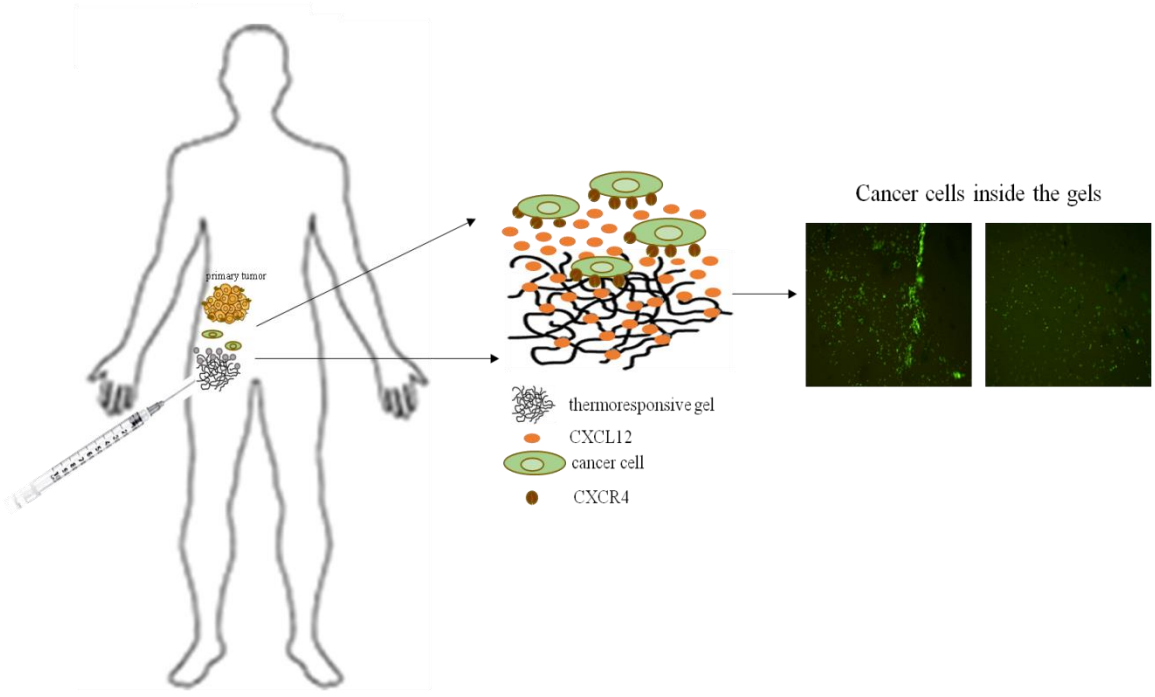

2.1 Introduction

Metastasis is the dissemination of cancer cells away from the site of origin. The process develop through several stages, such as: (i) loss of cell-cell contact; (ii) degradation of the basal lamina by malignant cells, resulting in local invasion; (iii) intravasation of cancer cells into the bloodstream and/or lymphatic system; (iv) migration of cancer cells in other organs and tissues; (v) creation of a pre-metastatic niche where metastasis may form if a permissive microenvironment for tumor cell colonization and proliferation is present [Arvelo *et al*., 2016; De la Fuente *et al*., 2015]. Chemoattraction through the CXCR4-CXCL12 axis has been shown to be an important mechanism to direct circulating tumor cells toward the host organ [Liu *et al*., 2016]. CXCL12, also known as stromal derived factor (SDF), is a highly effective chemokine with a marked action as chemotactic factor for T-lymphocytes and monocytes. In addition, it induces intracellular actin polymerization in lymphocytes, a process that is thought to be a prerequisite for cell motility [Bleul *et al*., 1996]. As result of alternative splicing of the same gene, it is secreted as six isoforms; CXCL12/α is the predominant form, present in almost all tissues [Yu *et al*., 2006]. In particular, while during embryogenesis, CXCL12 regulate the migration of hematopoietic cells from fetal liver to bone marrow and the development of blood vessels, in adults, it plays an important role in carcinogenesis process. Indeed, it is involved in angiogenesis by calling up endothelial progenitor cells (EPCs) from the bone marrow through a CXCR4 receptor dependent system [Zheng *et al*., 2007]. Also CXCL12 plays a key role in tumor metastasis: cancer cells expressing the CXCR4 receptor are attracted toward tissues releasing CXCL12 becoming, therefore, a target for metastasis formation [Müller *et al*., 2001]. While in many healthy tissues the expression of the CXCR4 receptor is low or absent, it was proved to be present in over 23 types of cancers, including breast, ovarian, prostate cancer and melanoma. Moreover, the CXCR4's expression in cancer cells seems to be related to tissues metastasis containing a high concentration of CXCL12 [Sun *et al*., 2010]. Despite the importance of the CXCL12-CXCR4 axis in tissue regeneration and in cell migration induced by chemotaxis, the use of CXCL12 in clinical use is limited by its short half-life and its highly time-dependent expression [Murphy *et al*., 2007].

2.2 Aim of the work

In this context, we investigated on the use of a fake metastatic niche consisting of a gel loaded with CXCL12 and able to create a steep concentration gradient of the chemokine in the proximity of the site of administration/injection, therefore diverting and capturing the circulating $CXCR4^+$ tumor cells. Thus, we have designed different thermoresponsive gels based on MC or poloxamers, with or without the addition of the polysaccharide HA. The gels were loaded with CXCL12 and their mechanical properties have been correlated with the *in vitro* ability to attract and capture $CXCR4^+$ human T-leukemia cells. Thermo-responsiveness is a pivotal attribute in this context; in particular, the gels were designed to have a lower critical solution transition temperature (LCST) close to the physiologic temperature. Thus, the matrices can be administered by means of a syringe being a viscous solution at 25 °C but, once at body temperature, they are able to form *in situ* a gel with mechanical properties suitable to capture $CXCR4^+$ circulating tumor cells [Klouda and Mikos, 2008].

2.3 Materials and methods

2.3.1 *Materials*

MC (viscosity: 4,000 cP) was purchased from Sigma (Milano, Italy). Poloxamers (Polox) used, designed with variable numbers of oxyethylene (a) and oxypropylene (b) units, were F127 (a = 100 and b = 65) and F68 (a = 76 and b = 29), obtained from Lutrol (Basf, Germany). Medium molecular weight (850 kDa) HA was supplied by Novozymes Biopharma (Bagsvaerd, Denmark). Potassium chloride (KCl) from Carlo Erba (Milano, Italy), dibasic sodium phosphate (Na_2HPO_4), sodium chloride (NaCl) from Sigma-Aldrich (St. Louis, USA) were used. CXCL12/α was purchased from R&D systems (Minneapolis, USA).

2.3.2 *Preparation of MC and MC-HA gels*

Gel made of bare MC was prepared by dissolving MC (2% w/v) in phosphate buffer saline (PBS, 120 mM NaCl, 2.7 mM KCl, 10 mM phosphate salts, pH=7.4), as previously reported [Mayol *et al.*, 2014]. Briefly, the solvent was divided into two aliquots of equal

volume: one was brought at 0 °C and the other one was heated until it reached the boiling point. MC was slowly solubilized in the hot solvent and then the cold solvent was added under magnetic stirring for about 4 hours, in an ice bath. The resultant solution was kept at 4 °C overnight. MC-HA gel was obtained by simply adding HA (0.1% w/v) into MC gel and mixing the resultant solution for one hour. For *in vitro* migration assay, CXCL12 was merely dispersed into the gel (0,00003% w/v).

2.3.3 *Preparation of Polox and Polox-HA based gel*

Polox gel was prepared as previously described with some modifications [Mayol *et al*., 2011]. Briefly, Polox F127 and F68 (21.43% w/v each) were mixed in distilled water under magnetic stirring, in an ice bath, until a clear solution was obtained. For complete solubilization, the solution was kept at 4 °C overnight. Polox-HA based formulation was obtained by adding HA (0.1% w/v) within the Polox solution under continuous stirring. The gels were stored at 4 °C until use. For *in vitro* migration assay, CXCL12 was merely dispersed into the gel.

2.3.4 *Cell culture*

CCRF-CEM, named CEM cells in the following, were grown in Roswell Park Memorial Institute (RPMI)-1640 medium (Hyclone; GE Healthcare Life Sciences, Logan, Utah, USA) with 10% fetal bovine serum (FBS), 2 mM glutamine, 1 mM sodium pyruvate, penicillin and streptomycin (50 µg/mL each).

2.3.5 *Cell migration assay*

Cell migration was assayed in 24-well Transwell® chambers (Corning Inc., Corning, NY) using inserts with 6.5-µm pore membrane. CEM cells, pre-stained with live dye green cell tracker *(*CellTracker Green CMFDA, Invitrogen, USA), were placed in the upper chamber (2.0×10^5cells/well) in the presence of a migration medium made of a 0.5% w/v bovine serum albumin (BSA) solution in 500µL RPMI. The lower chamber contained also the gels with or without CXCL12, bare cell culture medium as a control or CXCL12 solutions in

RPMI at 300 ng/mL. After 4 hours of incubation, cells on the upper surface of the filter were removed using a cotton wool swab; the membrane was then fixed in 4% paraformaldehyde for 15 min and the cells migrated toward the lower surface of the membrane were stained with 4,6-diamidino-2phenylindole (DAPI, 1:25000, AbD Serotec, UK), photographed and visually counted in 10 random selection of fluorescent microscope fields (Carlo Zeiss, Axio Scope.A1). Triplicate experiments were carried out. The amount of migrated cells was estimated through the migration index, defined as the ratio between number of migrating cells toward BSA containing media (CXCL12-loaded gels/gels or CXCL12/BSA).

2.3.6 *Rheological experiments*

The rheological properties of the gels were evaluated on a rotational rheometer (Malvern Kinexus) using a cone and plate geometry. In particular, the viscoelastic response of each formulation was evaluated by small-amplitude oscillatory shear tests. Briefly, each experiment was performed at 25 °C and 37 °C, in the 0.1 to 10 Hz oscillation frequency range with a shear strain fixed at which linear viscoelasticity is attained. The solutions were placed between the two plates with a gap < 1 mm. Thus, the shear storage or elastic modulus (G') and the shear loss or viscous modulus (G'') were measured as a function of frequency, which respectively characterize the solid-like contributions or the energy stored in the material during deformation and fluid-like contributions, or energy dissipated as heat, to the measured stress response. The value of G' allows estimating the features of the network structure. As G is proportional to the sum of the elastic contribution of the number of entanglements [D'Errico *et al*., 2008], it is possible to determine the average molecular weight of the polymer segments between two entanglements (M_e), through the Flory theory:

$$M_e = \frac{RTc}{G}$$

where RT is the thermal energy and *c* is the polymer concentration. Using the "equivalent network model" it is possible to estimate D_n, which is the average distance between the entanglements of polymer network:

$$D_n = \sqrt[3]{\frac{6 \cdot M_e}{\pi \cdot c \cdot A}}$$

where A is Avogadro constant [Flory, 1953].

2.3.7 *In vitro gel dissolution kinetics*

The *in vitro* dissolution kinetics of the obtained gels were evaluated by loading each them (1 mL) in a dialysis membrane (Spectra/Por® Biotech Cellular ester; molecular cut-off 12-14 kDa) and immersing them in 50 mL of PBS (pH=7.4), in a shaker bath at 37 °C. At predetermined time intervals, the gel-loaded membranes were recovered, washed three times for 30 minutes time with water to eliminate excess salts, dried for 3 hour at 25 °C and finally weighed. The residual mass of the gels was calculated as:

$$m_R = \frac{m(t = i)}{m(t = 0)} X100$$

where *t=i* is gel mass at a given time, while t=0 is the initial gel mass. All experiments were performed on at least three independents samples.

2.4 Results

2.4.1 *CXCL12 released from gels is biologically active*

The biological activity of the released CXCL12 was defined through CEM cell migration. The number of cells labelled with Green Cell Tracker migrated onto the membrane were counted using fluorescence imaging. The lower chamber contained CXCL12 in 0.5% BSA-culture medium, CXCL12-loaded gels or empty gels. Cells (2.0 x10^5 cells/well) were placed in the upper chamber and allowed to migrate toward CXCL12 (300 ng/mL), empty or CXCL12 (300 ng/mL)-loaded MC, MC-HA, Polox, Polox-HA in 0.5% BSA medium for 4 hours. The CXCL12 loaded gels induced higher CEM cell migration compared to corresponding empty gels (figure 2.1, Upper panel). The number of cells migrated to the lower chamber was also evaluated by flow-cytometry. In accordance, the number of migrated cells was higher in the wells containing CXCL12 loaded gels compared to empty

gels (figure 2.1, Lower panel). These results demonstrate that CXCL12 released from loaded gels is biologically active being able to attract $CXCR4^+$ cells.

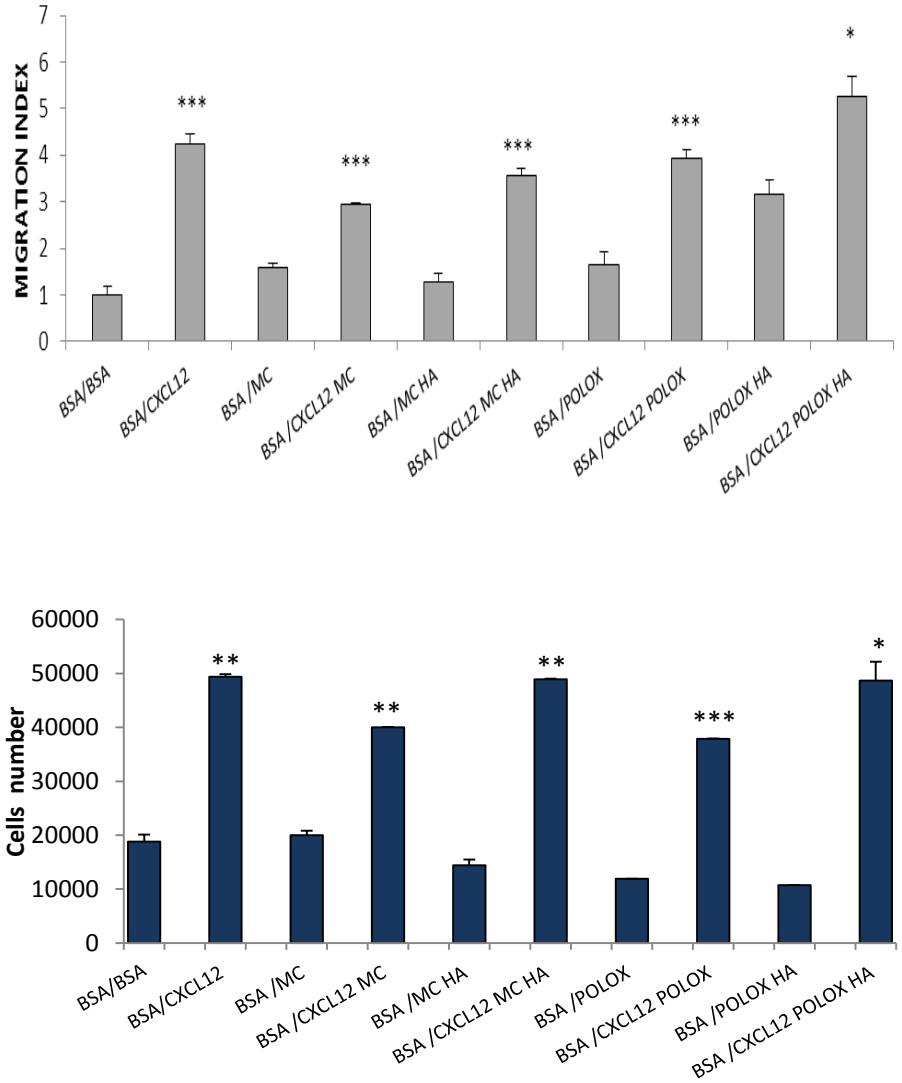

Figure 2.1: CXCL12 released from loaded gels MC, MC-HA, Polox, Polox-HA induced CEM cell migration. Upper: Migration was examined in CEM cell line in 24-well plates. Cells (2.0 $x10^5$cells/well) were placed in the upper chamber and allowed to migrate toward CXCL12 (300 ng/mL), empty or CXCL12 (300 ng/mL)-loaded MC, MC-HA, Polox, Polox-HA in 0.5% BSA medium for 4 hours. The cells (number of cells migrated through the membrane) were counted in ten different consecutive high power fields (magnification 200X). The results are expressed as migration index compared to BSA cells migration. Each column represents the mean ± S.D. (n=3). Statistical significances were calculated by student's t-test. * $p<0.05$, *** $p<0.001$ CXCL12 vs BSA or gel+CXCL12 vs gel. **Lower:** CEM cells migrated into the lower chamber were counted by flow cytometry. Statistical significances were calculated by student's t-test. **$p<0.01$, *** $p<0.001$ CXCL12 vs BSA or gel+CXCL12 vs gel

2.4.2 *CXCL12 embedded gel is biologically active*

The ability of the gels to recruit and capture tumor cells was assessed evaluating CEM cells migrated into the gels. In figure 2.2 (Upper and Intermediate panel), higher number of cells were detected on the bottom side of the filter comparing Polox+CXCL12 and Polox-HA+CXCL12 gels (panel C-D) versus Polox and Polox-HA gels (panel A-B). Moreover, higher cell number migrated to the bottom side of the filter toward the MC+CXCL12 and MC-HA+CXCX12 gels (panel G-H) with respect to MC and MC-HA gels (panel E-F). By comparing the two gels (Polox and MC), the Polox+CXCL12 (panel C) and the Polox-HA+CXCL12 (panel D) gels were overall more efficient in inducing transmembrane migration. Conversely, by evaluating the cells trapped into the gels, a higher number of cells migrated into the MC and MC-HA gels embedded with CXCL12 (figure 2.2, Lower panel). As it is shown MC+CXCL12 gels (C) were more efficient compared to MC-HA gels (D) (figure 2.2, Lower panel). In the Polox or Polox-HA gels no cells were detected into the gels (data not shown). To summarize, only MC and MC-HA gels embedded with CXCL12 captured CEM tumor cells although CXCL12-loaded gels MC, MC-HA, Polox and Polox-HA induced CEM cell migration.

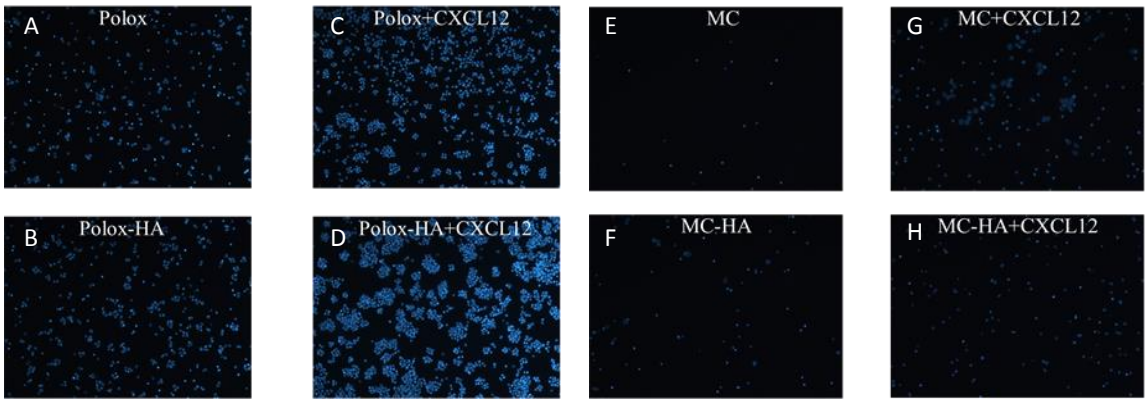

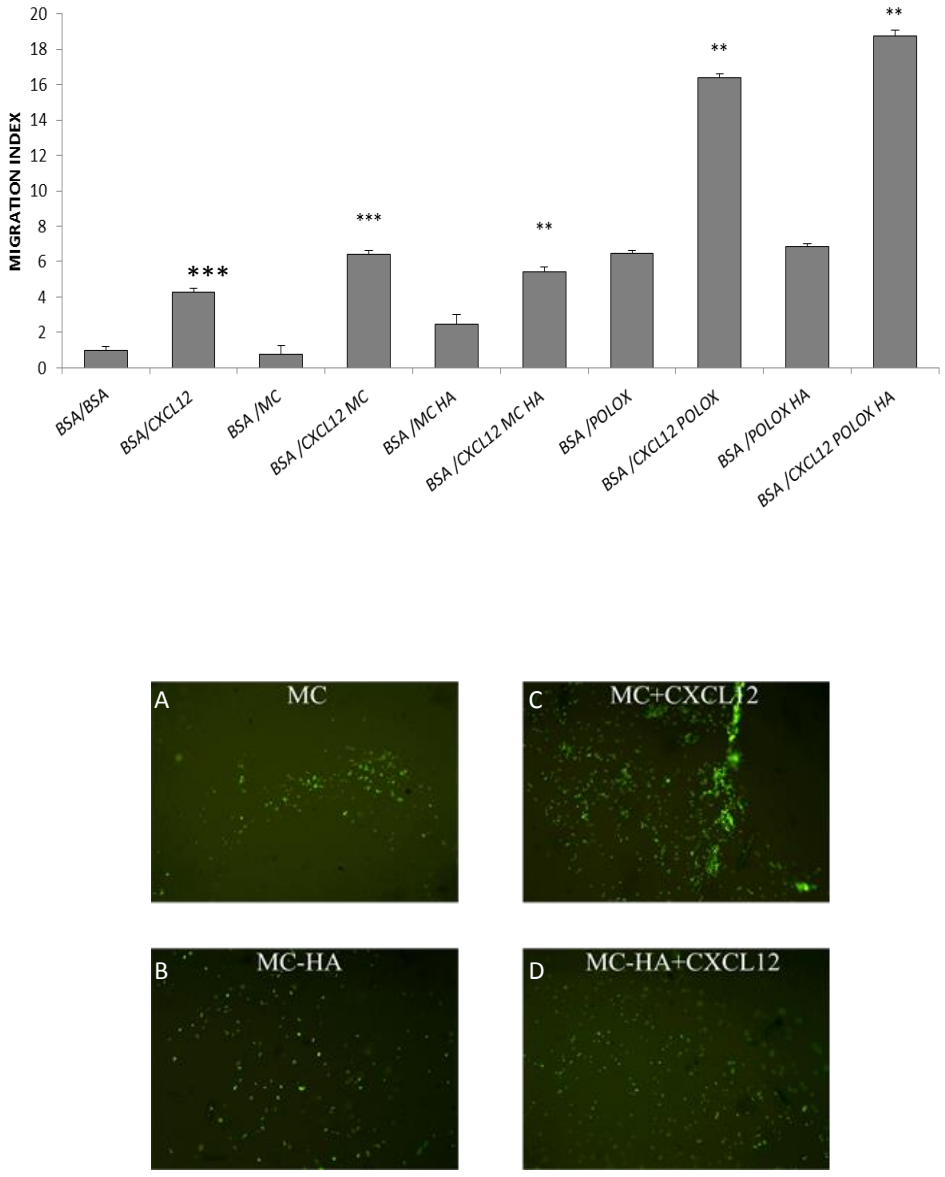

Figure 2.2: CEM cell migrated into MC and MC-HA gels. Upper panel: Representative images of filters displaying migrated CEM cells. Migration was examined in CEM cell line in 24-well plates. Cells (2.0 x10^5cells/well) were placed in the upper chamber and migrated toward CXCL12 (300 ng/mL), empty Polox (A), Polox-HA (B), MC (E), MC-HA (F), or CXCL12 (300 ng/mL)-loaded Polox (C), Polox-HA (D), MC (G), MC-HA (H). **Intermediate panel:** The quantitative results of migrated cells on filters. The cells (evaluated as number of cells migrated on the membrane) were counted in ten different consecutive high power fields (magnification 200X). The results are expressed as the migration index respect to basal migration of cells in BSA. Each column represents the mean ± S.D. (n=3). Statistical significances were calculated by Student's t-test. ** $p<0.01$, *** $p<0.001$ CXCL12 vs BSA or gel+CXCL12 vs gel. **Lower Panel**: Representative images of CEM cells inside the gel MC (A), MC-HA (B), MC+CXCL12 (C) and MC-HA+CXCL12 (D) after 4 hours of migration. In the Polox or Polox-HA gels no cells were detected into the gels (data not shown)

2.4.3 *Rheological studies*

Figures 2.3 and 2.4 display the results of rheological analyses of MC-based and Polox-based gels, in the presence or absence of HA. In particular, the storage shear modulus (G') and the loss shear modulus (G'') are reported as a function of oscillation frequency at two different temperatures (25 °C and 37 °C). It can be observed that MC-based systems show qualitatively similar mechanical behaviors. In particular, at 25 °C, G" is higher than G' in all cases and, therefore, the systems present a viscous/liquid-like behavior in all the analyzed frequency range. At 37 °C, however, the mechanical behavior is reversed and G' > G" by roughly one order of magnitude at all frequencies; therefore, a gel was formed, with both viscoelastic moduli being basically frequency-independent.

Moreover, in the presence of HA within MC systems, the mechanical properties of MC gels were significantly increased at 37 °C, therefore indicating the formation of a strong gel; on the contrary, at 25 °C, the mechanical spectra of the viscous liquids showed a qualitatively similar trend with the frequency. As depicted in figure 2.4, also the Polox gels showed a similar, temperature-dependent behavior. However, in this case, the strength of the gel was affected by the presence of HA to a lesser extent, showing an elastic modulus of approximately 10^4 Pa inherently unaffected by the frequency in the explored range, for both HA-containing and HA-free formulations.

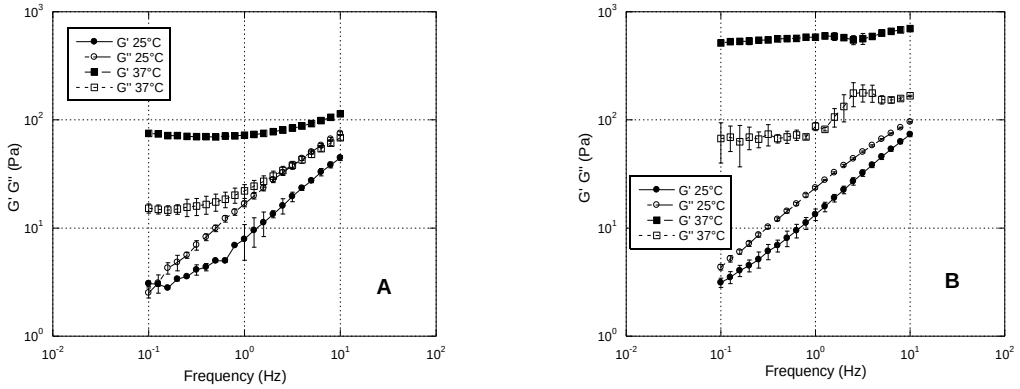

Figure 2.3: mechanical spectra of MC (A) and MC-HA (B), at 25 °C and 37 °C

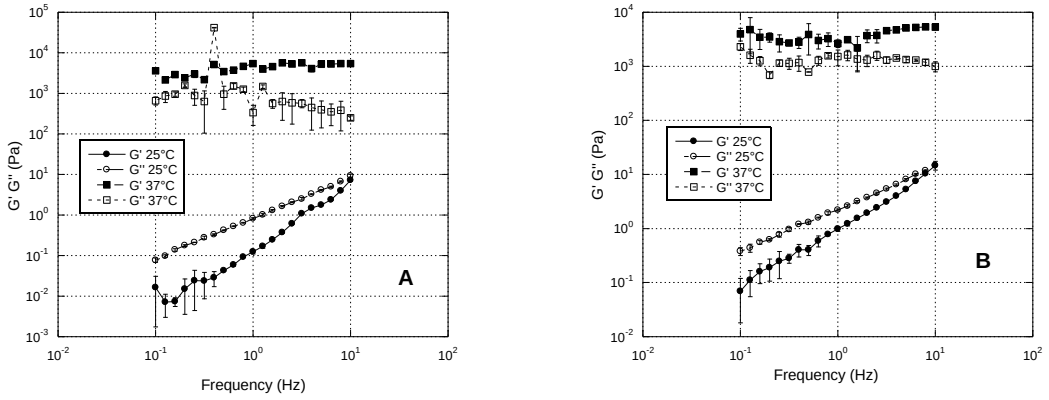

Figure 2.4: mechanical spectra of Polox (A) and Polox-HA (B), at 25 °C and 37 °C

The calculated M_e and D_n of the gels are reported in table 2.1. MC–based gel has shown the highest values of D_n, with a significant decrease after addition of HA in the formulation. Conversely, Polox formulations have been shown to possess a lower value of D_n, irrespective of HA addition.

Formultion	[Polymer] (% p/v)	[HA]* (% p/v)	G' (Pa)	$M_e \times 10^6$ (g/mol)	D_n (nm)
MC	2	-	75.2	97.6	54
MC-HA	2	0.1	515	15.0	28
Polox	42.9	-	3600	43.7	15
Polox-HA	42.9	0.1	3990	39.5	14

Table 2.1: network parameters of MC- and Polox-based different gels. G' is the value of the elastic modulus at 0.1 Hz, 37 °C. *Overall HA percentage in the final gel

2.4.4 *In vitro dissolution kinetics*

The dissolution kinetics of the gels, expressed as percentage of gel residual mass as a function of the time of immersion in PBS (pH=7.4) at 37 °C, are shown in figure 2.5. As it can be seen from the chart, MC and MC-HA gels dissolve more slowly than Polox gel. It must also be observed that the presence of HA in the MC formulation seems slightly

increase the rate of the gel dissolution. Instead the addition of HA to Polox gels strongly delays the *in vitro* dissolution kinetics.

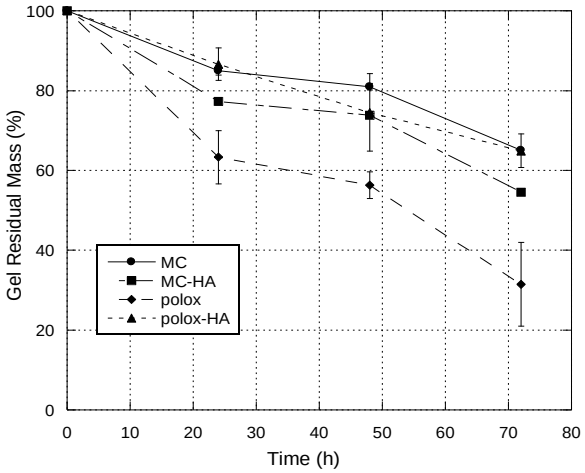

Figure 2.5: dissolution kinetics of different gels

2.5 Discussion

To date, despite the avalanche of new therapeutic regimens in cancer therapy, metastases are the primary determinants of mortality in patients [Yang *et al.*, 2014]. Metastasis targeting, a recent focus in cancer research, has been often addressed based on targeting specific genetic alterations in primary tumors. The outcomes of this have been, however, somehow unsatisfactory, mainly because of the genetic instability of metastatic tissues, which leads, in to mid-long term, to the selective outgrowth of therapy-resistant cells over sensitive ones [Cifone and Fidler, 1981; Fidler and Kripke, 2015]. Therefore, in this work we propose a possible, new paradigm to strive for the targeting of circulating metastases, to circumvent their genetic instability-driven elusiveness as a therapeutic goal. Actually, to the best of our knowledge, there are no scientific reports dealing with gel systems loaded with chemoattractants so as to work as metastasis traps. In this study, we have produced a novel device made up of a thermo-responsive gel loaded with CXCL12 to divert and capture circulating CEM cells, thus inhibiting their migration in other organs and tissues and, consequently, avoiding the establishment of a metastatic colony. All the formulated gels showed a thermo-sensitive behavior, with a gelification temperature

around body temperature, while being a viscous solution at room temperature [Mayol *et al*., 2011; Mayol *et al*., 2014]. This is a pivotal feature for syringeability, which is a crucial parameter of parenteral systems and, even more importantly, the ability to form gels at physiological temperature. Seemingly, the rheological properties of the gels at 37 °C influenced the capacity of CEM cells to migrate into the gels. Indeed, CEM cells are able to feel a CXCL12 chemotactic stimulus and cross the transwell membrane, whose pore size is 8 μm, irrespective of gel formulation. On the other hand, fluorescence microscope images have shown that, in MC-based systems, the presence of CXCL12 prompts cell migration toward the gels, this effect being more apparent when HA was present. In the case of Polox-based gels, both in the presence and absence of HA, the migration indexes were higher than in the case of MC-based systems. Despite this, cells were not found within the Polox-based gels, therefore indicating that, after the noticeable initial trigger to cell migration, cell invasion ability in Polox-based gels was thwarted. Actually, cell ability to migrate is highly dependent on the stiffnes of the matrix in which migration occurs [Da Silva *et al*., 2010; Engler *et al*., 2006]. More in detail, the amount of migrating cells is dictated by the cell ability to polarize in the sense of creating an asymmetric configuration of its subdomains resulting in cell movement activated by a protrusion–contraction sequence. In turn, cell polarization is influenced by matrix rigidity, and this results into durotaxis phenomenon which is the alignment of actin and myosin filaments along a gradient of matrix stiffness [De *et al*., 2008; Raab *et al*., 2017; Saez *et al*., 2007; Zemel and Safran, 2007]. Specifically, the traction forces involved in the contractile events of the filaments which trigger cell movement are higher when the cells experience stiffer matrices [Lam *et al*., 2011; Mitrossilis *et al*., 2010]. In actual fact, the elastic modulus of Polox-based gels at 37 °C was higher than that of MC-based systems in all the range frequency analyzed, and this is congruent with the observed high values in the migration index for such gels compared to MC-based systems. Results shown in figure 2.2 indicate that CEM cells are able to migrate within MC-based gels, while no cells were detectable within Polox-based matrices. This can be reasonably ascribed to the capacity of the CEM cells to diffuse inside the gels pores. Since gel pores (i.e. the mesh size of the gels) were found to be smaller then CEM cell dimensions (~15 μm), cell diffusion/penetration into the gels can be influenced by the ability of the polymer chians to disentagle each-other, thus enlarging their pores and so to the different viscous components of the various gels. In particular, as illustrated by rheograms in figure 2.4, at 37 °C and at low stress frequencies, the measured G" values of Polox-based gels are more than one order of magnitude higher compared to

G" values of MC-based gels. This can be considered a detriment to cell movement in the gel, which basically occurs via cavity-to-cavity steps. Indeed, it has been recently suggested that cell deformability, possibly combined with the deformation of the scaffold being intruded, is a limiting feature for migration [Da Silva *et al*., 2010].

The results shown in this work suggest that CEM cells are sensitive to both chemical and mechanical gradients, and that an optimization of the gel systems should probably take into account the possible existence of a limiting viscosity above which a gel matrix hampers the deformation of its pores therefore resulting in a significant impairment of cell migration.

2.6 Conclusions

The use of a fake metastatic niche to divert and capture $CXCR4^+$ circulating tumor cells can be helpful in capturing these target cells and possibly reducing/inhibiting the formation of metastasis. The optimized combination of chemical gradient and knowledge of durotaxis phenomenon is probably required to maximize the capturing ability of the tested gels. This approach, associated to typical surgical and chemotherapeutic clinical therapies, could be, in our opinion, very useful in cancer management. Further studies will be done to assess also *in vivo* the gel capability to divert $CXCR4^+$ circulating tumor cells.

REFERENCES

Arvelo F, Sojo F, Cotte C (2016). Tumor progression and metastasis. *Ecancermedicalscience*, 10:617.

Bleul C.C., Fuhlbrigge R.C., Casasnovas J.M., Aiuti A, Springer T.A. (1996). A highly efficacious lymphocyte chemoattractant, stromal cell-derived factor 1 (SDF-1). *The J of Exper Med*, 184: 1101–1109.

Cifone M.A., Fidler I.J. (1981). Increasing metastatic potential is associated with increasing genetic instability of clones isolated from murine neoplasms. *PNAS*, 78:6949-6952.

D'Errico G, De Lellis M, Mangiapia G, Tedeschi A, Ortona O, Fusco S, Borzacchiello A, Ambrosio L (2008). Structural and mechanical properties of UV-photo-cross-linked poly(N-vinyl-2-pyrrolidone) hydrogels. *Biomacromol*, 9:231-240.

Da Silva J, Lautenschläger F, Sivaniah E, Guck J.R. (2010). The cavity-to-cavity migration of leukaemic cells through 3D honey-combed hydrogels with adjustable internal dimension and stiffness. *Biomat*, 31:2201-2208.

De R, Zemel A, Safran S.A. (2008). Do cells sense stress or strain? Measurement of cellular orientation can provide a clue. *Biophys J*, 94:29-31.

De la Fuente A, Alonso-Alconada L, Costa C, Cueva J, Garcia-Caballero T, Lopez-Lopez R, Abal M (2015). M-trap: Exosome-based capture of tumor cells as a new technology in peritoneal metastasis. *J Natl Cancer Inst*, 107.

Engler A.J., Sen S, Sweeney H.L., Discher D.E. (2006). Matrix elasticity directs stem cell lineage specification. *Cell*, 126:677-689.

Fidler I.J., Kripke M.L. (2015). The challenge of targeting metastasis. *Cancer Metastasis Rev*, 34:635-641.

Flory P.J. (1953). Principles of Polymer Chemistry. Cornell University Press, Ithaca, NY, USA.

Klouda L, Mikos A.G. (2008). Thermoresponsive hydrogels in biomedical applications. *Eur J Pharm Biopharm*, 64:34-45.

Lam W.A., Chaudhuri O, Crow A, Webster K.D., Li T.D., Kita A, Huang J, Fletcher D.A. (2011). Mechanics and contraction dynamics of single platelets and implications for clot stiffening. *Nat Mater*, 10:61-66.

Liu P, Long P, Huang Y, Sun F, Wang Z (2016). CXCL12/CXCR4 axis induces proliferation and invasion in human endometrial cancer. *Am J Transl Res*, 8:1719-1729.

Mayol L, Biondi M, Quaglia F, Fusco S, Borzacchiello A, Ambrosio L, La Rotonda M.I. (2011). Injectable thermally responsive mucoadhesive gel for sustained protein delivery. *Biomacromol*, 12:28-33.

Mayol L, De Stefano D, De Falco F, Carnuccio R, Maiuri M, De Rosa G (2014). Effect of hyaluronic acid on the thermogelation and biocompatibility of its blend with methyl cellulose. *Carbohyd Polym*, 112:480-485.

Mitrossilis D, Fouchard J, Pereira D, Postic F, Richert A, Saint-Jean M, Asnacios A (2010). Real-time single-cell response to stiffness. *PNAS*, 107:16518-16523.

Müller A, Homey B, Soto H, Ge N, Catron D, Buchanan M.E., McClanahan T, Murphy E, Yuan W, Wagner S.N., Barrera J.L., Mohar A, Verástegui E, Zlotnik A (2001). Involvement of chemokine receptors in breast cancer metastasis. *Nature*, 410:50–56.

Murphy J.W., Cho Y, Sachpatzidis A, Fan C, Hodsdon M.E., Lolis E (2007). Strctural and functional basis of CXCL12 (stromal cell-derived factor-1 alpha) binging heparin. *Biol Chem*, 282:10018-10027.

Raab M, Swift J, Dingal P.C.D.P., Shah P, Shin J.W., Discher D.E. (2017). Crawling from soft to stiff matrix polarizes the cytoskeleton and phosphoregulates myosin-II heavy chain. *Int J of Cell Biol*, 199:669-683.

Saez A, Ghibaudo M, Buguin A, Silberzan P, Ladoux B (2007). Rigidity-driven growth and migration of epithelial cells on microstructured anisotropic substrates. *PNAS*, 104:8281-8286.

Sun X, Cheng G, Hao M, Zheng J, Zhou X, Zhang J, Taichman R.S., Pienta K.J., Wang J *(2010)*. CXCL1 /CXCR4/CXCR7 chemokine axis and cancer progression. *Cancer Met Rev*, 29:709–722.

Yang W, Zou L, Huang C, Lei Y (2014). Redox regulation of cancer metastasis: molecular signaling and therapeutic opportunities. *Drug Dev Res*, 75:331-341.

Yu L, Cecil J, Peng S.B., Schrementi J, Kovacevic S, Paul D, Su E.W., Wang J (2006). Identification and expression of novel isoforms of human stromal cell-derived factor 1. *Gene*, 374:174-179.

Zemel A, Safran S.A. (2007). Active self-polarization of contractile cells in asymmetrically shaped domains. *Phys Rev*, 76:021905.

Zheng H, Fu G, Dai T, Huang H (2007). Migration of endothelial progenitor cells mediated by stromal cell-derived factor-1alpha/CXCR4 via PI3K/Akt/eNOS signal transduction pathway. *J of Cardio Pharm*, 50:274–280.

CHAPTER 3

Chitosan-based polyelecrolyte complexes for doxorubicin and zoledronic acid combined therapy to overcame multidrug resistance

ABSTRACT

The aim of the present work was to develop PECs encapsulating Doxo and Zol for combined therapy against Doxo-resistant tumors. PECs were prepared by ionotropic gelation technique. The influence of some experimental parameters was evaluated in order to optimize the PECs in terms of size and polydispersity index. To study PEC stability, size and ζ-potential were monitored over the time. Moreover, HA-coated PECs were also developed. Finally, *in vitro* studies were carried out on wild type and Doxo-resistant cell lines, to assess both the synergism between Doxo and Zol, as well as the restoring of Doxo sensitivity. Moreover, targeting of CD44-overexpressing cells by using HA-coated PEC was also tested. Polymer concentration, incubation time and use of a surfactant were found to be crucial to achieve small size and monodisperse PECs. Doxo and Zol, only when encapsulated in PEC, showed synergism antiproliferative effect in all the tested cell lines. Moreover, the incubation of Doxo-resistant cell lines with Doxo/Zol co-encapsulating PEC resulted in restoration of Doxo sensitivity. Finally, in CD44-overexpressing cells, the addition of HA on PEC surface slightly enhanced the cytotoxicity of PEC encapsulating Doxo, but not of PEC co-encapsulating Doxo and Zol. PECs co-loaded with Doxo and Zol can be considered a promising approach to enhance Doxo cytotoxicity, overcaming drug resistance in Doxo-resistant cancer cells.

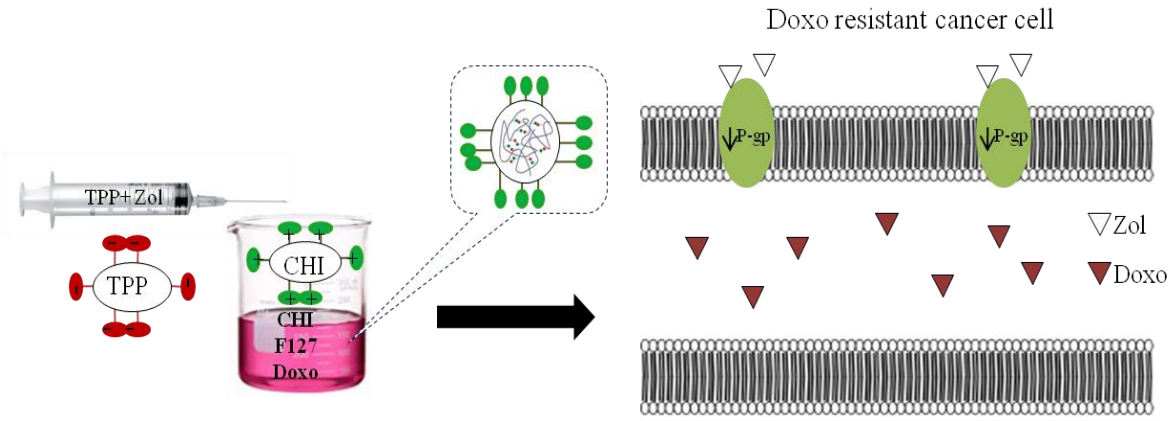

3.1 Introduction

One of the main limitation of the chemotherapy treatments is the development of malignant cell's resistance to one or more anticancer drugs; this process is known as "multidrug resistance" (MDR) which inevitably leads to a reduction of therapy effectiveness [Krishna and Mayer, 2000; Liscovitch and Lavie, 2002; Stavrovskaya, 2000; Szakács *et al*., 2006]. Generally, hydrophobic and amphipathic natural molecules, such as anthracyclines (e.g. Doxo) are more prone to develop resistance compared to other substances [Calcagno and Ambudkar, 2010; Thomas and Coley, 2003]. It is well known that the over-expression of some proteins of the efflux pumps ATP-binding cassette (ABC) family, is one of the major causes of the MDR [Choi, 2005; Gottesman and Pastan, 1993; Gottesman *et al*., 2002]. One of the main components of the ABC family is represented by P-glycoprotein (P-gp), also known as MDR protein 1(MDR1). P-gp is normally expressed in different normal tissues, such as kidney, liver, pancreas and colon where it is involved in the extrusion of neutral or weakly basic amphipathic substances penetrated into the cells [Dean *et al*., 2001; Sharom, 1997]. Therefore, tumors derived from these tissues have a greater expression of P-gp compared to others [Sharom, 2011]. The function, as well as the ATPase activity of the P-gp, seems to be affected by intra-cellular cholesterol levels since very high levels of cholesterol were found in the plasma membranes of MDR^+ tumor cells [Gimpl *et al*., 1997; Kapse-Mistry *et al*., 2014; Ozben, 2006; Thomas and Coley, 2003; Troost *et al*., 2004]. In our previous works we demonstrated that nanocarriers loaded with Zol, an aminobisphosphonate clinically used to treat bone diseases, increase the *in vitro* antiproliferative effects of Doxo in Doxo-resistant cell lines; this effect was explained with the effect of Zol on the inhibition of the cholesterol production and, consequently, on the P-gp activity [Caraglia *et al*., 2010; Kopecka *et al*., 2015; Kopecka *et al*., 2016].

Among the nanocarriers used as drug delivery systems, NPs based on PECs have attracted a great attention thanks to their low costs of manufacturing together with an easy scale-up and absence of organic solvents [Lankalapalli and Kolapalli, 2009; Patwekar *et al*., 2016]. In particular, ionotropic gelation process leads to spontaneous formation of PECs, as the result of electrostatic interactions between oppositely charged molecules. One of the main polymer suitable for gelation process is represented by CHI, a natural cationic polysaccharide composed of D-glucosamine and N-acetyl-D-glucosamine units, with well-known biodegradability, biocompatibility and bioadhesiveness properties. In acidic environment, CHI positive charges makes it suitable for electrostatic interactions with an

anionic counterpart, such as tripolyphosphate (TPP) and/or HA [Fan *et al*, 2012; Gan *et al*., 2005; Jonassen *et al*., 2012; Nasti *et al*., 2009; Ramasamy *et al*., 2014]. The latter is an anionic biocompatible and non-immunogenic glycosaminoglycan, also with ability to bind CD44 and RHAMM receptors over-expressed in different cancer cells [Gotte and Yip, 2006].

3.2 Aim of the work

In this context, the aim of the present work was to develop PECs co-loading Doxo and Zol by ionotropic gelation process. The preparation conditions were optimized to achieve PECs with low mean diameter, narrow size distribution, stability during storage, and high Doxo/Zol encapsulation efficiency. Finally, *in vitro* studies were carried out on osteosarcoma (SAOS), Doxo-resistant osteosarcoma (SAOS DX) and breast cancer (MCF7) cell lines, to assess both the possibility of combined therapy to overcame resistance in Doxo-resistant tumor cells and the HA targeting ability.

3.3 Materials and methods

3.3.1 *Materials*

CHI (molecular weight 300.000~500.000 Da, inherent viscosity: 200-400 mPa.s) and TPP were obtained from Sigma-Aldrich (USA). Poloxamer F127, a group of amphiphilic triblock polymer (number of oxyethylene units=100, number of oxyproptlene units=65) was purchased from Lutrol (Basf, Germany). HA (molecular weight ~ 180 kDa) was obtained from Contipro (Dolní Dobrouč, Czech Republic). Doxo hydrochloride from 3V Chimica (Rome, Italy), Zol monohydrate (1-Hydroxy-2-imidazol-1-ylethylidene) from U.S. Pharmacopeia Convention (Twinbrook Parkway, Rockville, USA) were used.

3.3.2 *Preparations of polyelectrolyte complexes (PECs)*

Uncoated blank PECs (PEC-CHI) were prepared by ionotropic gelation method. Briefly, CHI solution was prepared in 10 mL aqueous acetic acid (2% v/v); after complete solubilization the pH of the resulting solution was adjusted to 4.7 with NaOH (1N) and

filtrate trough 0.2 µm syringe filter. TPP solution was obtained by solubilizing TPP in 5 mL of distilled water followed by filtration trough 0.2 µm syringe filter. Afterwards, PECs were obtained by adding the anionic solution into the CHI solution and lefting them under magnetic stirring (700 rpm, at room temperature) for 30 minutes, to allow the cross-linking reaction. The resulted PECs suspension was purified by centrifugation (two washing at 10000 rpm, 10 min; Hettich Zentrifugen, Germany) and kept overnight at 4 °C. HA-coated PECs (PEC-HA) were prepared by using the same procedure described above for PEC-CHI. However, for PEC-HA formulations, HA aqueous solution was added immediately after PEC-CHI purification. In particular, the supernatant obtained after PEC-CHI purification was discarded and replaced with the same volume of HA solution. The obtained suspensions was stirred at 1200 rpm for 15 min, to allow the electrostatic interactions between PEC-CHI and HA, and purified by centrifugation (5000 rpm, 5 min). Various CHI, TPP and HA concentrations, times of interaction between them, as well as surfactant addiction to the formulation were investigated. Loaded PEC (HA-coated and uncoated) were obtained by simply adding Doxo (0.1mg/mL) to CHI solution and Zol (0.2 mg/mL) to TPP solution, prior to proceed with PEC preparation, forming: Zol loaded PEC (PEC-Zol); Doxo loaded PEC (PEC-Doxo); Zol and Doxo co-loaded PEC (PEC- Doxo-Zol); HA-coated PEC Zol-loaded (PEC-Zol-HA); HA-coated PEC Doxo-loaded (PEC-Doxo-HA); HA-coated PEC Zol and Doxo co-loaded (PEC- Doxo-Zol-HA).

3.3.3 *Size, polydispersity index and ζ potential*

The average diameters, polydispersity index (PI) and ζ-potential of the obtained formulations were measured *via* dynamic light scattering (N5, Beckman Coulter, USA and Nano-Z, Malvern Instruments, UK). For the analysis, each PEC formulations were properly diluted with ultrapure water and measured at room temperature. Results were calculated as average of 5 runs of three independent samples. To evaluate PEC dimensional stability size and ζ-potential measurements were monitored for at least 30 days, in water at 4 °C (i.e. storage conditions).

3.3.4 *Doxo and Zol encapsulation efficacy and preparation yield of the PECs*

PECs preparation yield was calculated from previously freeze-dried formulations (0.01 atm, 24 hours; Modulyo, Edwards, UK). In particular, it was gravimetrically obtained from the entire mass of recovered freeze-dried PECs. For the entrapment efficiency (EE), the supernatant obtained after purification of loaded PECs (or the pellet for HA-coated PECs) containing free drugs, was submitted to quantitative analyses. In particular, the percentage of Doxo entrapped into PECs was evaluated by spectrophotometric assay (UV-1800, Shimadzu Laboratory World, Japan) at λ=480 nm. The linearity of the response was verified over the concentration range 62,5-0,06 μg/mL (r^2> 0,99). Instead Zol encapsulation efficiency was measured by ultra-high-performance liquid chromatography (UHPLC, Shimadzu Nexera Liquid Chromatograph LC-30AD), performed on a Gemini C18, 110 Å column (250 mm × 4.6 mm, 5 μm) at a λ=220 nm, using a mobile phase composed of 20:80 (v/v) acetonitrile:tributyl-ammonium-phosphate buffer (pH=7). The flow rate was 1 mL/min and the run time was set at 15 min. The drugs encapsulation efficiency were calculated by the following equation:

$$EE\ (\%) = \frac{\text{Total amount of drugs in formulations} - \text{Free drugs}}{\text{Total amount of drugs in formulations}} \text{ x } 100$$

The values of the EE (%) were collected from three different batches.

3.3.5 *Cell culture*

SAOS, SAOS DX and MCF7 cell lines were obtained from American Type Culture Collection (ATCC; Rockville, MD). Wild type and SAOS DX cells were grown in Dulbecco's modified Eagle's medium (DMEM), while MCF7 were grown in Roswell Park Memorial Institute 1640 medium (RPMI). Both cell media were supplemented with 10% heat-inactivated fetal bovine serum, 20 mM HEPES, 100 U/mL penicillin, 100 mg/mL streptomycin, 1% L-glutamine and 1% sodium pyruvate. All the cells were cultured at a constant temperature of 37 °C in a humidified atmosphere of 5% carbon dioxide (CO_2).

3.3.6 *Cell proliferation assay*

After trypsinization, all the cell lines were plated in 100 µL of medium in 96-well plates at a density of $2x10^3$ cells/well. One day later, the cells were treated with free Doxo, free Zol, PEC-CHI, PEC-HA, PEC-Doxo, PEC-Doxo-HA, PEC-Zol, PEC-Zol-HA, PEC-Doxo-Zol and PEC-Doxo-Zol-HA, at concentrations ranging from 20 µM to 0.156 µM for Doxo and from 200 µM to 0,312 µM for Zol. Cell proliferation was evaluated by MTT assay. Briefly, cells were seeded in serum-containing media in 96-well plates at the density of 2×10^3 cells/well. After 24 hours incubation at 37 °C, the medium was removed and replaced with fresh medium containing all developed formulations at different concentrations. Cells were incubated under these conditions for 72 hours. Then, cell viability was assessed by MTT assay. The MTT solution (5 mg/mL in phosphate-buffered saline) was added (20 µL/well), and the plates were incubated for further 4 hours at 37 °C. The MTT-formazan crystals were dissolved in 1N isopropanol/hydrochloric acid 10% solution. The absorbance values of the solution in each well were measured at 570 nm using a Bio-Rad 550 microplate reader (Bio-Rad Laboratories, Milan, Italy). Percentage of cell viability was calculated as described in the following equation:

$$Cell\ viability\ (\%) = \frac{(\text{absorbance of the treated wells} - \text{absorbance of the blank control})}{(\text{absorbance of the negative control wells} - \text{absorbance of the blank control wells})} \text{x } 100$$

Then, the concentrations inhibiting 50% of cell growth (IC_{50}) were obtained and these values were used for subsequent experiments. MTT assay was carried out by triplicate determination on at least three separate experiments. All data are expressed as mean ± SD.

3.4 Results and discussion

3.4.1 *Uncoated PEC preparations and characterization*

PEC based on CHI were firstly obtained through manual ionotropic gelation technique exploiting the ability of the amine functional groups of CHI to be protonated in acidic environment; the resulting $-NH3^+$ groups are able to interact with negatively charged groups of TPP, leading to PEC formation [Janes *et al*., 2001]. Commonly, oppositely charged macromolecules aggregate due to their high charge density fluctuation in solutions

[Lankalapalli and Kolapalli, 2009]. Therefore, PECs formation and stability is affect by several factors [Masarudin *et al*., 2015]. Among these, CHI and TPP concentrations used during the preparation process play an important role. In table 3.1, the different polymer concentrations used, the size and PI of the different prepared PEC formulations are reported. In all the formulations, the volume ratios between CHI and TPP phases was fixed at 2:1.

Formulation	[CHI] mg/mL	[TPP] mg/mL	d (nm)	IP
$PEC_{(CHI\ 0.4\text{-}TPP\ 0.5)}$	0.4	0.5	236.9±31.2	1.14±0.5
$PEC_{(CHI\ 0.3\text{-}TPP\ 0.5)}$	0.3	0.5	231.9±9.50	0.23±0.1
$PEC_{(CHI\ 0.5\text{-}TPP\ 0.4)}$	0.5	0.4	272.1±86.7	0.42±0.1
$PEC_{(CHI\ 0.5\text{-}TPP\ 0.3)}$	0.5	0.3	314.2±14.5	1.03±0.6
$PEC_{(CHI\ 0.5\text{-}TPP\ 0.5)}$	0.5	0.5	132.7±11.2	0.43±0.1
$PEC_{(CHI\ 0.4\text{-}TPP\ 0.4)}$	0.4	0.4	185.1±0.81	0.27±0.1
$PEC_{(CHI\ 0.3\text{-}TPP\ 0.3)}$	0.3	0.3	132.3±6.80	0.42±0.1
$PEC_{(CHI\ 0.3\text{-}TPP\ 0.5)}$	0.3	0.4	287.8±15.4	0.15±0.1

Table 3.1: size and IP of different PEC formulations prepared using various CHI and TPP concentrations. All results are expressed as mean ± SD of at least three independent experiments

Results showed that PECs with smallest size (in the range from ~ 130 to ~ 180 nm) were obtained using the same concentrations of both CHI and TPP. By increasing the TPP/CHI ratio, the PEC size significantly increased. This could be probably ascribed to the excess of TPP in solution; negative charges of TPP might interact with free amino groups of pre-formed PECs, leading to a PEC aggregation. A similar size increase was observed by increasing CHI concentration. This effect was probably due to higher viscosity of the resulting solution, which slows down the cross-linking reaction between the polymers chains, with consequent formation of aggregates. Concentrations greater than 0.5 mg/mL of both components led to formation of visible macro-aggregates (data not shown). The time of interaction between CHI and the cross-linking agent was found to be another parameter influencing PEC size and PI. In particular, the optimal CHI and TPP concentrations, which led to the smallest PEC size, were used to prepare PECs with controlled-precipitation flow rate (Q). Results of dimensions, PI and ζ potential analysis of

PEC formulations, prepared by using different flow rate (Q = 500 and 133.3 μL/min, named A and B respectively), are summarized in table 3.2.

Formulation	[CHI] mg/mL	[TPP] mg/mL	Q (μL/min)	d (nm)	PI	ζ potential (mV)
$PEC_{(CHI\ 0.5\text{-}TPP\ 0.5)}$-A	0.5	0.5	500	223.3±3.8	0.67±0.3	18.1±1.5
$PEC_{(CHI\ 0.5\text{-}TPP\ 0.5)}$-B	0.5	0.5	133.3	187.0±9.1	0.45±0.2	21.3±1.1
$PEC_{(CHI\ 0.4\text{-}TPP\ 0.4)}$-A	0.4	0.4	500	147.7±2.9	0.49±0.1	19.1±1.9
$PEC_{(CHI\ 0.4\text{-}TPP\ 0.4)}$-B	0.4	0.4	133.3	129.4±2.7	0.42±2.7	19.1±0.8
$PEC_{(CHI\ 0.3\text{-}TPP\ 0.3)}$-A	0.3	0.3	500	127.5±2.2	0.51±0.3	17.8±2.9
$PEC_{(CHI\ 0.3\text{-}TPP\ 0.3)}$-B	0.3	0.3	133.3	104.4±1.4	0.41±0.3	21.4±1.9

Table 3.2: size, PI and ζ potential values of different PEC formulations prepared using different CHI and TPP concentrations and different Q. In all formulations, the inner diameter of the syringe used for the precipitation of TPP into CHI solution was set at 11.99 mm. All results are expressed as mean ± SD of at least three independent experiments

As it can be observed, PECs obtained using a lower flow rate showed smaller diameter. This size trend could be attributed to the time needed for the cross-linking reaction; thus, at lower flow rate, the possibility to achieve a homogeneous distribution of the polymer chains should be greater. This should promote their electrostatic interactions and formation of PECs with very small diameter (around ~ 100 nm). A positive charge, evaluated by ζ potential analysis, was found in all the formulations due to the presence of CHI primary free amino groups. On the basis of these results, formulation $PEC_{(CHI\ 0.3\text{-}TPP\ 0.3)}$-B, obtained by using a concentration of 0.3 mg/mL of both CHI and TPP and a flow rate of 133.3 μL/min, resulted in the optimal features in terms of mean diameter, although with a high PI (~ 0.4) indicating a poor homogeneity of the PEC dispersion (table 3.2). Therefore, the poloxamer F127 at different concentrations was added to CHI acetic acid solution before PEC preparation [Hosseinzadeh *et al*., 2012]. As expected, the addition of F127 resulted in significant IP reduction, depending on the poloxamer concentration. In particular, in the case of the $PEC_{(CHI\ 0.3\text{-}TPP\ 0.3)}$-B, the addition of F127 at 10% (w/w) allowed to get more monodisperse PECs (IP < 0.25), without significant change in size and ζ potential value (table 3.3).

Formulation	[CHI] mg/mL	[TPP] mg/mL	F127 (% w/w)	d (nm)	PI	ζ potential (mV)
$PEC_{(CHI\ 0.3\text{-}TPP\ 0.3)}$-$B_{20}$	0.3	0.3	20	114.1±5.1	0.48±0.1	17.2±2.5
$PEC_{(CHI\ 0.3\text{-}TPP\ 0.3)}$-$B_{16}$	0.3	0.3	16	114.8±6.9	0.32±0.2	16.9±2.1
$PEC_{(CHI\ 0.3\text{-}TPP\ 0.3)}$-$B_{10}$	0.3	0.3	10	110.8±3.5	0.23±0.2	21.2±3.3

Table 3.3: size, PI and ζ potential values of different PEC formulations prepared using different F127 concentrations

3.4.2 *HA-coated PEC preparations and characterization*

The optimized uncoated PEC formulation $PEC_{(CHI\ 0.3\text{-}TPP\ 0.3)}$-$B_{10}$ (from here named PEC) was considered to develop HA-coated PECs. The negatively-charged HA can coat PECs surface by taking advantage of its ability to make electrostatic interactions with a cationic counterpart. A such approach should result easy to scale-up and avoid organic solvents and chemical reactions between polymers. The addition of different HA concentrations and time required for the interaction between anionic HA and cationic PEC, were investigated in order to achieve optimized formulations in terms of size. As shown in table 3.4, the HA addition resulted in a significant increase in PEC size.

Formulation	[HA] mg/mL	Time of interaction (min)	d (nm)	PI	ζ potential (mV)
$PEC\text{-}HA_{(0.3\text{-}15\ min)}$	0.3	15	249.2±2.4	0.59±0.1	-17.1±1.1
$PEC\text{-}HA_{(0.3\text{-}30\ min)}$	0.3	30	278.8±6.9	0.49±0.1	-12.6±1.2
$PEC\text{-}HA_{(0.6\text{-}15\ min)}$	0.6	15	180.9±6.7	0.08±0.1	-23.1±1.2
$PEC\text{-}HA_{(0.6\text{-}30\ min)}$	0.6	30	196.7±2.5	0.19±0.1	-26.8±1.3
$PEC\text{-}HA_{(0.9\text{-}15\ min)}$	0.9	15	170.8±13	0.29±0.2	-20.1±0.9
$PEC\text{-}HA_{(0.9\text{-}30\ min)}$	0.9	30	175.6±1.1	0.29±0.1	-16.5±1.5

Table 3.4: size, PI and ζ potential values of different PEC-HA formulations prepared using different HA concentrations and times of interaction between HA solution and PEC formulations

In particular, results showed that very homogeneous size distribution of PEC-HA (IP<0.1) was obtained when using a HA concentration of 0.6 mg/mL and a time of interaction of 15

min (PEC-HA(0.6-15 min)). Therefore, this formulation (from here named PEC-HA) was considered for the following step of the study. Furthermore, upon the addition of HA to the formulation, a switch in ζ potential value was observed from ~ +21 mV (PEC formulation) to ~ - 23 mV (PEC-HA formulation). The negative ζ potential was ascribed to the ionization of HA carboxyl groups, thus demonstrating the presence of the external HA moieties on PEC surface.

3.4.3 *Preparation and characterization of PEC encapsulating Doxo and Zol*

Doxo and Zol were loaded into PEC and PEC-HA formulations, to obtain a co-delivery of these drugs in a combined therapy. Doxo and Zol encapsulation efficiencies and preparation yield of different formulations are summarized in table 3.5.

Formulation	[Zol] mg/mL loaded	[Doxo] mg/mL loaded	E.E. Zol (%)	E.E. Doxo (%)	Yield (%)
PEC	-	-	-	-	80.8±0.1
PEC-HA	-	-	-	-	92.5±0.4
PEC-Zol	0.2	-	55.1±1.8	-	77.8±1.3
PEC-Zol-HA	0.2	-	53.6±5.6	-	96.5±0.4
PEC-Doxo	-	0.1	-	37.7±9.4	79.4±0.1
PEC-Doxo-HA	-	0.1	-	29.1±7.7	80.9±0.1
PEC-Zol-Doxo	0.2	0.1	58.7±1.6	37.6±3.9	81.6±0.1
PEC-Zol-Doxo-HA	0.2	0.1	52.9±3.3	31.3±3.1	83.3±0.1

Table 3.5: Doxo and Zol encapsulation efficiency (%) and yield (%) of different formulations prepared. In all cases CHI (0.3 mg/mL), TPP (0.3 mg/mL) and HA (0.6 mg/mL) were used

As shown, the prepared formulations were characterized by a high yield, greater than 70% in all cases. Zol and Doxo encapsulation efficiency was found to be similar in PECs loaded with one or both drugs. Furthermore, the presence of HA into the formulation did not seem to significantly affect the percentage of drugs loaded into the PECs. The mean size, as well as the PI of PECs loaded with one or both drugs, resulted slightly increased. On the other hand, the two molecules did not affect the behaviors of PEC-HA, which showed a diameter

of about 170 nm with a polydispersity index of ~ 0.1 (table 3.6). As it can be observed in table 3.6, when HA was added to the formulations, ζ potential of the formulations shifted from positive to negative values.

Formulation	d (nm)	PI	ζ potential (mV)
PEC-Zol	131.1±0.1	0.32±0.1	20.2±1.3
PEC-Zol-HA	180.9±1.4	0.18±0.2	-18.6±0.3
PEC-Doxo	120.5±4.7	0.42±0.4	22.9±1.6
PEC-Doxo-HA	173.7±9.7	0.11±0.1	-22.1±0.4
PEC-Zol-Doxo	111.5±0.1	0.39±0.4	23.1±2.3
PEC-Zol-Doxo-HA	176.5±1.2	0.12±0.1	-18.8±0.5

Table 3.6: size, PI and ζ potential of different loaded PEC formulations

3.4.4 *Stability studies*

In order to evaluate the stability of prepared formulations, mean diameters, PI and ζ-potential were analyzed up to 30 days of storage in water at 4 °C. As shown in figure 3.1, PECs coated with HA had a narrow size distribution than PECs without HA. This suggesting that HA could act as stabilizer presumably conferring high density of negative charges on the PEC surface and/or due to a "steric clamping" effect of HA on the PEC surface. For all analyzed formulations ζ potential values resulted stable up to 30 days, thus suggesting the permanence of HA on PEC surface (data not shown).

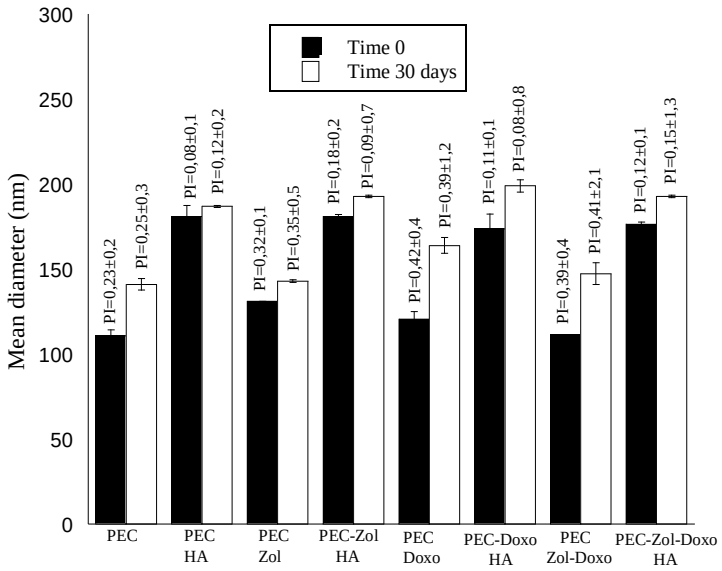

Figure 3.1: size and PI of different PECs formulations, at 0 time and after 30 days in water at 4 °C

3.4.5 *Cell proliferation assay*

The effects of free Doxo, free Zol, PEC, PEC-HA, PEC-Doxo, PEC-Doxo-HA, PEC-Zol, PEC-Zol-HA, PEC-Doxo-Zol and PEC-Doxo-Zol-HA, were evaluated on the proliferation of wild type SAOS, SAOS DX and MCF7 cancer cell lines by MTT assay. All the tested formulations induced a dose-dependent growth inhibition in all the cell lines analyzed after 72 hours, while treatment with blank PEC did not produce significant cytotoxic effects (figure 3.2).

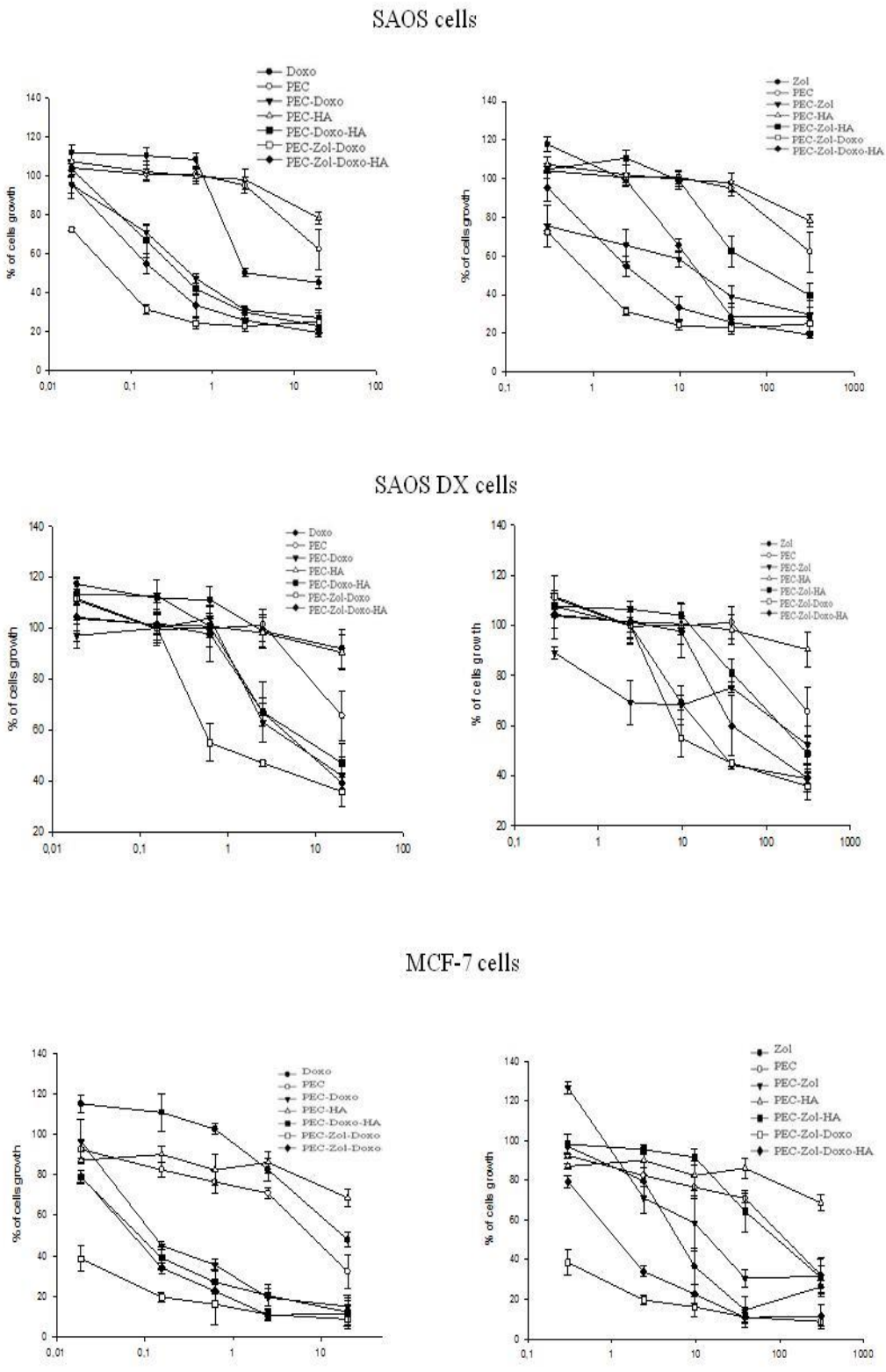

Figure 3.2: effect of all developed formulations on wild type and doxo–resistant SAOS and MCF proliferation

In table 3.7, results are reported as concentrations inhibiting 50% of cell growth (IC_{50}) after 72 hours of treatment.

SAOS	IC50
Doxo	2
PEC-Doxo	0.5
PEC-Doxo-HA	0.4
PEC-Doxo-Zol	0.05
PEC-Doxo-Zol-HA	0.2
PEC	-
PEC-HA	-

SAOS	IC50
Zol	17
PEC-Zol	16
PEC-Zol-HA	108
PEC-Doxo-Zol	0.8
PEC-Doxo-Zol-HA	2.7
PEC	-
PEC-HA	-

SAOS DX	IC50
Doxo	>20
PEC-Doxo	10.04
PEC-Doxo-HA	12.29
PEC-Doxo-Zol	0.9462
PEC-Doxo-Zol-HA	6.456
PEC	-
PEC-HA	-

SAOS DX	IC50
Zol	23.41
PEC-Zol	>200
PEC-Zol-HA	>200
PEC-Doxo-Zol	13.84
PEC-Dox-Zol-HA	98.19
PEC	-
PEC-HA	-

MCF-7	IC50
Doxo	18
PEC-Doxo	0.12
PEC-Doxo-HA	0.09
PEC-Doxo-Zol	< 0.019
PEC-Doxo-Zol-HA	0.07
PEC	-
PEC-HA	-

MCF 7	IC50
Zol	6.2
PEC-Zol	14
PEC-Zol-HA	90
PEC-Doxo-Zol	<0.3
PEC-Doxo-Zol-HA	1
PEC	-
PEC-HA	-

Table 3.7: IC_{50} of all developed formulations on wild type, Doxo–resistant SAOS and MCF, after 72 hours of treatment

In details, IC_{50s} of free Doxo were equal to 2μM for wild type SAOS, superior to 20μM for SAOS DX and equal to 18 μM for MCF7. The Doxo encapsulated in PEC (PEC-Doxo) induced a 50% growth inhibition at a concentration of 0.5, 10 and 0.12 μM in wild type, SAOS DX and MCF7, respectively (table 3.7). These data demonstrated that PECs, also without the co-encapsulation of Zol, are able to strongly increase the cytotoxicity of Doxo. It is worthy of note that Doxo encapsulation in other nanocarriers, e.g. stealth liposomes, results in a reduced Doxo cytotoxicity [Alberts and Garcia, 1997; Gabizon and Martin, 1997; Working *et al*., 1999]. In the case of PEC, it is possible to hypothesize an enhanced uptake into the cells and consequent higher Doxo intracellular delivery. On the other hand, the PEGylated nanocarriers have been shown to reduce the drug uptake into the target cells [Verhoef and Anchordoquy, 2013]. IC_{50}s of free ZOL were equal to 17μM in wild type SAOS, 23 μM in SAOS DX and 6.2 μM in MCF7. The encapsulation of ZOL in PECs did not potentiate its antitumor activity, in fact IC_{50} for PEC-Zol values were 16, >200 and 14 for wild type, SAOS DX and MCF7, respectively. These results are in contrast with our previous finding in which different lipid-based nanocarriers encapsulating Zol were useful to increase Zol uptake in different cancer cell lines [Marra *et al*., 2011; Salzano *et al*., 2011]. Here, when incubating wild type SAOS and MCF-7 with PEC-Zol only a citotoxicity similar or slightly higher, compared to naked Zol, was found. Thus, the strong interaction between CHI and Zol could slow the delivery of the bisphosphonate into the cytoplasm. Further studies are needed to understand the disappearance of Zol toxicity when incubating SAOX DX with PEC-Zol. On the other hand, PEC-Doxo-Zol inhibited the 50% of cell growth at a concentration of 0.05, 0.9 and 0.019 μM for Doxo and 0.8 13 and <0.3μM for Zol on wild type, SAOS DX and MCF7, respectively, by enhancing significantly the effects of both the drugs. The functionalization of PECs with HA resulted in different effect depending on the type of cancer cells. In particular, PEC-Doxo-HA induced a 50% growth inhibition at a concentration of 0.4, 12 and 0.09 μM in wild type, SAOS DX and MCF7, respectively. IC_{50s} of PEC-Zol-HA were equal to 108 μM for wild type SAOS, superior to 200 μM for Doxo-resistant SAOS and equal to 90 μM for MCF7. On the other hand, PEC-Doxo-Zol-HA inhibited 50% of cell growth at a concentration of 0.2, 6.4 and 0.07 μM for Doxo and 2.7, 98 and 1 μM for Zol on wild type, SAOS DX and MCF7, respectively. As summarized in table 3.7, a synergic effect was found when co-encapsulating Doxo with Zol. Interestingly, the data on SAOX DX strongly confirm

our previous finding on the association of Doxo and Zol to revert resistance to Doxo [Kopecka *et al*., 2016]. In particular, it has been hypothesized that Zol is able to restore the sensitivity in Doxo resistant cancer cells by acting on the mevalonate pathway, reducing P-gp expression and thus re-inducing the direct Doxo cytotoxicity. Here, in addition, a synergic effect was also found in wild type cells, thus suggesting that other mechanism different than the inhibition of the P-gp could arrive when associating these two drugs. On the other hand, the functionalization of PECs with HA potentiated the antitumor efficacy of Doxo but not the cytotoxicity of Zol. Indeed, PEC-Doxo-Zol-HA was more potent than free Doxo and Zol but not than PEC-Doxo-Zol, this effect was more evident in MCF7 that overexpressed CD44 receptor. This could be probably ascribed to the saturable cells receptor effect, on which the HA-uptake mechanism is based [Ouasti *et al*., 2012]. After administration into the body, free HA in solution could compete with PEC-HA to bind the same receptors expressed on cells surface. HA-CD44 interaction cause receptor internalization and consequently degradation by cellular enzymes; afterwards, CD44 expression takes about 24-48 hours. During this time frame, only a limited number of receptors will be available to cluster around HA-coated PEC, thus resulting in significantly decrease of receptor-mediated endocytosis of PEC-HA in CD44 overexpressing cancer cells [Almalik *et al*., 2013].

3.5 Conclusions

In the present study, CHI/TPP/HA based-PECs co-loaded with Doxo and Zol were successfully prepared with a simple and easily up-scalable method. Some parameters such as polymer concentration, times of interaction between them and surfactant addiction to the formulations were found to be crucial for PEC formation and technological features. The presence of HA moieties on PEC surface increases their stability over time. PEC co-delivery of Doxo and Zol enhances Doxo delivery in Doxo-resistant cell lines, thus providing a promising approach to overcome MDR. Differently to what was expected, despite HA-coated PECs are able to increase the cytotoxicity compared to free drugs, they were no more potent compared with uncoated PEC-Doxo-Zol, also in MCF7 cell lines overexpressing CD44 receptor. Additional studies will be done to confirm this effect and to evaluate the *in vivo* pharmacokinetics of the carriers.

REFERENCES

Alberts D.S., Garcia D.J. (1997). Safety aspects of pegylated liposomal doxorubicin in patients with cancer. *Drugs*, 4:30-35.

Almalik A, Karimi S, Ouasti S, Donno R, Wandrey C, Day P.J., Tirelli N (2013). Hyaluronic acid (HA) presentation as a tool to modulate and control the receptor-mediated uptake of HA-coated nanoparticles. *Biomat*, 34:5369-5380

Calcagno A.M., Ambudkar S.V. (2010). The molecular mechanisms of drug resistance in single-step and multi-step drug-selected cancer cells. *Methods Mol Biol*, 596:77-93.

Caraglia M, Marra M, Naviglio S, Botti G, Addeo R, Abbruzzese A (2010). Zoledronic acid: an unending tale for an antiresorptive agent. *Expert Opin Pharmacother*, 11:141–154.

Choi C.H. (2005). ABC transporters as multidrug resistance mechanisms and the development of chemosensitizers for their reversal. *Cancer Cell Int*. 5:30.

Dean M, Rzhetsky A, Allikmets R (2001). The human ATP-binding cassette (ABC) transporter superfamily. *Genome Res*, 11:1156-1166.

Fan W, Yan W, Xu Z, Ni H (2012). Formation mechanism of monodisperse, low molecular weight chitosan nanoparticles by ionic gelation technique. *Coll Surf B Bio*, 90:21–27.

Gabizon A, Martin F (1997). Polyethylene glycol-coated (pegylated) liposomal doxorubicin. Rationale for use in solid tumours. *Drugs*, 4:15-21.

Gan Q, Wang T, Cochrane C, McCarron P (2005). Modulation of surface charge, particle size and morphological properties of chitosan-TPP nanoparticles intended for gene delivery. *Coll Surf B Bioint*, 44:65–73.

Gimpl G, Burger K, Fahrenholz F (1997) Cholesterol as modulator of receptor function. *Biochem*, 36:10959–10974.

Gotte M, Yip G.W. (2006). Heparanase, hyaluronan, and CD44 in cancers: A breast carcinoma perspective. *Canc Res*, 66:10233–10237.

Gottesman M.M., Pastan I (1993). Biochemistry of multidrug resistance mediated by the multidrug transporter. *Annu Rev Biochem,* 62:385-427.

Gottesman M.M., Fojo T, Bates S.E. (2002). Multidrug resistance in cancer: role of ATP-dependent transporters. *Nat Rev Cancer,* 2:48-58.

Hosseinzadeh H, Atyabi F, Dinarvand R, Ostad S.N. (2012). Chitosan–Pluronic nanoparticles as oral delivery of anticancer gemcitabine:preparation and in vitro study. *Int J Nanomed,* 7: 1851–1863.

Janes K.A., Fresneau M.P., Marazuela A, Fabra A, Alonso M.J. (2001). Chitosan nanoparticles as delivery systems for doxorubicin. *J Control Release,* 73:255–61.

Jonassen H, Kjøniksen A.L., Hiorth M (2012). Stability of chitosan nanoparticles cross-linked with tripolyphosphate. *Biomacromol,*13:3747–3756.

Kapse-Mistry S, Govender T, Srivastava R, Yergeri M (2014). Nanodrug delivery in reversing multidrug resistance in cancer cells. *Front Pharmacol*, 5:159.

Kopecka J, Porto S, Lusa S, Gazzano E, Salzano G, Giordano A, Desiderio V, Ghigo D, Caraglia M, De Rosa G, Riganti C (2015). Self-assembling nanoparticles encapsulating zoledronic acid revert multidrug resistance in cancer cells. *Oncotarget,* 6:31461-31478.

Kopecka J, Porto S, Lusa S, Gazzano E, Salzano G, Pinzòn-Daza M.L., Giordano A, Desiderio V, Ghigo D, De Rosa G, Caraglia M, Riganti C (2016). Zoledronic acid-encapsulating self-assembling nanoparticles and doxorubicin: a combinatorial approach to overcome simultaneously chemoresistance and immunoresistance in breast tumors. *Oncotarget*, 7:20753-20772.

Krishna R, Mayer L.D. (2000). Multidrug resistance (MDR) in cancer. Mechanisms, reversal using modulators of MDR and the role of MDR modulators in influencing the pharmacokinetics of anticancer drugs. *Eur J Pharm Sci*, 11:265–283.

Lankalapalli S, Kolapalli V.R.M. (2009) Polyelectrolyte complexes: a review of their applicability in drug delivery technology. *Indian J PharmSci*, 71:481–487.

Liscovitch M, Lavie Y (2002). Cancer multidrug resistance: a review of recent drug discovery research. *IDrugs,* 5:349–355.

Marra M, Salzano G, Leonetti C, Tassone P, Scarsella M, Zappavigna S, Calimeri T, Franco R, Liguori G, Cigliana G, Ascani R, La Rotonda M.I., Abbruzzese A, Tagliaferri P, Caraglia M, De Rosa G (2011). Nanotechnologies to use bisphosphonates as potent anticancer agents: the effects of zoledronic acid encapsulated into liposomes. *Nanomed*, 7:955-964.

Masarudin M.J., Cutts S.M., Evison B.J., Phillips D.R., Pigram P.J. (2015). Factors determining the stability, size distribution, and cellular accumulation of small, monodisperse chitosan nanoparticles as candidate vectors for anticancer drug delivery: application to the passive encapsulation of [^{14}C]-doxorubicin. *Nanotec Sci Appl*, 8:67–80.

Nasti A, Zaki N.M., Leonardis P.D., Ungphaiboon S, Sansongsak P, Rimoli M.G., Tirelli N (2009). Chitosan/TPP and chitosan/TPP-hyaluronic acid nanoparticles: systematic optimisation of the preparative process and preliminary biological evaluation. *Pharm Res*, 26:1918–1930.

Ouasti S, Kingham P.J., Terenghi G, Tirelli N (2012). The cd44/integrins interplay and the significance of receptor binding and re-presentation in the uptake of rgd-functionalized hyaluronic acid. *Biomat*, 33:1120-1134.

Ozben T (2006). Mechanism and strategies to overcame multiple drug resistance in cancer. *FEBS Lett*, 580:2903-2909.

Patwekar S.L., Potulwar A.P., Pedewad S.R., Gaikwad M.S., Khan S.A., Suryawanshi A.B. (2016). Review on Polyelectrolyte Complex as Novel Approach for Drug Delivery System. *IJPPR*, 5:97-109.

Ramasamy T, Tran T.H., Cho H.J., Kim J.H., Kim Y.I., Jeon J.Y., Choi H.G., Yong C.S., Kim J.O. (2014). Chitosan-Based Polyelectrolyte Complexes as Potential Nanoparticulate Carriers: Physicochemical and Biological Characterization. *Pharm Res*, 31:1302–1314.

Salzano G, Marra M, Porru M, Zappavigna S, Abbruzzese A, La Rotonda M.I., Leonetti C, Caraglia M, De Rosa G (2011). Self-assembly nanoparticles for the delivery of bisphosphonates into tumors. *Int J Pharm*, 403:292-297.

Sharom F.J. (1997). The P-Glycoprotein Efflux Pump: How Does it Transport Drugs? *J Membrane Biol*, 160:161–175

Sharom F.J. (2011). The P-glycoprotein multidrug transporter. *Essays Biochem*, 50:161-178.

Stavrovskaya A.A. (2000). Cellular mechanisms of multidrug resistance of tumor cells. *Biochemistry (Mosc)*, 65:95–106.

Szakács G, Paterson J.K., Ludwig J.A., Booth-Genthe C, Gottesman M.M. (2006). Targeting multidrug resistance in cancer. *Nar Rev Drug Discov*, 5:219-234.

Thomas H, Coley H.M. (2003). Overcoming multidrug resistance in cancer: an update on the clinical strategy of inhibiting p-glycoprotein. *Cancer Control*, 10:159–165.

Troost J, Lindenmaie J, Haefeli W.E., Weiss J (2004) Modulation of cellular cholesterol alters P-glycoprotein activity in multidrug-resistant cells. *Mol Pharmacol*, 66:1332–1339.

Verhoef J.J.F., Anchordoquy T.J. (2013). Questioning the Use of PEGylation for Drug Delivery Drug Deliv Transl Res, 3:499–503.

Working P.K., Newman M.S., Sullivan T, Yarrington J (1999). Reduction of the cardiotoxicity of doxorubicin in rabbits and dogs by encapsulation in long-circulating, pegylated liposomes. J *Pharmacol Exp Ther*, 289:1128-1133.

CHAPTER 4

Spontaneous arrangement of a tumor targeting hyaluronic acid shell on irinotecan loaded PLGA nanoparticles

ABSTRACT

The arrangement of tumor targeting HA moieties on irinotecan (IRIN)-loaded PLGA NPs has been directed by means of a gradient of lipophilicity between the oil and water phases of the emulsion used to produce the NPs. PLGA constitutes the NP bulk while HA is superficially exposed, with amphiphilic poloxamers acting as a bridge between PLGA and HA. Differential scanning calorimetry, zeta potential analyses and ELISA tests were employed to support the hypothesis of polymer assembly in NP formulations. The presence of flexible HA chains on NP surface enhances NP size stability over time due to an increased electrostatic repulsion between NPs and a higher degree of hydration of the device surface. IRIN *in vitro* release kinetics can be sustained up to 7–13 days. *In vitro* biologic studies indicated that HA-containing NPs were more toxic than bare PLGA NPs against CD44-overexpressing breast carcinoma cells, therefore indicating their ability to target CD44 receptor.

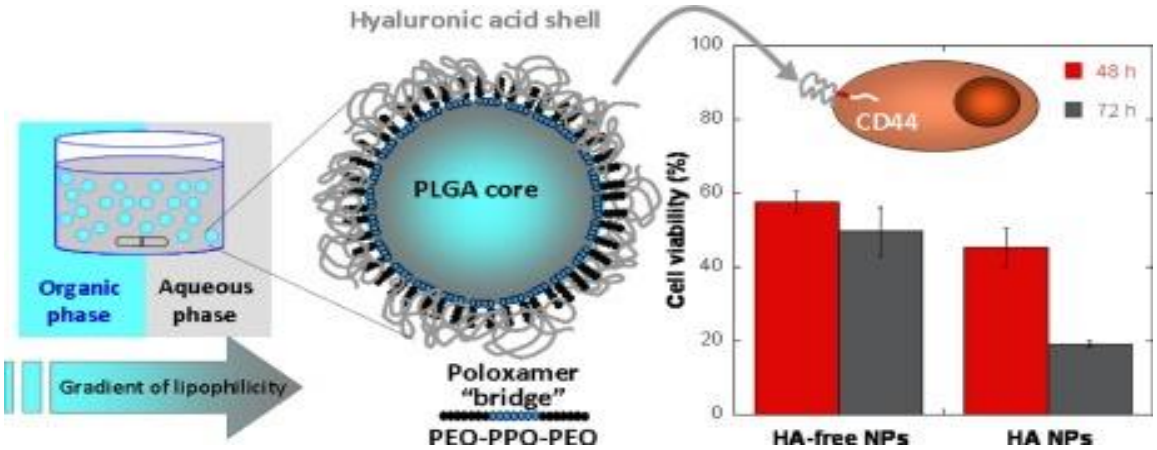

4.1 Introduction

New cancer therapies based on polymeric NPs have attracted great deal of interest due to their ability to encapsulate a wide array of anticancer drugs and to control their release at tumor target site [Brigger *et al*., 2002; Cho *et al*., 2008]. Among the materials used to produce polymeric NPs, PLGA play a dominant role [Athanasiou *et al*., 1996; Jain, 2000]. It is a synthetic copolymer of lactic acid (hydrophobic portion) and glycolic acid (hydrophilic portion), approved from FDA for clinical applications, thanks to its biocompatibility, non-toxicity and total *in vivo* biodegradability [Jalil and Nixon, 1990]. Bioerosion causes the chemical degradation by forming low molecular weight water-soluble derivatives, which are then eliminated through the typical metabolic processes of the body. NPs can increase the drug concentration in cancer cells and help overcoming the limitations of conventional chemotherapy, which lacks specificity and elicits severe toxic effects toward healthy cells [Ricci and Zong, 2006]. As already mentioned in the first chapter (paragraph 1.5), one known strategy to promote NPs accumulation into tumor cells and tissues relies on passive targeting, taking advantage of the EPR effect [Bae *et al*., 2011; Wang *et al*., 2005]. It must be underlined that size, surface-charge and hydrophobicity of NPs in which the drug is loaded strongly affect the drug bioavailability. In previous work we exploited the possibility to formulate PLGA NPs coated with hydrophilic poly (ethylene oxide) (PEO) moieties without a chemical reaction between the two polymers, therefore avoiding the presence of chemical reaction solvents and wastes [Mayol *et al*., 2015]. This helps overcoming the above mentioned tolerability/approval issues and representing an obvious advantage from a formulative point of view. Indeed, taking advantage of the amphiphilic properties of the blends, a hydrophilic coating of the NPs can spontaneously form, thus endowing NPs with a higher dimensional stability and the ability to take advantage of EPR effect. However, the effectiveness of the drug bioavailability can be probably enhanced when NPs uptake is optimized. In particular, NP internalization faces a size threshold limitation and, for this reason, in another study we have explored the nanoprecipitation technique with the aim to obtain NPs smaller in size and narrower in size distribution, and thus more suitable for cell uptake [Serri *et al*., 2017]. In this study we verified that an efficient uptake of NPs in malignant mesothelioma cell line (MSTO-211H) is strongly affected by size and polydispesity index of the developed nanodevices. Actually, uptake data indicate that a size reduction of only 20 nm leads to an evident increase in NP internalization. In this scenario, nanoprecipitation method was

found to improve the control of NP size and size distribution that, in turns, enhances cell internalization as showed in MSTO-211H. The uptake experiments clearly showed a cytoplasmic regionalization of the NPs and a rapid internalization increasing over the time. Actually, an optimization of NP uptake can significantly affect the biological efficacy of the platform/payload. Therefore, the identification of a clear subcellular localization may also indicate the feasibility of the formulation.

Even if EPR does enhance some drug accumulation at tumor target sites through the preferential extravasation of long-circulating devices, its efficacy is limited to a few percent of the administered dose and is associated to a possible lack of NPs cell internalization and/or to the undesired release of the loaded drugs before NPs uptake [Bae *et al*., 2011; Choi *et al*., 2010]. To overcome these issues, a significant research effort is devoted to endow NPs with biomolecular active targeting through suitable modifications of device surface. Functionalized NPs can recognize and bind tumor cells, and can also be internalized by receptor-mediated endocytosis [Byrne *et al*., 2008; Peer *et al*., 2007; Torchilin, 2006]. In this frame, the polysaccharide HA has attracted significant research attention for tumor-targeted delivery since it is biocompatible and non-immunogenic, and can specifically bind CD44 and RHAMM receptors, which are overexpressed in many key forms of cancer [Ossipov, 2010; Choi *et al*., 2010; Toole, 2004]. Several HA-based drug carriers have been studied for tumor targeting. Since HA has multiple functional groups available for chemical conjugation, several HA-drug conjugates have been developed as macromolecular prodrugs [Auzenne *et al*., 2007; Pouyani and Prestwich, 1994]. HA has also been chemically anchored onto manifold drug-loaded NPs; moreover, amphiphilic HA derivatives have been synthesized by chemically grafting several hydrophobic moieties so as to produce HA-based micellar systems for the release of hydrophobic chemotherapeutic drugs [Borzacchiello *et al*., 2007; Choi *et al*., 2011; Lee *et al*., 2009; Mayol *et al*., 2014; Yadav *et al*., 2010]. These HA modified macromolecular prodrugs and nano-sized drug carriers exhibited enhanced tumor targeting ability and therapeutic efficacy, compared to free anticancer agents [Nishiyama, 2007]. However, HA-modified macromolecular prodrugs and nano-sized drug carriers have been obtained by means of a chemical reaction, which is likely to alter HA biological properties. Besides, the preparation of HA NPs by a chemical reaction is still facing regulatory and technological challenges such as the absence of FDA approval and the limited upscalability of the process. It must be underlined that HA-coated solid lipid NPs which do not involve a chemical reaction have

been recently developed. Unfortunately, despite the promising results, the control of drug delivery kinetics is less than satisfactory and the delivery of the drug payload is most likely to occur before NPs reach the tumor site [Tran *et al*., 2014]. In this panorama, NPs produced by Layer-by-Layer (LbL) technology are an emerging class of self-assembled polymeric drug carrier that addresses several challenges in the delivery of small molecule therapeutics and imaging agents [Dreaden *et al*., 2014]. With this approach, an electrostatically driven self-assembly of oppositely charged polymers allows the functionalization of NP surface with HA. Different methods to directed the self-assembly of tumor targeting HA moieties with an easily upscalable method, could be a promising alternative to LbL thecnology.

4.2 Aim of the work

In this work, a novel and simple method based on single emulsion technique to produce NP has been proposed. This technique is based on the self-aggregation of polymers driven by a lipophilicity gradient between the oil and water phases of the emulsion, thus allowing the simultaneous NP formation and coating with HA in a single step, differently from LbL. Here IRIN-loaded biodegradable PLGA NPs have been formulated and coated with non-chemically modified HA for tumor targeting toward CD44-overexpressing cell lines. IRIN is a topoisomerase I inhibitor which causes DNA strand breakage and widely employed in chemotherapy, also in combination with Doxo [Biondi *et al*., 2013a; Biondi *et al*., 2013b]. Besides topotecan, IRIN is the only topoisomerase I-targeted anticancer drug and its efficacy is strongly limited since a chemical equilibrium between the lactone form and the ring-opened form exists in solution [Teicher, 2008]. The ring-opened carboxylate form is 90% less effective than the lactone form and its cell membrane crossing is hampered [Hertzberg *et al*., 1989]. Therefore, the administration of IRIN suspended within a nanodevice able to cross the cell membrane may be promising to overcome these issues. Furthermore, an active targeting to tumor cells and tissues is helpful to reduce the side effects associated to the IRIN interaction with non-target tissues and organs. The stability of the formulated IRIN-loaded NPs was evaluated by measuring their size over time and *in vitro* drug release studies have been taken to evaluate the capacity of the produced NPs to control and prolong IRIN release. Differential scanning calorimetry (DSC), potential analyses and ELISA tests were employed to investigate polymer assembly in NP

formulations. Finally, *in vitro* biological test on both cells overexpressing and not overexpressing CD44 receptor, respectively human breast carcinoma cells (HS578T) and L-929 cells, were performed to assess NP toxicity and targeting ability to CD44 receptor.

4.3 Materials and methods

4.3.1 *Materials*

HA with a weight-average molecular weight (MW) of 850,000 Da was provided by Novozymes Biopharma (Denmark). Equimolar PLGA (RG504H, MW 12,000 Da) was purchased from Boheringer Ingelheim (Germany). Poloxamers (PEOa-PPOb-PEOa) F127 (a = 100 and b = 65) and F68 (a = 76 and b = 29), obtained from Lutrol (Basf, Germany), were used. IRIN, acetone and dimethyl sulfoxide (DMSO) were obtained from Sigma–Aldrich (USA). Phosphate buffer saline (PBS) tablets without calcium and magnesium were obtained from MP Biomedicals Inc. (France).

4.3.2 *NPs preparation*

Blank and IRIN-loaded NPs were prepared by a single emulsion-solvent evaporation technique (oil in water). Formulations with different amounts of HA, PLGA and poloxamers are summarized in table 4.1.

Acronym	**OIL PHASE (O)**			**WATER PHASE (W_1)**		
	PLGA	F68	F127	HA	F68	F127
P	2	-	-	-	0.05	0.05
PP	1	0.5	0.5	-	0.05	0.05
PPHA30	1	0.5	0.5	2	0.05	0.05
PPHA60	1	1.5	1.5	4	0.05	0.05

Table 4.1: composition and acronyms of the different NP formulations; all concentrations are expressed as % (w/w)

Briefly, 1 mL of PLGA solutions in acetone alone or blended with polox (F127 and F68 1:1 w/w) were prepared with a PLGA-polox weight ratio fixed at 1:1 and an overall polymer concentration of 2% w/v. The organic phase was emulsified by sonication using a Branson Ultrasonic Cleaners (Model 3510) for 5 min with 40 mL of water phase, possibly containing different HA and polox amounts, as schematically represented in figure 4.1. More in detail, for HA containing NPs, two water phases were prepared (W_1 and W_2) and consecutively added; W_1 phase contained different amounts of HA and polox in 15 mL, were emulsified with oil phase by sonication then W_2 phase containing pure bidistilled water (25 mL) was added, to enhance the separation of the nanodroplets. The resulting emulsion was evaporated at 35 °C for 35 minutes by means of a rotary evaporator (Laborota 4010 digital, HEIDOLPH). NPs were finally separated from supernatant by centrifugation at 13000 rpm for 60 minutes (Hettich Zentrifugen, Germany) and stored at -80 °C. As regards to the IRIN-loaded NPs, IRIN (10 mg) were added in the oil phase at a polymer concentration of 2%.

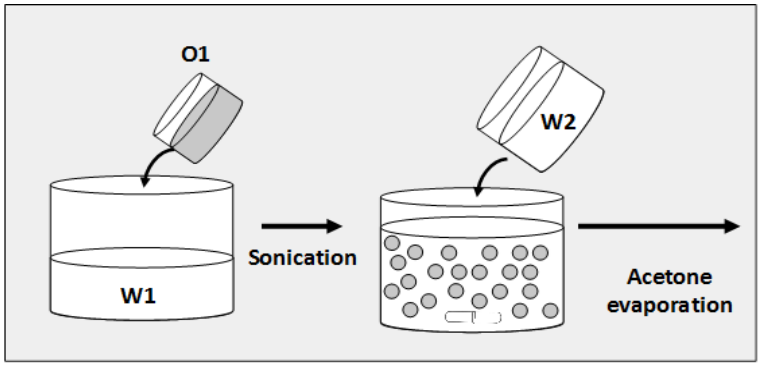

Figure 4.1: schematic representation of NPs preparation

4.3.3 *NP characterization: morphology, mean size, size distribution and ζ potential*

NPs morphology was investigated through a transmission electron microscope (TEM, FEI Tecnai G12 Spirit Twin) with emission source LaB6 (120 kV, spotsize 1) using 400 mesh carbon-coated copper grids at room temperature. The carbon-coated copper grid was immersed in ultradiluted NP suspension and, after the drying phase, the grid was placed on a rod holder for the TEM characterization. Three grids per NP suspension were prepared and a minimum of four micrographs *per* grid were acquired. Surface topography and phase

signals of NPs were recorded by atomic force microscopy (AFM, NanoWizard II-AFM, standalone top View Optics, JPK Instruments, Germany) by placing one drop of NP suspension (1 mg/mL) on a freshly cleaved mica surface. For AFM observations, the suspension was air-dried at room temperature. Particle size and ζ potentials of NPs were determined *via* dynamic light scattering (DLS) measurements with a Zetasizer Nano (Malvern Instruments, Malvern, UK). For particle size measurements, NPs were suspended in ultrapure water. To study the agglomeration dynamics of NPs in bidistilled water at 4 °C, NPs size measurements were taken for ten days. Furthermore, ζ potential assay was performed at different pH values (from 7.4 to 2) at room temperature. Results were averaged on at least five measurements.

4.3.4 *Thermal analyses*

Aiming to study the interactions between the different polymers in NP formulation, thermoanalytical tests were carried out on PLGA and poloxamer powders, along with freeze-dried P, PP and PPHA NPs, to study the interactions between the different polymers in NP formulation. The heat involved in the phase transitions of polymers was determined by a differential scanning calorimeter (DSC; DSC Q20, TA Instruments, U.S.A.), calibrated with a pure indium standard. The samples were placed in aluminum pans and underwent a double scan; the first was carried out from 10 to 80 °C to eliminate the thermal history of the samples and the second one from -60 °C to 80 °C. Heating rate was set at 5 °C/min. Measurements were carried out under an inert nitrogen atmosphere, purged at a flow rate of 50.0 mL/min. The heat evolved during polymer crystallization and fusion (W/g) was calculated from the recorded DSC thermograms by integrating the exothermic/endothermic peaks, while the glass transition temperature (T_g) was obtained from thermogram inflection point.

4.3.5 *Drug entrapment efficiency*

Drug entrapment efficiency (EE) was calculated by dissolving freeze-dried NPs (1 mg) in 1 mL of DMSO. The resulting solution was sonicated for 1 hour in a water bath at 59 kHz, 100% power. IRIN content was quantified by spectrophotometric assay (UV-1800, UV-VIS spectrophotometer, Shimadzu, Japan) at 370 nm. The linearity of the response was

verified on IRIN solutions in DMSO (0.04–10 μg/mL concentration range; r^2>0.99). Entrapped IRIN percentage was calculated as

$$EE = 100X \frac{D_E}{D_T}$$

where D_E is the amount of entrapped drug in the NPs and D_T is the total amount of the drug used to prepare the NPs. Results were averaged on at least three independent batches.

4.3.6 *In vitro release kinetic of IRIN*

For release experiments, NPs were suspended in 10 mL of release medium (PBS at pH 7.4) and incubated at 37 °C in an orbital incubator (SI50, Stuart R, UK) operating at 100 rpm. At scheduled time intervals, 1 mL aliquots were withdrawn and replaced with the same volume of fresh medium. The aliquots were ultracentrifuged and the supernatant was analyzed through spectrophotometric analysis (λ=364.5 nm) to quantify IRIN content. The instrument response was linear over the concentration range 0.1–50 μg/mL (r^2>0.99). The experiments were run in triplicate.

4.3.7 *Quantification of HA*

The amounts of HA incorporated in/on the NPs were quantified as reported elsewhere [Mondalek *et al*., 2010]. Briefly, HA was determined after conjugation with a specific enzyme provided by a HA ELISA kit (Biorbyt LLC, USA), followed by spectrophotometric analysis at 450 nm after each washing step. More in detail, the amount of HA incorporated in the NP was determined by subtracting, from the initial mass of HA, the amount lost in the three NP washes. The linearity of the kit response was assessed in the 0–250 ng/mL HA concentration range (r^2 > 0.96).

4.3.8 *Cell culture studies*

L929 cells originating from Mouse C34/An connective tissue were obtained from the European Collection of cell cultures (Sigma-Aldrich, USA) and were used at a passage 15-

23. CD44-overexpressing human breast carcinoma HS578T cells, kindly gifted by Dr. Olga Zeni (IREA-CNR), were used. The cells were grown at 37 °C and 5% CO_2 in T-75 cell culture flask (Falcon, Italy), using DMEM (Hyclone, USA) cell culture medium supplemented with 10% fetal bovine serum and antibiotics (penicillin G sodium 100 U/mL, streptomycin 100 µg/mL). In the case of HS578T cells, the culture medium was enriched with 10 µl/mL bovine insulin. When confluent growth was reached, the cells were detached with 0.25% trypsin-EDTA solution and washed twice with fresh PBS. The resulting cell suspensions were centrifuged for 5 min at 10000 rpm (BRK55/10 Centrifuge, Centurion Scientific Ltd, UK). Finally, the supernatant was separated and the cells resuspended in fresh culture medium. Viable cells were counted using the TC20 automated cell counter (Biorad, USA).

4.3.9 *In vitro cytotoxicity*

L929 and HS578T cells were seeded in 48-well plates at a density of 5 x 10^3 cells *per* well in the presence of 200 µL of cell culture medium. Five wells were used as blank control. To determine the 50% inhibitory concentration (IC50) of the drug, the cells were exposed at IRIN solutions at concentrations ranging from 10 to 230 µM. In particular, after 24 hours incubation at 37 °C in 5% CO_2 atmosphere, the incubation medium was removed and 200 µL of IRIN solution at the same concentration was added. Afterwards, the cells were incubated for 48 hours and their viability assessed by alamar blue test. The biocompatibility of void PP and PPHA30 NPs as well as the bio-efficacy of IRIN loaded PP and PPHA30 NPs were estimated using an amount of NPs equivalent to that used to load an IRIN dose correspondent to IRIN IC50. Both L929 and HS578T cells were incubated with the tested NPs for 48 hours, and their viability was assessed by alamar blue test. HS578T cells, after the test, were rinsed and an amount of NPs equivalent to IRIN IC50 was added; the cells were then incubated for further 72 hours and their viability assessed by alamar blue test.

Alamar blue test was performed by adding the alamar blue (AB) reagent to the samples (at 10% v/v with respect to the medium) and incubated at 37 °C for 4 hours. The absorbance of the samples was measured using a spectrophotometer plate reader (Multilabel Counter, 1420 Victor, Perkin Elmer) at 570 nm and 600 nm. AB is an indicator dye that incorporates an oxidation-reduction indicator whose color changes in response to the chemical

reduction in growth medium resulting from cell viability. Data are calculated as the percentage difference between treated and control samples with the following formula:

$$\%\,reduction = \frac{(O_2 \times A_1) - (O_1 \times A_2)}{(O_2 \times P_1) - (O_1 \times P_2)} \times 100$$

where O_1 is the molar extinction coefficient (E) of oxidized AB at 570 nm; O_2 is the E of oxidized AB at 600 nm; A_1 is the absorbance of test wells at 570 nm; A_2 is the absorbance of test wells at 600 nm; P_1 is the absorbance of positive growth control well at 570 nm; P_2 is the absorbance of positive growth control well at 600 nm.

4.3.10 *Statistical analyses*

In all cases, quantitative data are reported as mean value ± standard deviation (SD). The statistical significance of the results has been assessed by one-way analysis of variance ANOVA. An p value < 0.05 was considered to identify statistically different groups.

4.4 Results and discussion

4.4.1 *NPs preparation and characterization*

In recent years, many 'smart' nanosystems for targeted cancer therapy have been developed, in order to increase the safety of use and the effectiveness of the loaded chemotherapy drugs [Cho *et al*., 2008; Brigger *et al*., 2002; Huang *et al.*, 2013; Ding *et al*., 2012]. Furthermore, it is also desirable to endow the produced devices with targeting ability toward cancer cells. A convenient way of developing such NPs can exploit their spontaneous assembly in emulsion, driven by a lipophicity gradient between the core and the external surface of the NPs, which forms core-shell NPs in aqueous environment. Here, we have developed a one-step procedure to obtain amphiphilic PLGA-based NPs decorated with an external HA corona, in which hydrophilic HA was combined to hydrophobic PLGA *via* amphiphilic poloxamer bridging. In particular, HA is the hydrophilic domain of NPs and therefore would arrange on the outer shell of the devices, while hydrophobic PLGA would form the core of the NPs, as schematically represented in figure 4.2. These

nanosystems have been engineered to combine device stability and targeting ability to CD44-overexpressing cancer cells.

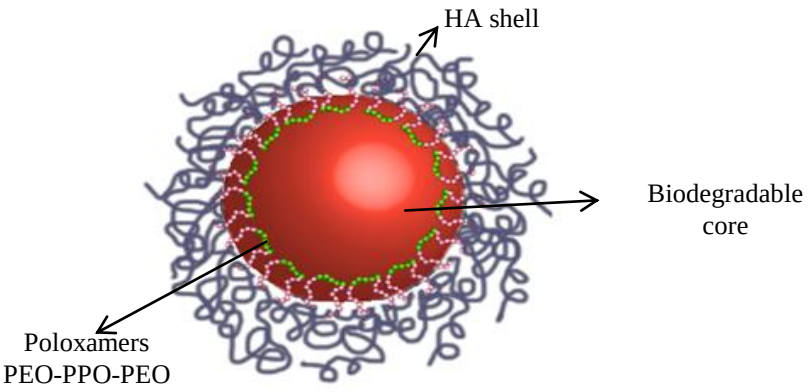

Figure 4.2: schematic representation of the NPs characterized by HA shell, biodegradable PLGA-core and poloxamers that act as bridge between PLGA and HA

HA-decorated NPs have been formulated by dissolving PLGA and poloxamers in acetone and by emulsifying the obtained solution in an aqueous phase containing HA and, in case, poloxamers. The overall polymer concentration (PLGA and poloxamers) in the oil phase has been fixed at 2% w/v, while different amounts of HA and poloxamers in the external aqueous phase have been added. HA is known to be a strong polyanion at physiological pH and, therefore, the robustness of HA self-assembly on NP surface can be monitored by ζ potential analyses.

Results of size and ζ potential measurements are summarized in table 4.2 and shown that NPs size is progressively increasing with increasing HA concentration in the external aqueous phase, while ζ potential values significantly decrease from ~ -27mV of PP to ~ -57 mV for PPHA60.

Forms	$PDI_{t=0}$	$d(nm)_{t=0}$	$d(nm)_{t=10\ d}$	ζ potential $(mV)_{t=0}$	ζ potential $(mV)_{t=10\ d}$
P	0.156 ± 0.01	154 ± 2.0	190 ± 10	-15.0 ± 0.8	-26.1 ± 1.7
PP	0.082 ± 0.01	106 ± 1.1	110 ± 10	-25.5 ± 1.2	-29.1 ± 1.8
PPHA30	0.884 ± 0.01	184 ± 4.3	161 ± 20	-49.7 ± 1.4	-49.3 ± 0.9
PPHA60	1.230 ± 0.01	306 ± 14	258 ± 14	-56.2 ± 1.0	-57.0 ± 2.1

Table 4.2: NP size and zeta potential at time zero and after 10 days in bidistilled water at 4°C. The mean values and standard deviations were calculated from at last three independent experiments

These results indicate the formation of an external HA shell, driven by a lipophilicity gradient between the oil and water phases of the emulsion used to produce the NPs. A ζ potential value equal to -50 mV is more negative than the one observed in the case of NPs coated by HA, prepared through LbL procedure, thus suggesting a more uniform and efficacious cover of the polysaccharide on NP surface with the novel production method presented in this work [Dreaden *et al*., 2014]. A negative zeta potential, which is due to the ionization of the carboxyl groups of HA, can prevent NP aggregation and binding to plasma proteins, therefore promoting their stability and prolonged circulation *in vivo*. Furthermore, the ζ potential of NPs was found to be increasing with decreasing pH and, in particular, a quasi-neutral surface charge was found in the case of PPHA NPs, at a pH close to HA pK_a (pH ~ 2), due to the protonation of the carboxyl groups on HA under decreasing pH (figure 4.3) [Huang *et al*., 2014]. Differently, HA-free NPs neutralize their superficial charge at the pK_a of PLGA (pH ~ 4) [Yoo and Mitragotri, 2010].

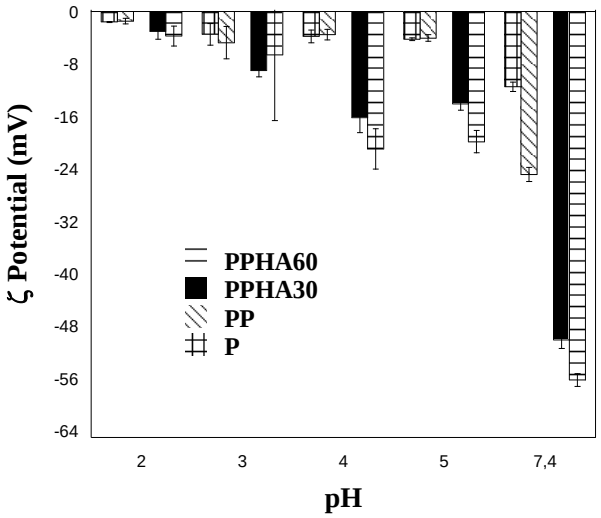

Figure 4.3: zeta potential values of different NP formulations as a function of pH. The mean values and standard deviations were calculated from at last three independent experiments

The presence of 0.2 % w/v of poloxamers in the external aqueous phase allows to obtain NPs with a lower mean diameter, without affecting the zeta potential value. This can be reasonably ascribed to the 'bridging' action of poloxamers between the inner hydrophobic PLGA and the outer hydrophilic HA domains. Indeed, it can be easily hypothesized that the surfactant properties of poloxamers help creating a less steep gradient of lipophilicity, which encourages the interaction and arrangement of HA chains on the surface of PLGA NPs.

In the clinical administration of NPs, the phenomenon of particle aggregation represents, of course, a crucial issue, affecting the drug release profile and possibly increasing the risk of vessel occlusion. For these reasons, the electrostatic and/or steric stabilization of NPs is an important aspect to be considered. In table 4.2, the results of NP dimensional stability experiments are reported. These findings point that a tumor-targeting HA corona enhances NP dimensional stability over time thanks to the higher electrostatic repulsion of PPHA NPs which, in turn, depends on the lower ζ potential values, i.e. a higher density of negative charges at NP surface. Moreover, the presence of flexible HA chains on NP surface may help to improve NP steric stability and hydration.

Selected TEM micrographs of P, PP and PPHA NPs are reported in figures 4.4, 4.5 and 4.6, respectively.

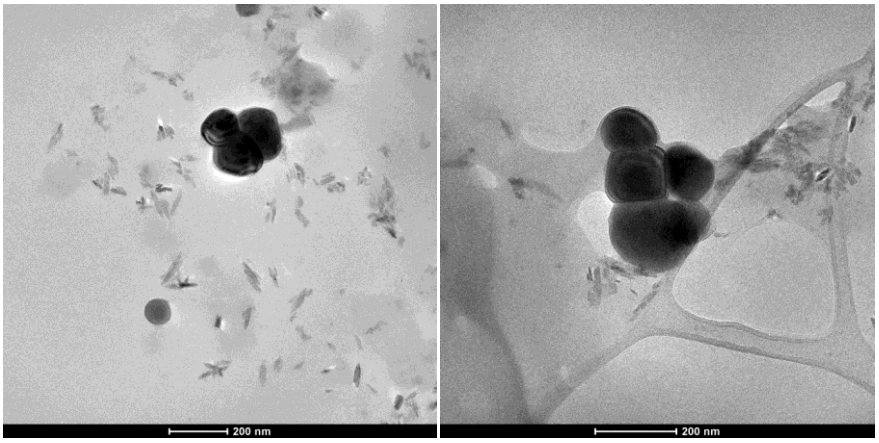

Figure 4.4: selected TEM micrographs of P NPs

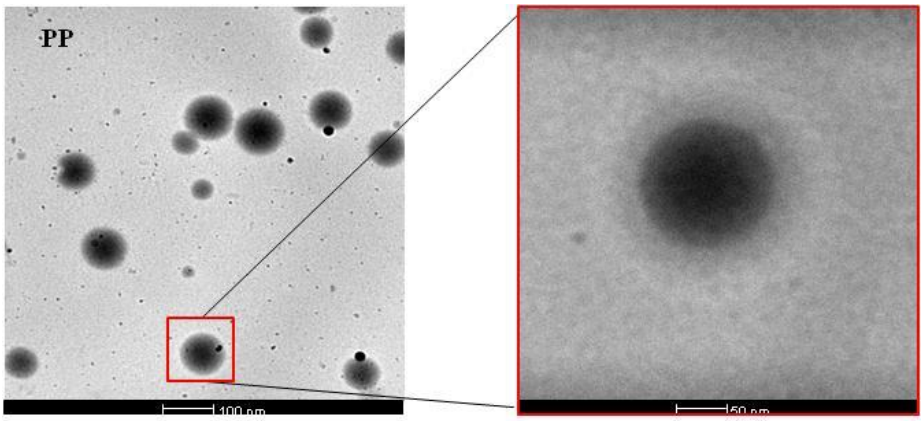

Figure 4.5: selected TEM micrographs of PP NPs

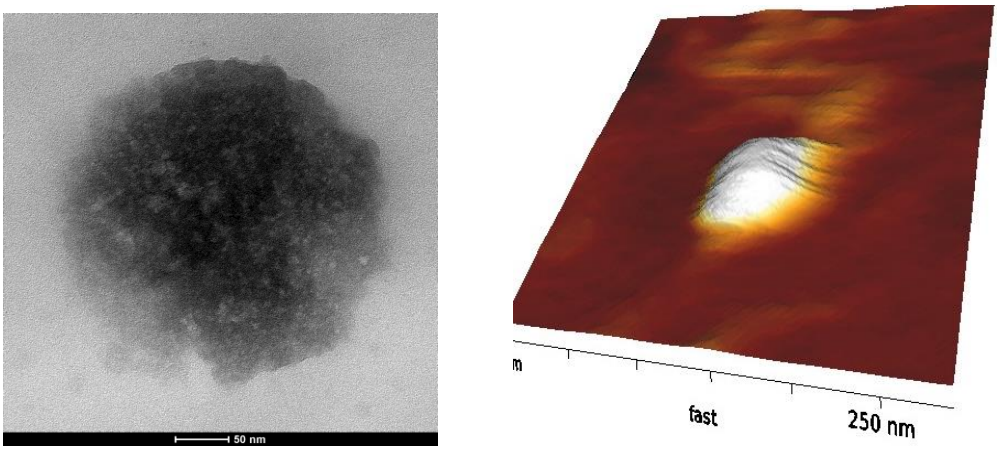

Figure 4.6: selected TEM (left) and AFM (right) micrographs PPHA NPs

The images revealed discrete, spherical particles for all NP formulations. However, it must be underlined that PPHA NPs have a completely different appearance compared to P and PP NPs. Indeed, in the case of HA-containing NPs, there is, clearly, a sort of surface discontinuity, which cannot be noticed in both P and PP which, on the contrary, have a very smooth surface. These findings further corroborate the hypotheses of superficial HA arrangement/deposition. The shape and outer HA corona was also visible in AFM images (figure 4.6, right).

The PP2HA30 formulation, hereafter named PPHA, has been selected for all the experiments reported in the following since it is optimized in terms of small size and dimensional stability.

4.4.2 *Theramal analyses*

The results of thermal analyses are shown in figure 4.7 and summarized in table 4.3.

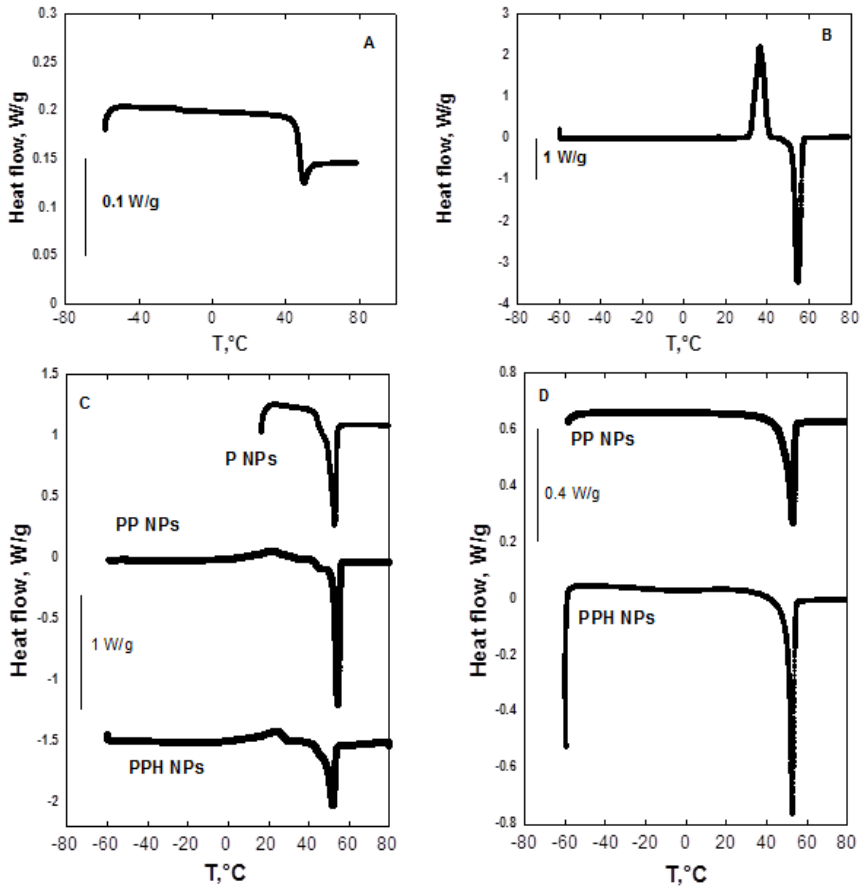

Figure 4.7: DSC thermograms of PLGA powder (A) and poloxamer powder (B); P, PP and PPHA NPs first scan (C); P, PP and PPHA NPs, second scan (D). Results were obtained from at last three independent experiments

	T_g, °C	T_f, °C	ΔH_f, J/g	T_c, °C	ΔH_c, J/g
PLGA powder	47.7±0.1	-	-	-	-
Poloxamers	-	54.2±0.1	140±3	36.3±0.2	127±3
P NPs	44.0±0.5	-	-	-	-
PP NPs	43.3±0.3	54.3±0.2	28.1±9.4	27.8±4.8	23.3±9.2
PPHA NPs	43.6±0.8	51.7±0.2	37.3±4.2	26.8±3.2	28.6±15.1

Table 4.3: results of thermal analyses. The mean values and standard deviations were calculated from at last three independent experiments

As it can be seen, the PLGA thermogram shows a glass T_g around 48 °C while, as for the poloxamers, crystallization and melting are shown at about 36 °C and 54 °C, respectively. As for HA powder, DSC traces showed no thermodynamic transition in the temperature

range here examined (data not shown). In the case of P NPs, the T_g is lower than that of the powder of PLGA (~ 44 °C instead of ~ 48 °C), therefore pointing at a plasticizing action of the poloxamers used as surfactants in the aqueous phase of the emulsion. The T_g values were found very similar also when the poloxamers have been blended in the organic phase of the emulsion (*i.e.* for PP and PPHA NPs), therefore indicating the same plasticizing effect of poloxamers also when they are in the bulk of NPs. Furthermore, as depicted in figure 4.7, when analyzing PP NPs, a broadening of poloxamer crystallization peak, along with a decrease of their crystallization heat (ΔH_c) and temperature (T_c) has been observed. This suggests an amorphous interaction between the polymeric chains of PLGA and poloxamers when they are solubilized into the organic phase of the emulsion used to produce the NPs. In actual fact, as we have previously hypothesized, due to the amphiphilic nature of poloxamers, the hydrophobic PO segments preferentially self-orient towards the PLGA NP core, while the hydrophilic EO segments direct towards the aqueous phase [Mayol *et al.*, 2015]. In the presence of HA in NP formulation, melting and crystallization do not significantly change compared to PP NPs, demonstrating that poloxamer crystallization is not further hampered. Moreover, it must be underlined that, in the first heating ramp, the T_g of PLGA is observable in NPs while, in the second scan (figure 4.7 D), after poloxamer melting, PLGA T_g and poloxamer crystallization peak are no longer visible. This may support the hypothesis that, in PPHA NPs, PLGA and HA do not interact since PLGA constitute NP bulk while HA is superficially exposed with the poloxamers acting as a bridge between the PLGA and HA. After poloxamer melting, this configuration is lost and a polymeric blend, with thermal properties different from the ones of the starting polymers, is formed. This hypothesis of polymer self-assembly into the NPs is also corroborated by the previously shown morphologic and ζ potential results.

4.4.3 *IRIN encapsulation efficiency, NPs yield and HA quantification*

PPHA drug entrapment efficiency was found to be 61.2 % (w/w), while for P NP it was 58.8 % (w/w), as reported in table 4.4. Results of ELISA assay showed a loss of 34.3% w/w of HA in the supernatant (data not shown).

Forms	Polymer:drug ratio	Drug encapsulation efficiency (%)	NP yield (%)
P	10.5 ± 0.4	62.6 ± 2.5	65.9 ± 4.2
PP	8.2 ± 0.5	64.9 ± 3.3	53.0 ± 7.8
PPHA30	10.0 ± 0.5	62.7 ± 3.4	48.0 ± 6.8
PPHA60	9.7 ± 0.3	64.1 ± 1.8	38.9 ± 10.0

Table 4.4: polymer-to-drug ratio, drug encapsulation efficiency and NP yield. The mean values and standard deviations were calculated from at last three independent experiments

4.4.4 *In vitro release kinetic of IRIN*

Experimental *in vitro* release profiles of IRIN from P and PPHA NPs are reported in figure 4.8.

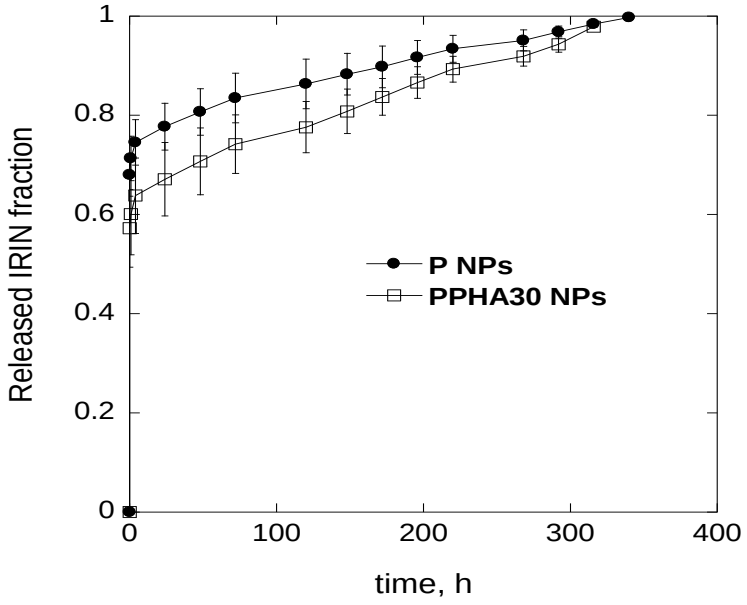

Figure 4.8: *in vitro* IRIN release profiles from P and PPHA30 NPs

The results demonstrated that IRIN is completely released in less than two weeks, with > 85% of the loaded drug eluted within 7 days. In both formulations, a strong burst is evidenced. It can also be seen that IRIN release is slightly slower in the case of HA-containing NPs. This can be probably ascribed to a slightly higher affinity of IRIN for the amphiphilic HA-containing NPs compared to simple P NPs.

4.4.5 *In vitro cytotoxicity studies*

HS578T and L929 cell lines were employed to investigate the cytotoxicity of PP NP and PPHA30 NPs using alamar blue assay. The IRIN IC50 for L929 cells was found to be 51.7 µM, while the IRIN IC50 for HS578T cells was 100.5 µM. The NP concentrations used in the experiments were chosen as those able to load IRIN at a dose equivalent to its IC50. Results from cell culture studies related to *in vitro* bioefficacy of IRIN-loaded PPHA30 NPs and PP NPs are presented in figure 4.9.

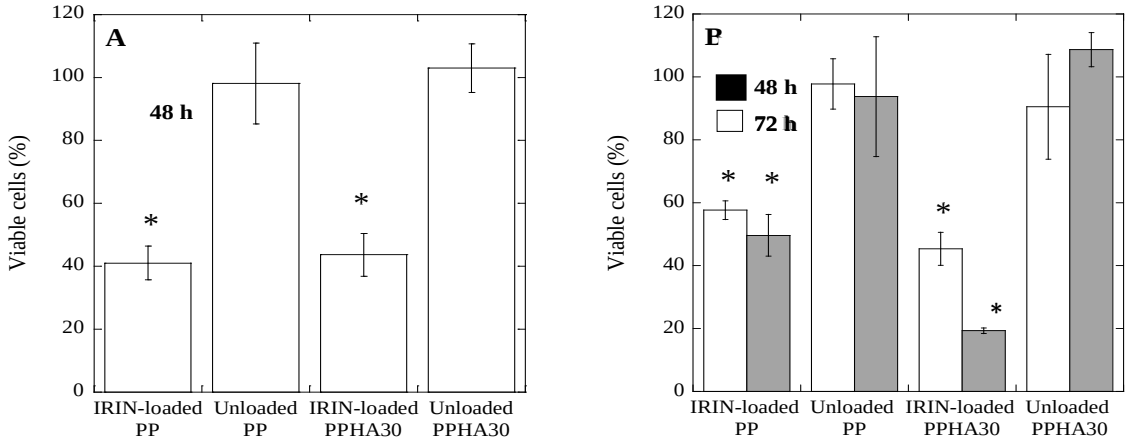

Figure 4.9: results of cytotoxicity assay. Percentage of viable L929 cells after 48 hours incubation (A) and of HS578T cells after 48 and 72 hours of incubation (B). Cell viability was calculated with respect to the non-treated control cells. *P < 0.05 vs the respective unloaded NP

As to L929 cells (figure 4.9 A) it is possible to observe unloaded NPs are not toxic. Indeed, the percentage of viability, compared to the control, for PP and PPHA30 is almost 100%. Differently, for both the IRIN-loaded particles, the percentage of viability is about 40%. This result indicates that PP and PPHA30 particles are able to inhibit the cells growth and that HA coating does not influence this ability. Also in the case of HS578T cells (figure 4.9 B), the unloaded NPs are not cytotoxic. Interestingly, in the case of IRIN-loaded NPs, the behaviors of PPHA30 and PP NPs are different both at 48 and, in a significant way, at 72 hours. In particular, the percentage of cell viability is about 60% and 45% after 48 hours for PP and PPHA30 NPs, respectively, therefore indicating that HA-coated NPs can inhibit cellular growth more effectively compared to PP NPs. A more evident result was obtained

at 72 hours, being the percentage of viable cells about 20% and 50% for PPHA30 and PP NPs, respectively. Taken all together, these results suggest that PPHA30 NPs can deliver more drugs into cancer cells and resulting in a stronger cell killing effect, probably due to the HA receptor-mediated endocytosis and therefore a better NP cellular uptake in $CD44^+$ cells.

4.5 Conclusions

In this study, a novel strategy to directed the self-assembly of tumor targeting HA moieties on IRIN-loaded PLGA NPs is proposed. This novel NP production method is easily up-scalable, being a single step process. The NPs showed a spherical shape and a size ranging from 100 to 306 nm. Thermal analyses revealed that in the produced NP formulations PLGA, poloxamer and HA act as independent entities and not as a polymeric blend. These results, together with the results of ζ potential analyses, suggest a polymer self-organization driven by a gradient of lipophilicity between the oil and water phases of the emulsion used to prepare the NPs. The HA cover enhances NP size stability over time due to an enhanced electrostatic repulsion of HA coated NPs and also to a higher degree of hydration and/or to a steric stability caused by the presence of flexible HA chains on NP surface. The amphiphilic nature of these NPs, characterized by an inner hydrophobic core and a hydrophilic shell, allowed to obtain a drug encapsulation efficiency of 61.2% w/w. The *in vitro* release profiles showed a sustained IRIN release up to 7-13 days. Cell cytotoxicity tests showed that PPHA30 NPs can deliver more drugs into cancer cells resulting in a stronger cell killing effect on CD44-overexpressing cells, probably due a positive effect of HA on NP internalization.

Taken all together, these results designate PPHA NPs as promising candidates for targeted drug delivery to solid tumors for a number of significant cancer types.

REFERENCES

Athanasiou K.A., Niederauer G.G., Agrawal C.M. (1996). Sterilization, toxicity, biocompatibility and clinical applications of polylactic acid/polyglycolic acid copolymers. *Biomat*, 17:93-102.

Auzenne E, Ghosh S.C., Khodadadian M, Rivera B, Farquhar D, Price R.E. (2007). Hyaluronic acid–paclitaxel: Antitumor efficacy against CD44(+) humanovarian carcinoma xenografts. *Neoplasia*, 9:479–486.

Bae K.H., Chung H.J., Park T.G. (2011). Nanomaterials for cancer therapy and imaging. *Mol Cel*, 31:295-302.

Biondi M, Fusco S, Lewis A.L., Netti P.A. (2013a) Investigation of the mechanisms governing doxorubicin and irinotecan release from drug-eluting beads: mathematical modeling and experimental verification. *J Mater Sci Mater Med*, 24:2359-2370.

Biondi M, Guarnieri D, Yu H, Belli V, Netti P.A. (2013b) Sub-100 nm biodegradable nanoparticles: in vitro release features and toxicity testing in 2D and 3D cell cultures. *Nanotec*, 24:045101.

Borzacchiello A, Mayol L, Ramires P.A., Pastorello A, Di Bartolo C, Ambrosio L, Milella E (2007). Structural and rheological characterization of hyaluronic acid-based scaffolds for adipose tissue engineering. *Biomat*, 28:4399-4408.

Brigger I, Dubernet C, Couvreur P (2002). Nanoparticles in cancer therapy and diagnosis. *Adv Drug Del Rev*, 54:631-651.

Byrne J.D., Betancourt T, Brannon-Peppas L (2008). Active targeting schemes for nanoparticle systems in cancer therapeutics. *Adv Drug Deliv Rev*, 60:1615-1626.

Cho K, Wang X, Nie S, Chen Z.G., Shin D.M. (2008). Therapeutic nanoparticles for drug delivery in cancer. *Clin Canc Res*, 14:1310-1316.

Choi K.Y., Chung H, Min K.H., Yoon H.Y., Kim K, Park J.H., Kwon I.C., Jeong S.Y. (2010). Self-assembled hyaluronic acid nanoparticles for active tumor targeting. *Biomat*, 31:106-114.

Choi K.Y., Min K.H., Yoon H.Y., Kim K, Park J.H., Kwon I.C., Choi K, Jeong S.Y. (2011). PEGylation of hyaluronic acid nanoparticles improves tumor targetability in vivo. *Biomat*, 32:1880-1889.

Ding H, Wang X.J., Zhang S, Liu X.L. (2012). Applications of polymeric micelles with tumor targeted in chemotherapy. *J Nanoparticle Res*, 14:1254-1261.

Dreaden E.C., Morton S.W., Shopsowitz K.E., Choi J.H., Deng Z.J., Cho N.J. (2014). Hammond PT. Bimodal tumor-targeting from microenvironment responsive hyaluronan layer-by-layer (LbL) nanoparticles. *ACS Nano*, 8:8374-8382.

Hertzberg R.P., Caranfa M.J., Holden K.G., Jakas D.R., Gallagher G, Mattern M.R., Mong S.M., Bartus J.O., Johnson R.K., Kingsbury W.D. (1989). Modification of the hydroxyl lactone ring of camptothecin: Inhibition of mammalian topoisomerase I and biological activity. *J Med Chem*, 32:715–720.

Huang S, Shao K, Liu Y, Kuang Y, Li J, An S, Guo Y, Ma H, Jiang C (2013). Tumor-targeting and microenvironment-responsive smart nanoparticles for combination therapy of antiangiogenesis and apoptosis. *ACS Nano*, 7:2860-2871.

Huang J, Zhang H, Yu Y, Chen Y, Wang D, Zhang G, Zhou G, Liu J, Sun Z, Sun D, Lu Y, Zhong Y (2014). Biodegradable self-assembled nanoparticles of poly (D,L-lactide-co-glycolide)/hyaluronic acid block copolymers for target delivery of docetaxel to breast cancer. *Biomat*, 35:550-566.

Jain R.A. (2000). The manufacturing techniques of various drug loaded biodegradable poly(lactide-co- glycolide) (PLGA) devices. *Biomat*, 21:2475-2490.

Jalil R, Nixon J.R. (1990). Biodegradable poly(lactic acid) and poly(lactide-co-glycolide) microcapsules: problems associated with preparative techniques and release properties. *J Microencapsulation*, 7:297-325.

Lee H, Ahn C.H., Park T.G. (2009). Poly[lactic-co-(glycolic acid)]-grafted hyaluronic acid copolymer micelle nanoparticles for target-specific delivery of doxorubicin. *Macrom Bios*, 9:336-342.

Mayol L, Biondi M, Russo L, Malle B.M., Schwach-Abdellaoui K, Borzacchiello A (2014). Amphiphilic hyaluronic acid derivatives towars the design of micelles for the sustained delivery of hydrophobic drugs. *Carb Pol*, 102:110-116.

Mayol L, Serri C, Menale C, Crispi S, Piccolo M.T., Mita L, Giarra S, Forte M, Saija A, Biondi M, Mita D.G. (2015). Curcumin loaded PLGA-poloxamer blend nanoparticles induce cell cycle arrest in mesothelioma cells. Eur J Pharm Biopharm, 93:37-45.

Mondalek F.G., Ashley R, Roth C.C., Kibar Y, Shakir N, Ihnat M.A., Fung K, Grady B.P., Kropp B.P., Lin H (2010). Enhanced angiogenesis of modified porcine small intestinal submucosa with hyaluronic acid-poly(lactide-co-glycolide) nanoparticles: from fabrication to preclinical validation. *J Biomed Mater Res*, 94:712-719.

Nishiyama N (2007). Nanomedicine: Nanocarriers shape up for long life. *Nature Nanothec*, 2:203-204.

Ossipov D.A. (2010). Nanostructured hyaluronic acid-based materials for active delivery to cancer. *Expert Opin Drug Deliv*, 7:681-703.

Peer D, Karp J.M., Hong S, Farokhzad O.C., Margalit R, Langer R (2007). Nanocarriers as an emerging platform for cancer therapy. *Nature Nanotec*, 2:751-760.

Pouyani T, Prestwich G.D. (1994). Functionalized derivatives of hyaluronic acid oligosaccharides: Drug carriers and novel biomaterials. *Bioconjugate Chem*, 5:339-347.

Ricci M.S., Zong W.X. (2006). Chemotherapeutic approaches for targeting cell death pathways. *Oncologist*, 11:342-357.

Serri C, Argirò M, Piras L, Mita D.G., Saija A, Mita L, Forte M, Giarra S, Biondi M, Crispi S, Mayol L (2017). Nano-precipitated curcumin loaded particles: effect of carrier size and drug complexation with (2-hydroxypropyl)-b-cyclodextrin on their biological performances. *Int J Pharm*, 520:21-28.

Teicher, B.A. (2008). Next generation topoisomerase I inhibitors: Rationale and biomarker strategies. *Biochem Pharm*, 75:1262–1271.

Toole B.P. (2004). Hyaluronan: From extracellular glue to pericellular cue. *Nature Rev Canc*, 4:528-539.

Torchilin V.P. (2006). Multifunctional nanocarriers. *Adv Drug Del Rev*, 58:1532-1555.

Tran T.H., Choi J.Y., Ramasamy T, Truong D.H., Nguyen C.N., Choi H.G., Yong C.S., Kim J.O. (2014). Hyaluronic acid-coated lipid nanoparticles for targeted delivery of vorinostat to CD44 overexpressing cancer cells. *Carbo Pol*, 114:407-415.

Wang J, Mongayt D, Torchilin V.P. (2005). Polymeric micelles for delivery of poorly soluble drugs: Preparation and anticancer activity in vitro of paclitaxel incorporated into mixed micelles based on poly(ethylene glycol)-lipid conjugate and positively charged lipids. *J of Drug targ*, 13:73-80.

Yadav A.K., Agarwal A, Rai G, Mishra P, Jain S, Mishra A.K. (2010). Development and characterization of hyaluronic acid decorated PLGA nanoparticles for delivery of 5-fluorouracil. *Drug Del*, 17:561-572.

Yoo J.W., Mitragotri S (2010). Polymer particles that switch shape in response to a stimulus. *Proc Natl Acad Sci USA*; 107:11205-11210.

CHAPTER 5

In vitro evaluation of tumor targeting ability of enoxaparin-coated self-emulsifying drug delivery systems (SEDDS) for parenteral administration

ABSTRACT

Aim: To develop parenteral Enox-coated SEDDS for tumor targeting. **Methods**: Enox moieties have been chemically conjugated to palmitoyl chloride. Coated SEDDS were prepared by mixing the Enox-palmitoyl conjugate with uncoated SEDDS and characterized regarding size and ζ potential. Cell uptake studies were performed on human breast adenocarcinoma and on human epithelial colorectal adenocarcinoma cell lines. **Results**: Enox-coated SEDDS exhibited a size of 102 nm and a ζ potential of -11 mV. About 89% of loaded Enox-palmitoyl conjugate was found on SEDDS surface. Cell uptake of Enox-coated SEDDS was found to increase on both cell lines, compared to uncoated SEDDS. **Conclusions**: Enox-coated SEDDS can be considered as a promising carrier for targeted administration of anticancer drugs.

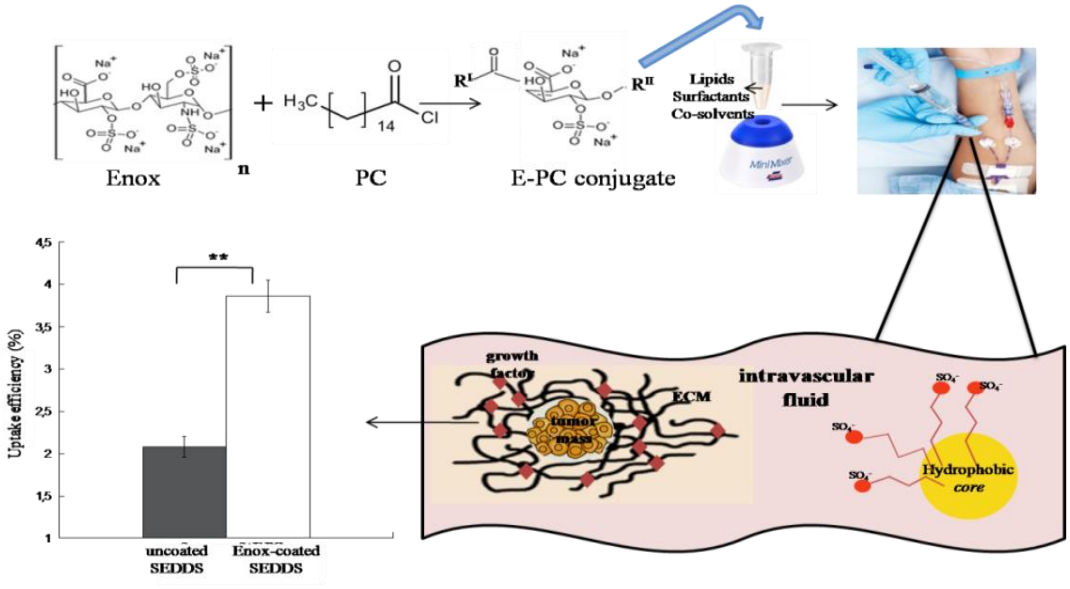

5.1 Introduction

Novel cancer therapies based on active targeting to malignant cells represent a promising approach to overcome the numerous and serious side effects being associated with conventional chemotherapeutic drugs. The active targeting is achieved by decorating drug delivery systems with specific ligands having high affinity toward surface-receptors and/or antigens over-expressed in tumor tissues [Bar-Zeev *et al*., 2017; Bhadra *et al*., 2002; Bi *et al*., 2016; Ding *et al*., 2012; Giarra *et al*., 2016; Kommareddy *et al*., 2005; Li *et al*., 2016; Torchilin, 2006]. In this context, several studies demonstrated that LMWH, obtained by chemical or enzymatic depolymerization of UFH, exhibit anticancer properties against different types of tumors [Castelli *et al*., 2004; Petit *et al*., 2000; Yang *et al*., 2015]. Their antitumor activity is related to their ability to bind various extracellular targets involved in the metastasis formation and over-expressed in many tumor tissues [Achour *et al*., 2016; Bouris *et al*., 2015; Chen *et al*., 2015]. Moreover, LMWH can also inhibit the activity of P- and L-selectins being involved in cell-cell interactions, and of fibroblast growth factor (FGF) as well as vascular endothelial growth factor (VEGF), involved in angiogenesis process [Casu *et al*., 2008; Gomes *et al*., 2015; Läubli and Borsig, 2010; Zhong *et al*., 2015]. In particular, Enoxaparin (Enox) has attracted great attention as tumor-active targeting ligand, due to its high binding affinity towards fibrinogen-derived products and angiogenic growth factors, which are over-expressed in the stroma of some tumors but not in healthy tissues [Chung *et al*., 2010; Liang and Kiick, 2014; Nurunnabi *et al*., 2012; Ye *et al*., 2015].

On the other hand, SEDDS are encountering a growing interest as drug delivery systems. They are based on a mixture of lipids, surfactants and co-solvents that, once in aqueous medium, under gentle agitation, spontaneously form transparent and kinetically stable nanoemulsions [Cherniakov *et al*., 2015; Khan *et al*., 2012; Kollipara and Gandhi, 2014]. Apart from their oral use, SEDDS have also attracted attention for the parenteral administration of hydrophobic drugs, particularly because of their physical stability, low costs of manufacturing and ease scale-up [Date and Nagarsenker, 2008a; Date and Nagarsenker, 2008b; Talegaonkar *et al*., 2008].

5.2 Aim of the work

In this work, we investigated the possibility to develop Enox coated SEDDS as novel carriers for systemic administration and targeting tumors. Palmitoyl chloride was therefore covalently attached to Enox and the resulting conjugate (E-Pa) was incorporated into SEDDS. Then, the SEDDS were characterized in terms of size, ζ potential, protein adsorption, stability in serum and hemolytic activity. Finally, cellular uptake of E-Pa coated SEDDS was evaluated on two different cancer cell lines and compared with the uncoated SEDDS formulation.

5.3 Materials and methods

5.3.1 *Materials*

Enox (average MW 4500 Da) was purchased from Sanofi-Aventis GmbH (Austria). Capmul® PG8 (propylene glycol monocaprylate) was a gift from Abitec (USA); Peceol™ (glyceryl monooleate) and Labrafil® M 1944 (oleoyl polyoxyl-6 glycerides) were a gift from Gattefossé (France). Palmitoyl chloride (PC), Cremophor EL (polyoxyl-35 castor oil), propylene glycol (PG), Fe (III) chloride, L-cysteine ethyl ester hydrochloride, toluidine blue, sodium chloride (NaCl), triton X-100, fluorescein diacetate (FDA), sodium hydroxide (NaOH), tetrahydrofuran (THF), bovine serum albumin (BSA) and n-hexane were obtained from Sigma-Aldrich (Austria). L-Arginine from Alfa Aesar GmbH (Germany), hydroxylamine hydrochloride from Acros Organics (USA) and potassium hydroxide (KOH) from Gatt-Koller (Austria) were used. Fetal bovine serum (FBS), phosphate buffer saline (PBS), Minimum Essential Medium (MEM) and penicillin/streptomycin were purchased from Stricker (Austria). Opti-MEM and RPMI medium were obtained from Gibco (Austria). All solvents, chemicals and media were of analytical grade and used as received.

5.3.2 *Uncoated SEDDS preparation*

Uncoated SEDDS were prepared as previously described by Zupančič et al. [Zupančič *et al.*, 2016] with some modifications. Briefly, 20% Peceol, 40% Cremophor EL, 30%

Labrafil-1944 and 10% PG were gently mixed by vortex and kept at room temperature until use.

5.3.3 *Synthesis of Enox-palmitoyl conjugate (E-Pa)*

The E-Pa conjugate was obtained through ester bond formation between a highly reactive acid halide and Enox hydroxyl groups; the reaction involves HCl release. Briefly, 500 µL of PC dissolved in tetrahydrofuran were added dropwise to 500 µL of Enox aqueous solution (500 µg/mL), at different molar ratios (E-$Pa_{1:1}$; E-$Pa_{1:50}$; E-$Pa_{1:100}$; E-$Pa_{1:150}$; E-$Pa_{1:200}$). The resultant solution was mixed on a vortexer for 2 minutes and then included on a thermo-mixer (Eppendorf), at 37 °C and 700 rpm for one hour. Afterwards, the temperature was set at 25 °C and the samples were shaken at 700 rpm overnight to allow the evaporation of the organic solvent. The obtained aqueous phase, containing the E-Pa conjugate, was centrifuged at 13000 rpm for 20 minutes (Minispin, Eppendorf) to remove the unreacted PC, lyophilized (Christ Gamma 1-16 LSC Freeze dryer) and stored at 4 °C until use. Bromophenol blue (0.03% w/v) was added to the resultant solution to test the progression of the reaction by measuring the pH of the different prepared conjugates.

5.3.4 *Size exclusion HPLC (SEC-HPLC) for E-Pa quantification*

The amount of unreacted Enox and of different E-Pa conjugates in the reaction mixture was quantified by SEC-HPLC following a method previously described by Matanović et al. [Matanović *et al*., 2015], but with some modifications. The Chromaster Hitachi HPLC-systems was equipped with 5430 diode array detector, 5310 column oven, 5260 autosampler and 5160 pump. Analyses were performed on a BioSep-SEC-S 2000 column (300 x 7.80 mm, 5 µm) at a detection wavelength of 215 nm using a mobile phase composed of 1 mg/mL L-arginine solution (pH arranged to 6.5 with 0.1 M HCl). The flow rate was 1 mL/min, the injection volume was 90 µL and the temperature was set at 40 °C.

5.3.5 *Evaluation of the degree of Enox-OH substitution by iron (III)/hydroxylamine assay*

The degree of Enox-OH substitution was evaluated indirectly through iron (III)/hydroxylamine assay, a quantitative colorimetric method for carboxyl-ester determination previously described by Kakáč et al. [Kakáč and Vejdělek, 1976]. Briefly, 250 µL of 15% (w/v) hydroxylamine hydrochloride solution and 10.5 M potassium hydroxide solution were added to 500 µL of about 1.2 mg/mL of sample solution in water and left to react for 15 min. Then, 750 µL of 3 M hydrochloric acid solution was added to the resultant mixture and the pH was adjusted to 1.1-1.5 with NaOH. Afterwards, 250 µL of 0.37 M iron (III) solution in 0.1 M hydrochloric acid and 125 µL of isopropyl alcohol were added to the sample solution and left to react for 10 min, thus obtaining a red to purple solution. The used reagents were kept at 4 °C until use. All steps were performed in ice bath at a temperature around 1±0.1 °C. The ester concentrations were evaluated by measuring the absorbance at λ=520 nm using a calibration curve of L-cysteine ethyl ester hydrochloride in the concentration range of 1.25- 20 mg/mL (r^2=0.995).

5.3.6 *E-Pa coated SEDDS preparations and characterization*

The lyophilized E-Pa conjugates were dissolved in DMSO and added to the SEDDS formulation at a final concentration of 1 mg/g, respectively. The resultant emulsion was included on a thermo-mixer at 25 °C and 700 rpm overnight. Afterwards, the formulation was purified by dialysis membrane (cut-off 16000 Da) in water for 4 hours. The ζ-potential of the uncoated formulation and of the E-Pa coated SEDDS formulation was measured by emulsifying the pre-concentrate in water (1% w/v) (Malvern, UK).

5.3.7 *SEDDS stability studies*

The adsorption of proteins on SEDDS surface is a critical issue for their *in vivo* stability after intravenous injection. The interaction with serum proteins and the possibility of self-aggregation were evaluated by monitoring the mean size and polydispersity index of the uncoated formulation (named 1) and of the corresponding E-Pa coated formulation (1+E-$Pa_{1:200}$, 1% w/v) in serum albumin (1% w/v in water) and in plasma (diluted 1:100 in 20

mM phosphate buffer, pH 7.4) up to 4 hours at 37 °C. ζ potential stability analyses were also performed in water up to 4 hours at 37 °C.

5.3.8 *Quantification of the amount of E-Pa$_{1:200}$ on SEDDS surface by toluidine blue assay*

The amount of E-Pa$_{1:200}$ conjugate on the SEDDS surface was evaluated indirectly by toluidine blue colorimetric assay exploiting the capability of toluidine blue to bind to the free sulfate groups of Enox [Han *et al*., 2006]. Briefly, during the 1+E-Pa$_{1:200}$ purification process, aliquots of the external water phase, containing the E-Pa$_{1:200}$ conjugate released from the SEDDS, were withdrawn at predetermined time points and kept at 4°C. Afterwards 300 µL of toluidine blue solutions (25 mg in 500 mL 0.01 M HCl, containing 0.2% w/v NaCl) were added to 200 µL of each aliquot and left to react in a thermo-mixer at 25 °C and 700 rpm for 30 minutes. Then, 300 µL of n-hexane were added to the resultant solution, shortly mixed and the absorbance of the unreacted toluidine blue in the aqueous phase was measured at λ=631 nm (Microplate-reader, TECAN Infinite M200). The amount of E-Pa$_{1:200}$ conjugate on the SEDDS surface was determined by subtracting the amount lost during the purification from the loaded one. The linearity of the response was assessed in the 7.8-125 µg/mL E-Pa$_{1:200}$ concentration range (r^2=0.996).

5.3.9 *In vitro hemolysis assay and sterility test*

The *in vitro* hemolysis assay is a fast and reliable test for evaluating the damage and lysis of erythrocytes cytoplasmic membrane. It was carried out with a method previously described by Mahmoud et al. [Mahmoud *et al*., 2014], but with some modifications. Briefly, human blood was diluted 1:10 with NaCl 0.9% (w/v) and then 0.2% (w/v) of uncoated and E-Pa$_{1:200}$ coated formulations were added, mixed at 600 rpm for 30 s by vortex and incubated in a shaker bath at 37 °C for 4 hours. The negative control (0% hemolysis) was obtained by diluting 1:10 human blood in NaCl 0.9% (w/v), whereas the positive control (100% hemolysis) was prepared by adding 0.5% (v/v) of Triton-X in diluted 1:10 human blood with NaCl 0.9% (w/v). Afterwards, the samples were withdrawn, placed on ice for 2 minutes to quench erythrocyte lyses and centrifuged (3000 rpm for 5 minutes) to separate the supernatant from the pellet, consisting of intact red blood cells.

The obtained supernatant was centrifuged another time (3000 rpm for 5 minutes) and the content of hemoglobin was measured at λ=540 nm. To verify the possibility to sterilize SEDDS by filtration, the formulations were diluted in NaCl (0.9% w/v) at a final concentration of 1% (w/v). The droplet mean diameter and polydispersity index were measured before and after filtration trough cellulose acetate filter (0.2 µm).

5.3.10 Cell cultures

Human breast adenocarcinoma MDA-MB-231 cell line, kindly donated by Professor Ira-Ida Skvortsova (EXTRO-lab, Department for Therapeutic Radiology and Oncology, Medical University Innsbruck), was cultured as monolayer in culture flask using RPMI medium, supplemented with 10% (v/v) FBS, 2 mM L-glutamine and penicillin/streptomycin solution (100 units/0.1 mg/L). Human epithelial colorectal adenocarcinoma Caco-2 cell line, obtained from European Collection of Cell Culture (ECACC, Health Protection Agency, Porton Down, Salisbury, Wiltshire, UK) was cultured as monolayer in culture flask using MEM medium supplemented with 10% (v/v) heat inactivated FBS and penicillin/streptomycin solution (100 units/0.1 mg/L). Both cell cultures were maintained at 95% humidity and 37 °C in 5% CO_2 atmosphere.

5.3.11 In vitro toxicity assay

The *in vitro* potential toxicity effect of the formulations 1 and 1+E-$Pa_{1:200}$ were evaluated by resazurin assay using two different cell lines. Briefly approximately $1x10^5$ MDA-MB-231 and $2x10^5$ Caco-2 cells/well were seeded to a 24-well plate and incubated with 500 µL of different SEDDS concentrations (0.5 w/v, 0.25 w/v, 0.1 w/v) in opti-MEM for 4 hours. Untreated cells were used as negative control. After 4 hours the formulations were removed and cells were washed twice with sterile PBS (pH=7.1) and incubated with 500 µL of resazurin solution (44 µM) in White Medium for 2 hours. After incubation, the absorbance of the supernatant was measured by fluorometric assay (Microplate-reader, TECAN Infinite M200) (λ_{ex}=540 nm, λ_{em}= 590 nm). Results were calculated as follows:

$$\text{Cell viability (\%)} = \frac{\text{Fluorescence of treated cells}}{\text{Fluorescence of untreated cell}} \text{ x } 100$$

5.3.12 In vitro cellular uptake studies

Fluorescent SEDDS were prepared by adding 20 µL of FDA solution (25 mg/mL in ACN) to 500 mg of formulations 1 and 1+E-$Pa_{1:200}$. Approximately $1x10^5$ MDA-MB-231 and $2x10^5$ Caco-2 cells/well were seeded to a 24-well plate. Afterwards, cells were incubated with 0.25 % (w/v) of formulations in opti-MEM. After 4 hours of incubation, cells were washed twice with prewarmed sterile PBS (pH=7.1), lysed with 5 M NaOH containing 1% w/v Triton-X and re-incubated for 30 min. The lysed cells without the removal of the formulations after 4 hours of incubations were used as positive control (100% uptake), whereas untreated cells were used as negative control (0% uptake). At the end of the incubation time all samples were transferred in 2 mL tubes, centrifuged (13000 rpm, 5 min) and the intensity of fluorescence of the lysates were measured by fluorimeter (λ_{ex}=485 nm, λ_{em}= 555 nm). Results were expressed through the equation:

$$\text{Uptake (\%)} = \frac{\text{Fluorescence of lysate with removing formulation}}{\text{Fluorescence of positive control}} \times 100$$

5.3.13 Statistical data analysis

Statistical data analyses were performed using Student's t-test for comparison of two paired groups, assuming $p<0.05$, $p<0.01$ and $p<0.001$ as levels of significance. All experiments were performed in triplicate and the results are reported as the means ±SD.

5.4 Results and discussion

5.4.1 *Synthesis and characterization of E-Pa conjugate*

The E-Pa conjugate was obtained by covalently attaching palmitoyl chloride to the hydroxyl groups of Enox, through an ester bond formation as schematically represented in figure 5.1.

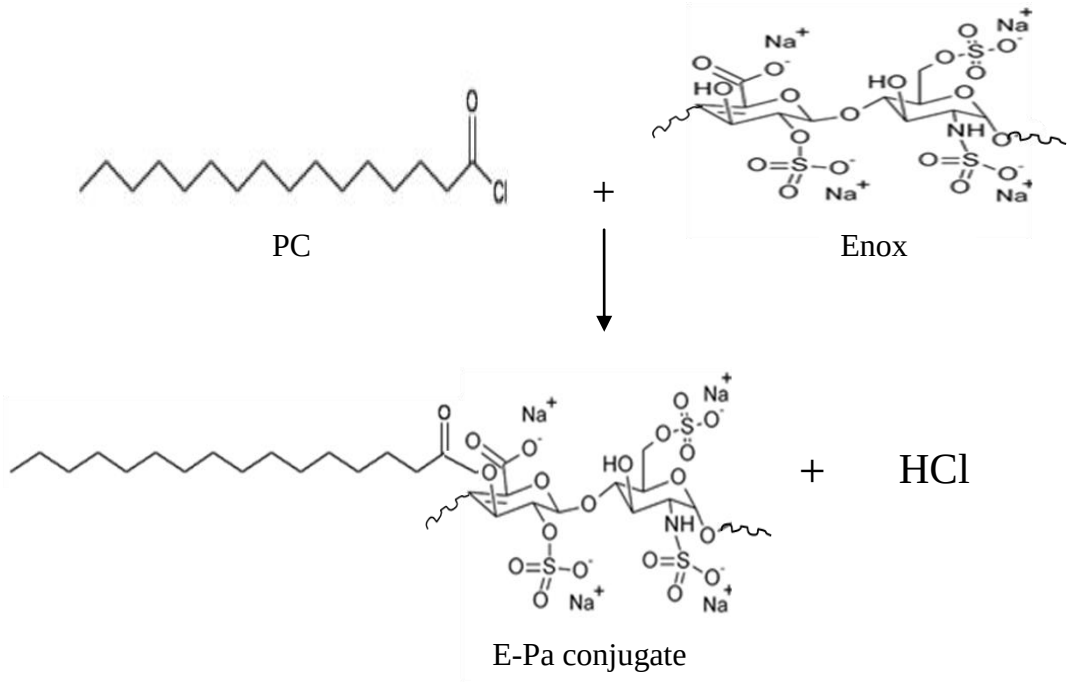

Figure 5.1: schematically representation of synthetic reaction and chemical structures of Enox, PC and E-Pa conjugate

A simple acylation reaction in aqueous environment was carried out, thus not requiring the removal of any organic solvent [Kočevar *et al*., 2007; Kabanov *et al*., 1990]. This approach was considered advantageous especially for formulations that could be proposed for further clinical and industrial development. Acronyms and the molar ratios of the different components used for the preparations of conjugates are summarized in table 5.1.

Conjugates Acronym	Enox (mol)	PC (mol)	Degree of Enox-OH substitution (%)
E-Pa$_{1:1}$	1	1	0.000±0.61
E-Pa$_{1:50}$	1	50	45.26±3.70
E-Pa$_{1:100}$	1	100	62.10±2.32
E-Pa$_{1:150}$	1	150	70.54±1.15
E-Pa$_{1:200}$	1	200	84.38±2.13

Table 5.1: acronyms, composition and degree of Enox-OH substitutions (%), measured by iron (III)/hydroxylamine assay, of the different E-Pa conjugates

The acylation reaction produces one mole of HCl *per* mole of formed esters. The HCl release leads to a pH change in the solution, which was used to evaluate the progression of the reaction, by adding bromophenol blue at the final solution. As expected, when increasing PC content, the pH value shifted from ~ 5.3 (only Enox) to ~ 1.8 (E-$PC_{1:200}$) (figure 5.2).

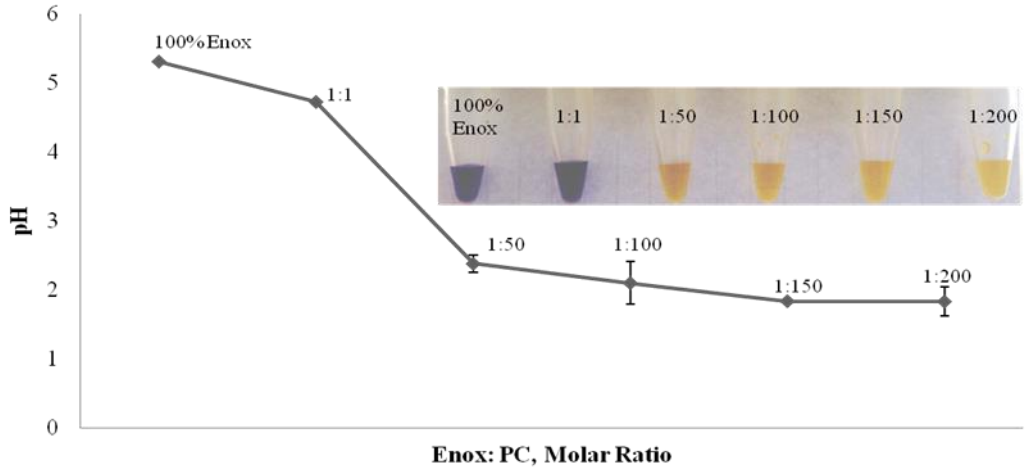

Figure 5.2: pH evaluation of different conjugates after the addiction of bromophenol blue (0.03% w/v) at the solutions

Then, SEC-HPLC analysis was performed to investigate the yield of the conjugation reaction. A single peak was found in Enox SEC-HPLC chromatogram at the retention time of 8.5 min, while no peaks were observed in the PC chromatogram. Differently, in the chromatograms of E-$Pa_{1:50}$, E-$Pa_{1:100}$ and E-$Pa_{1:150}$ a second peak appeared at retention time of about 11.6 min, ascribable to the conjugate formation. In detail, the area of the peak attributed to the conjugate increased whit increasing PC concentration, while the area of the peak at 8.5 min decreased. In the chromatogram of E-$Pa_{1:200}$ only the peak at retention time 11.6 min was observed, thus suggesting that using E/PC molar ratio of 1:200, 100% of the Enox was converted into E-Pa conjugate. Representative chromatograms of Enox and E-$Pa_{1:200}$ conjugate are illustrated in figure 5.3 A. The concentration (expressed as % v/v) of the different E-Pa conjugates obtained as well as of the unreacted Enox, measured by integrating the area of the peaks acquired by SEC-HPLC chromatograms, are reported in figure 5.3 B.

In order to confirm the E-Pa conjugate formation and to evaluate the degree of Enox-OH substitution, iron (III)/hydroxylamine colorimetric assay was performed. The assay is based on the reaction between the ester groups with hydroxylamine to form a hydroxamic acid, which then reacts with ferric ion forming a spectrophotometrically visible chelate ferric hydroxamate complex. In this way, it was possible to determine the degree of Enox-OH groups reacted with the acyl halide PC. Results shown in table 5.1 confirmed that the degree of Enox-OH substitution progressively increases with increasing amounts of PC being present at the coupling reaction, resulting in a maximum of 84.38% substitution for E-Pa$_{1:200}$ conjugate.

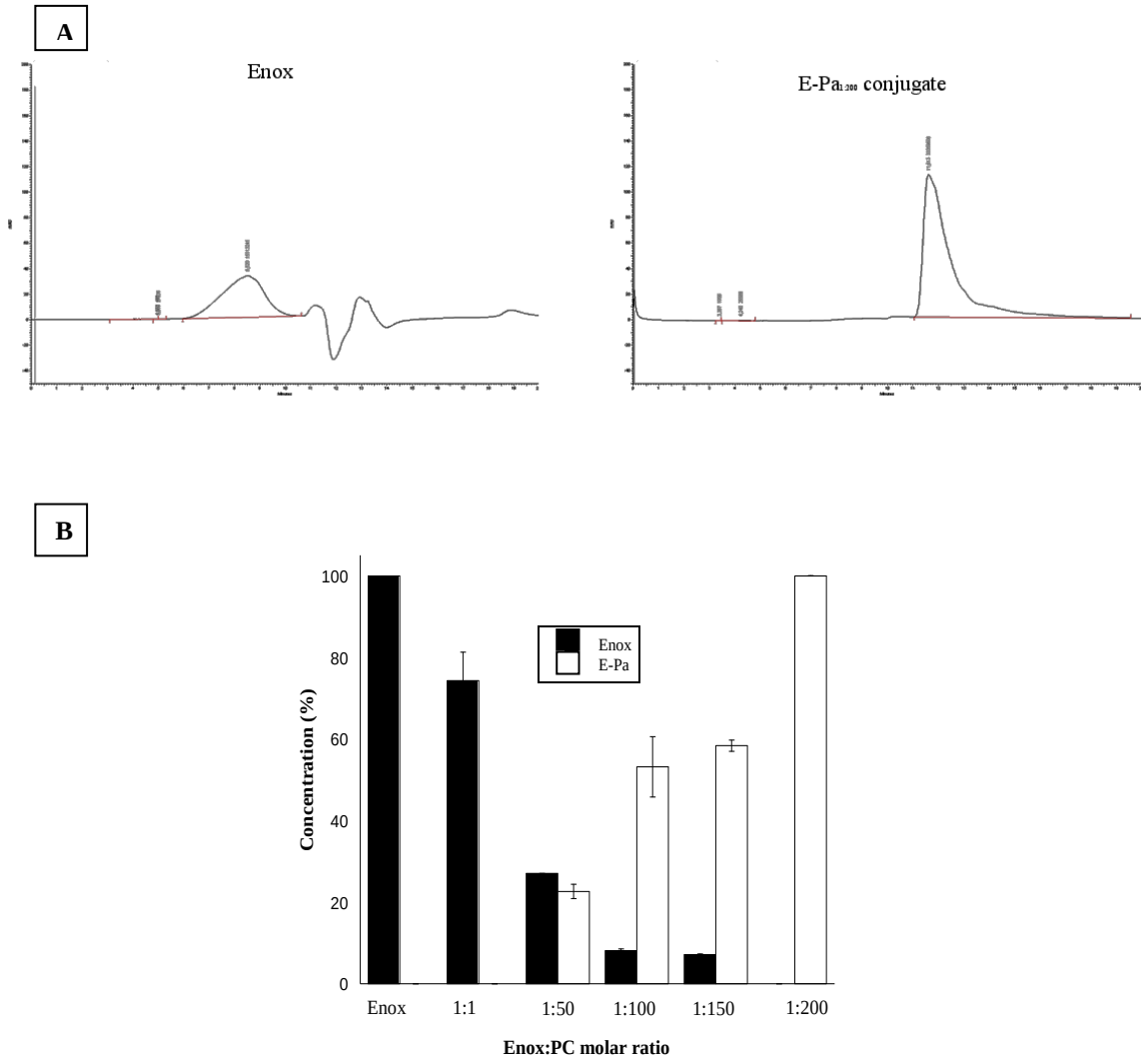

Figure 5.3: representative SEC-HPLC chromatograms of Enox and E-Pa$_{1:200}$ conjugate (A) and concentrations (% v/v) of E-Pa conjugates and unreacted Enox in function of Enox:PC molar ratios (B), measured by integrating the area of the peaks acquired by SEC-HPLC chromatograms

5.4.2 *Preparation and characterization uncoated and E-Pa coated SEDDS*

Uncoated SEDDS formulation 1 was prepared and mixed with E-Pa conjugates prepared with different Enox/PC molar ratios, in order to obtain various E-Pa coated SEDDS as summarized in table 5.2.

Formulation	d (nm) $_{t=0}$	PI $_{t=0}$	ζ potential (mV)$_{t=0}$
1	91.09±1.05	0.255±0.02	-4.040±0.29
1+ E-PC$_{1:50}$	94.05±0.31	0.210±3.20	-6.735±0.54
1+ E-PC$_{1:100}$	92.30±1.20	0.190±2.10	-7.730±0.30
1+ E-PC$_{1:150}$	99.02±0.28	0.200±1.20	-7.285±0.23
1+ E-PC$_{1:200}$	102.3±0.04	0.234±0.04	-11.20±0.03

Table 5.2: size, polydispersity index and ζ potential of formulations, before and after addition of different conjugates E-Pa, in deionized water at 0 times

Both uncoated and E-Pa coated SEDDS were diluted in water (final concentration 1% w/v), resulting in a clear nanoemulsion. Mean diameter, polydispersity index and ζ potential measurements of the prepared SEDDS are summarized in table 5.2. The mean diameter of the SEDDS droplets was influenced by the addition of conjugates to formulations, as well as by the type of E-Pa conjugate. On the other hand, SEDDS showed a polydispersity index ranging from 0.190 to 0.255, suggesting that even due to the inclusion of E-Pa conjugates, SEDDS remained homogeneous in size. Moreover, the E-Pa addition resulted in a decrease of ζ potential from -4 mV to -11 mV. This could be ascribed to the amphiphilic properties of the conjugate that could locate its hydrophobic fatty acid ester chain into the lipid core of nanoemulsions, while exposing the hydrophilic and negatively charged Enox on SEDDS surface.

5.4.3 *SEDDS stability studies*

The adsorption of proteins on the surface of nanocarriers is considered a crucial issue for their *in vivo* stability following administration. After injection, nanovectors are rapidly eliminated from the systemic circulation since they are able to recognize and adsorb serum

proteins on their surface [Leroux *et al*., 1995]. This could promote their fast aggregation rendering them easily recognizable for macrophages of endoplasmic reticulum (RES) and resulting in their subsequent elimination and liver accumulation, where they may cause side effects, and/or vessel occlusion [Lenaerts *et al*., 1984; Owens and Peppas, 2006]. Nanocarriers surface properties play therefore a key role in the opsonisation process since a more negative ζ potential can prevent aggregation through electrostatic stabilization. Table 5.2 shows a decrease of the ζ potential values obtained by adding E-Pa conjugates to the formulation. This can be reasonably ascribed to the negative charge of Enox, presumably present on the droplet surface. In line with this, the lowest ζ potential was observed in case of the conjugate with the highest content in PC, namely of E-$Pa_{1:200}$, for which a more efficient intercalation between E-Pa fatty acid chains and the lipid phase of the droplets can be hypothesized. Therefore, it was considered for further studies. The mean diameter and the polydispersity index, before and after adding E-$Pa_{1:200}$, were monitored in serum albumin and in human plasma at 37 °C. As it can be observed in tables 5.3 and 5.4, the formulation was stable in presence of E-$Pa_{1:200}$ conjugate up to 4 hours.

Form	**BSA 37°C**			
	$d(nm)_{t=0}$	**$PI_{t=0}$**	**$d(nm)_{t=4h}$**	**$PI_{t=4h}$**
1	113.1±1.07	0.21±0.08	114.1±4.88	0.16±0.04
1+E-$Pa_{1:200}$	111.8±1.34	0.23±0.01	106.7±4.46	0.21±0.01

Table 5.3: size stability and polydispersity index of formulations 1, with and without E-$Pa_{1:200}$, in BSA (1% w/v) at 0 time and after 4 hours at 37 °C

Form	**PLASMA 37°C**			
	$d(nm)_{t=0}$	**$PI_{t=0}$**	**$d(nm)_{t=4h}$**	**$PI_{t=4h}$**
1	108.3±8.41	0.23±0.01	111.8±1.81	0.24±0.05
1+E-$Pa_{1:200}$	103.4±4.31	0.20±0.01	110.1±3.11	0.24±0.02

Table 5.4: size stability and polydispersity index of formulations 1, with and without E-$Pa_{1:200}$, in plasma (1:100) at 0 time and after 4 hours at 37 °C

The inclusion of the E-Pa conjugate did not significantly affect the SEDDS stability in BSA and in serum. As for size and polydispersity index, also the ζ potential values of both

E-$Pa_{1:200}$ coated formulations resulted stable for 4 hours at 37 °C (data not shown). Based on these results, it might be assumed that the prepared SEDDS, independently on the presence of E-Pa, should be stable in the blood stream.

5.4.4 *Quantification of the amount of E-$Pa_{1:200}$ on SEDDS surface by toluidine blue assay*

It has been reported that the amount of heparin on the surface of nano-devices significantly influence their *in vivo* performance [Han *et al*., 2006]. In this study, it was possible to reach a maximum of E-Pa conjugate concentration of 1 mg/g (E-Pa conjugate/SEDDS). When adding a concentration higher than 1 mg/g, increase in droplet size and instability of the dispersion were observed. The amount of E-Pa on SEDDS surface was indirectly evaluated by toluidine blue assay. Results showed a loss of 11% of E-$Pa_{1:200}$ conjugate after 10 min from the preparation in the external water phase during the purification step. Afterwards, a plateau was reached suggesting no further release of conjugate up to 4 hours (figure 5.4).

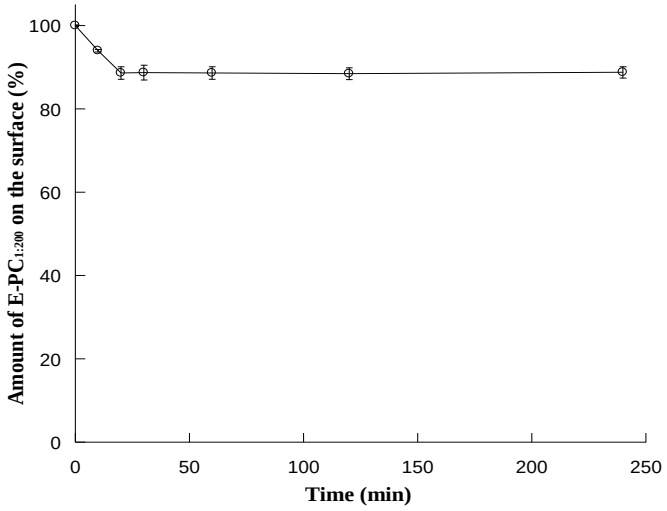

Figure 5.4: amount (%) of E-$Pa_{1:200}$ on 1+E-$Pa_{1:200}$ coated SEDDS surface, evaluated by toluidine blue assay during the purification process, up to 4 hours

5.4.5 *In vitro hemolysis assay and sterility test*

One of the key requirements for a preparation intended for parenteral administration is its hemocompatibility. The results of the hemolysis assay showed for both uncoated and E-Pa coated SEDDS a hemolysis lower than 2% generally regarded as non-toxic level (data not shown) [Salzano *et al*., 2016]. Furthermore, another key requirement for systemic administration is the possibility to sterilize the formulation. Thus, both 1 and 1+E-$Pa_{1:200}$ formulations were diluted in physiologic solution (NaCl 0.9% w/v) and filtrated using 0.22 μm cellulose acetate filters. The size as well as the polydispersity index of both formulations did not undergo a significantly change after filtration (table 5.5). These results indicated that it is possible to obtain a *sterile* formulation by filtration, thus avoiding the high-temperature autoclave sterilization procedure, which may result detrimental for the formulation [Khachane *et al*., 2015].

Formulation	d(nm) in NaCl (0.9% w/v) pre-filtration	IP in NaCl (0.9% w/v) pre-filtration	d(nm) in NaCl (0.9% w/v) post-filtration	IP in NaCl (0.9% w/v) post-filtration
1	92.79±10.2	0.23±0.01	96.23±5.06	0.20±0.03
1+E-$Pa_{1:200}$	111.8±1.34	0.23±0.01	106.7±4.46	0.21±0.01

Table 5.5: size and polydisperisty index of formulations 1, with and without E-$Pa_{1:200}$, in NaCl (0.9% w/v), pre- and post-filtration through cellulose acetate filter (0.2 μm)

5.4.6 *In vitro cell uptake studies*

Viability of MDA-MB-231 and Caco-2 cells in the presence of uncoated and E-Pa coated SEDDS was assessed *via* resazurin assay. Cells were incubated with 1 and 1+E-$Pa_{1:200}$ formulations at different concentrations. Any cytotoxicity was observed when testing both uncoated and E-Pa coated SEDDS in concentrations up to 0.25% (w/v) on both cell lines (data not shown). Cell uptake of uncoated and E-Pa coated SEDDS, loaded with fluorescein diacetate (FDA) was evaluated *via* cell uptake studies on both MDA-MB-231 and Caco-2 cell lines by measuring fluorescence derived from hydrolytic cleavage of FDA with NaOH. The uptake of 1+E-$Pa_{1:200}$ coated SEDDS was found to increase 1.36-fold and 1.86-fold on MDA-MB-231 and Caco-2 cells, respectively, compared to uncoated formulation (figure 5.5 A and B).

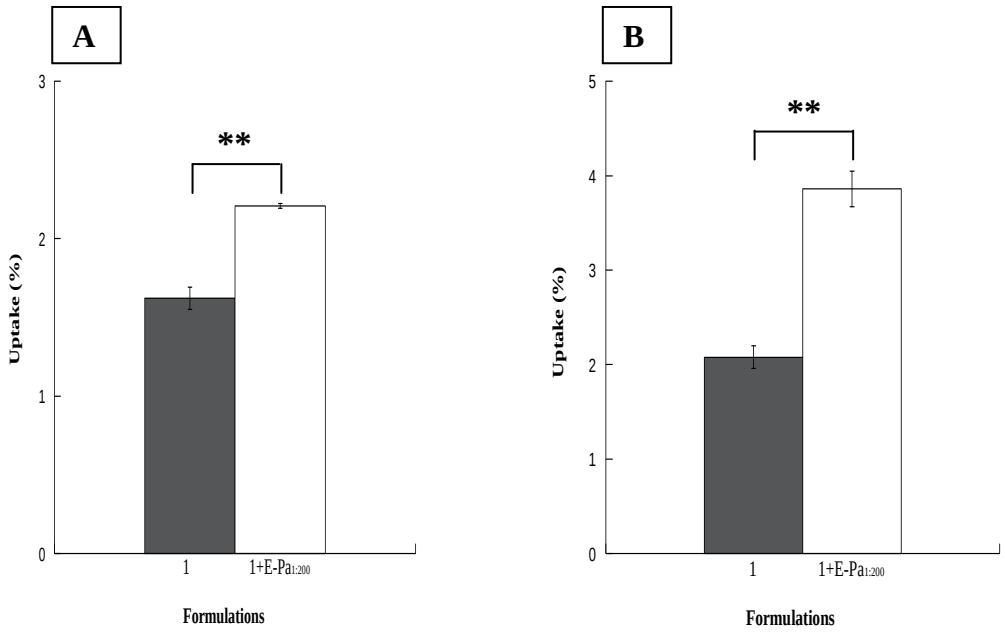

Figure 5.5: uptake efficiency (%) of formulations 1 and 1+E-$PC_{1:200}$ (0.25% w/v), after 4 hours of incubation upon MDA-MB-231 cells (A) and Caco-2 cells (B). Results are expressed as means of three independent experiments ± SD (** $p < 0.01$)

It is well known that several components of the ECM, such as different cytokines and grow factors are over-expressed in different kind of tumors exhibiting binding domains for UFH and its derivatives [Salatin and Khosroushahi, 2017]. Based on these considerations the presence of sulfate motif of Enox seems to be crucial for the interactions between the ECM binding domains and Enox coated delivery systems. As previously described, the acylation reaction between Enox and PC, to form E-Pa conjugate leads to an ester bond formation between the fatty acid and the hydroxyl groups of Enox. In this way, it was possible to preserve the sulfate groups, as confirmed by toluidine blue assay and consequently the Enox binding activity. These interactions enhanced the internalization of the 1+E-$Pa_{1:200}$ coated SEDDS into cancer cells *via* an Enox endocytosis mediated process.

5.5 Conclusions

In the present study, sterically stabilized Enox coated SEDDS for tumor targeting were successfully prepared with an easily upscalable method. This was achieved by firstly

preparing an amphiphilic conjugate able to direct the spontaneous exposition of Enox moieties on SEDDS surface. The *in vitro* cell uptake studies showed that the decoration of SEDDS with Enox increases the internalization efficiency on both MDA-MB-231 and Caco-2 cells, when compared with uncoated formulation. According to these results Enox-coated SEDDS can be considered as a promising carrier for targeted administration of anticancer drugs.

REFERENCES

Achour O, Poupard N, Bridiau N, Bordenave Juchereau S, Sannier F, Piot J.M., Fruitier Arnaudin I, Maugard T (2016). Anti-heparanase activity of ultra-low-molecular-weight heparin produced by physicochemical depolymerization. *Carbohydr Polym*, 135:316-323.

Bar-Zeev M, Livney Y.D., Assara Y.G. (2017). Targeted nanomedicine for cancer therapeutics: Towards precision medicine overcoming drug resistance. *Drug Resistance Updates*, 31:15-30.

Bhadra D, Bhadra S, Jain P, Jain N.K. (2002). Pegnology: a review of PEG-ylated systems. *Pharmazie*, 57:5-29.

Bouris P, Skandalis S.S., Piperigkou Z, Afratis M, Karamanou K, Aletras A.J., Moustakas A, Theocharis A.D., Karamanos N.K. (2015). Estrogen receptor alpha mediates ephitelial to mesenchymal transition, expression of specific matrix effectors and functional properties of breast cancer cells. *Matrix Biol J Int Soc Matrix Biol*, 43:42-60.

Bi Y, Hao F, Yan G, Teng L, Lee R.J., Xie J (2016). Actively Targeted Nanoparticles for Drug Delivery to Tumor. *Curr Drug Metab*, 17:763-782.

Castelli R, Porro F, Tarsia P (2004). The heparins and cancer: review of clinical trials and biological properties. *Vasc Med*, 9:205-13.

Casu B, Vlodavsky I, Sanderson R.D. (2008). Non-anticoagulant heparins and inhibition of cancer. *Pathophysiol Haemost Thromb*, 36:195-203

Chen X.P., Luo J.S., Tian Y, Nie C.L., Cui W, Zhang W.D. (2015). Downregulation of Heparanase Expression Results in Suppression of Invasion, Migration, and Adhesion Abilities of Hepatocellular Carcinoma Cells. *Biomed Res Int*, 241983.

Cherniakov I, Domb A.J., Hoffman A (2015). Self-nano-emulsifying drug delivery systems: an update of the biopharmaceutical aspects. *Expert Opin Drug Deliv*, 12:1121-33

Chung Y.I., Kim J. C., Kim Y. H., Tae G, Lee S. Y., Kim K, Kwon I. C. (2010). The effect of surface functionalization of PLGA nanoparticles by heparin- or chitosan-conjugated Pluronic on tumor targeting. *J Control Release*, 143:374-382.

Date A.A., Nagarsenker M.S. (2008a). Parenteral microemulsions: An overview. *International Journal of Pharmaceutics*, 355: 219-230.

Date A.A., Nagarsenker M.S. (2008b). Design and evaluation of microemulsions for improved parenteral delivery of propofol. *AAPS PharmSciTech*, 9:138-145.

Ding H, Wang X.J., Zhang S, Liu X.L. (2012). Applications of polymeric micelles with tumor targeted in chemotherapy. *J of Nano Res*, 14:1254.

Giarra S, Serri C, Russo L, Zeppetelli S, De Rosa G, Borzacchiello A, Biondi M, Ambrosio L, Mayol L (2016). Spontaneous arrangement of a tumor targeting hyaluronic acid shell on irinotecan loaded PLGA nanoparticles. *Carbohydr Polym*, 140:400-407.

Gomes A.M., Kozlowski E.O., Borsig L, Teixeira F.C., Vlodavsky I, Pavão M.S. (2015). Antitumor properties of a new non-anticoagulant heparin analog from the mollusk Nodipecten nodosus: Effect on P-selectin, heparanase, metastasis and cellular recruitment. *Glycobiology*, 25:386-93

Han H.D., Lee A, Song C.K., Hwang T, Seong H, Lee C.O., Shin B.C. (2006). *In vivo* distribution and antitumor activity of heparin-stabilized doxorubicin-loaded liposomes. *Int J Pharm*, 313:181-88.

Kabanov A.V., Levashov A.V., Alakhov V.Y., Martinek K, Severin E.S. (1990). Fatty acylation of proteins for translocation across cell membranes. *Biomed Sci*, 1:33-6.

Kakáč B, Vejdělek Z.J. (1976). Handbuch der photometrische Analyse organischer Verbindungen. *Ergänzungsband*, 1. Ed: Verlag Chemie.

Khachane P.V., Jain A.S., Dhawan V.V., Joshi G.V., Date A.A., Mulherkar R, Nagarsenker M.S. (2015). Cationic nanoemulsions as potential carriers for intracellular delivery. *Saudi Pharm J*, 23:188-194.

Khan A.W., Kotta S, Ansari S.H., Sharma R.K., Ali J (2012). Potentials and challenges in self-nanoemulsifying drug delivery systems. *Expert Opin Drug Deliv*, 9:1305-17

Kočevar N, Obermajer N, Štrukelj B, Kos J, Kreft S (2007). Improved acylation method enables efficient delivery of functional palmitoylated cystatin into epithelial cells. *Chem Biol Drug Des*, 69:124-131.

Kollipara S, Gandhi R.K. (2014). Pharmacokinetic aspects and in vitro-in vivo correlation potential for lipid-based formulations. *Acta Pharm Sin B*, 4:333-49

Kommareddy S, Tiwari S.B., Amiji M.M. (2005). Long-circulating polymeric nanovectors for tumor-selective gene delivery. *Technol Cancer Res Treat*, 4:615-625.

Läubli H, Borsig L (2010). Selectins promote tumor metastasis. *Semin Cancer Biol*, 20:169-77.

Lenaerts V, Nagelkerke J.F., Van Berkel T.J., Couvreur P, Grislain L, Roland M, Speiser P (1984). In vivo uptake of polyisobutyl cyanoacrylate nanoparticles by rat liver Kupffer, endothelial, and parenchymal cells. *J Pharm Sci*, 73:980-982.

Leroux J.C., De Jaeghere F, Anner B, Doelker E, Gurny R (1995). An investigation on the role of plasma and serum opsonins on the internalization of biodegradable poly(D,L-lactic acid) nanoparticles by human monocytes. *Life Sci*, 57:695-703.

Li M, Zhang W, Wang B, Gao Y, Song Z, Zheng Q.C. (2016). Ligand-based targeted therapy: a novel strategy for hepatocellular carcinoma. *Int J Nanomedicine*, 11:5645-5669.

Liang Y, Kiick K.L. (2014). Heparin-functionalized polymeric biomaterials in tissue engineering and drug delivery applications. *Acta Biomater*, 10:1588-1600.

Mahmoud D.B., Shukr M.H., Bendas E.R. (2014). *In vitro* and *in vivo* evaluation of self-nanoemulsifying drug delivery systems of cilostazol for oral and parenteral administration. *Int J Pharm*, 476:60-69.

Matanović M.R., Grabnar I, Grabnar P.A., Roškar R (2015). Development and validation of a simple and sensitive size-exclusion chromatoghraphy method for quantitative determination of heparin in pharmaceuticals. *Acta Pharm*, 65:43-52.

Nurunnabi M, Khatun Z, Moon W. C., Lee G, Lee Y. K. (2012). Heparin based nanoparticles for cancer targeting and noninvasive imaging. *Quant Imaging Med Surg*, 2:219-226.

Owens D.E., Peppas N.A. (2006). Opsonization, biodistribution, and pharmacokinetics of polymeric nanoparticles. *Int J Pharm*, 307:93-102.

Petit T, Ghnassia J.P., Petit J.C. (2000). Antitumour activity of heparin on metastatic colon cancer. *Clin Oncol (R Coll Radiol)*, 12:249-50.

Salatin S, Khosroushahi Y (2017). Overviews on the cellular uptake mechanism of polysaccharide colloidal nanoparticles. *J. Cell. Mol. Med*, 21:1668-1686.

Salzano G, Zappavigna S, Luce A, D'Onofrio N, Balestrieri M.L., Grimaldi A, Lusa S, Ingrosso D, Artuso S, Porru M, Leonetti C, Caraglia M, De Rosa G (2016). Transferrin-targeted nanoparticles containing zoledronic acid as a potential tool to inhibit glioblastoma growth. *J Biomed Nanotechnol*, 12:811-830.

Talegaonkar S, Azeem A, Ahmad F.J., Khar R.K., Pathan S.A., Khan Z.I. (2008). Microemulsions: a novel approach to enhanced drug delivery. *Recent Pat Drug Deliv Formul*, 2:238-57.

Torchilin V.P. (2006). Multifunctional nanocarriers. *Adv Drug Del Rev*, 58:1532-1555.

Yang X, Du H, Liu J, Zhai G (2015). Advanced nanocarriers based on heparin and its derivatives for cancer management. *Biomacromolecules*, 16:423-436.

Ye T, Jiang X, Li J, Yang R, Mao Y, Li K, Li L, Chen F, Yao J, Wu Y, Yang X, Wang S, Pan W (2015). Low molecular weight heparin mediating targeting of lymph node metastasis based on nanoliposome and enzyme-substrate interaction. *Carbohydr Polym*, 122:26-38.

Zhong G.X., Gong Y, Yu C.J., Wu S.F., Ma Q.P., Wang Y, Ren J, Zhang X.C., Yang W.H., Zhu W (2015). Significantly inhibitory effects of low molecular weight heparin (Fraxiparine) on the motility of lung cancer cells and its related mechanism. *Tumour Biol*, 36:4689-97

Zupančič O, Grießinger J.A., Rohrer J, Pereira de Sousa I, Danninger L, Partenhauser A, Sündermann N.E., Laffleur F, Bernkop-Schnürch A (2016). Development, *in vitro*

and *in vivo* evaluation of a self-emulsifying drug delivery systems (SEDDS) for oral enoxaparin administration. *Eur J Pharm Biopharm*, 109:113-121.

CHAPTER 6

Summary and future perspectives

Due to several limitations and side effects of conventional anticancer therapy, new strategies based on controlled drug delivery systems have been attracting a great deal of interest over the last years. In particular, polysaccharide-based systems possess peculiar favorable properties, such as biodegradability, biocompatibility, large availability as natural source, low cost manufacturing process and easiness of chemical functionalization due to the presence of multiple reactive groups in their structures. For these reasons, in the present thesis, different aspects of using polysaccharides in innovative formulations with potential application in tumors treatment have been studied. More in detail, two different strategies were envisaged.

In the first strategy, different thermoresponsive gels based on methylcellulose or poloxamers, with or without the polysaccharide hyaluronic acid, were designed, loaded with the chemokine CXCL12 and their *in vitro* ability to act as metastasis trap were analyzed (chapter 2). The use of this fake metastatic niche to divert and capture $CXCR4^+$ circulating tumor cells resulted helpful in capturing these target cells and possibly reducing/inhibiting the formation of metastasis. This work is also presented in two research articles submitted for publication in international sceinfific journals [Giarra S, Ieranò C, Biondi M, Napolitano M, Campani V, Pacelli R, Scala S, De Rosa G, Mayol L. Engineering of thermoresponsive gels as a fake metastatic niche toward the capture of $CXCR4^+$ circulating tumor cells. *Carbohydr Polym: under revision*; Ieranò C, D'Alterio C, Giarra S, Napolitano M, Santagata A, Barbieri A, Campani V, Luciano A, Arra L, Anniciello A.M., Botti G, Mayol L, De Rosa G, Pacelli R Scala S. In vivo capture of early metastatic cells through a CXCL12 loaded-dermal filler. *Theranostics: submitted*].

The second strategy concerned the use of polysaccharides both as structural and coating component for different types of nano-carriers. In particular, polyelectrolyte complexes co-loaded with doxorubicin and zoledronic acid were prepared with the main aim to overcome multidrug resistance against doxorubicin resistant tumors (chapter 3). Chitosan was used as structural component of such complexes that were prepared with a simple and easily up-

scalable method. The co-delivery of the two active molecules resulted in an enhanced doxorucin delivery in doxorubicin resistent cancer cells, thus providing a promising approach to overcome multidrug resistance. A research article is currently in prepraration collecting the results of this study [Giarra S, Zappavigna S, Mayol L, Leonetti C, Caraglia M, De Rosa G. Chitosan-based polyelecrolyte complexes for doxorubicin and zoledronic acid combined therapy to overcome multidrug resistance. *In Preparation*].

In chapter 4, a novel strategy to modify irinotecan-loaded poly lactic-co-glycolic acid nanoparticles with hyaluronic acid moieties for tumor targeting has been proposed. This preparation method, based on a self-assembling strategy, is easy to scale-up and consist on a single step process. Cell cytotoxicity tests showed that hyaluronic acid-coated nanoparticles can enhance drug delivery into $CD44^+$ cancer cells, probably due to the hyaluronic acid-receptor endocytosis mediated process. The results of this study are described in three research articles published in international scientific journals, all belonging to Q1 class [Mayol L, Serri C, Menale C, Crispi S, Piccolo M.T., Mita L, Giarra S, Forte M, Saija A, Biondi M, Mita D.G. (2015). Curcumin loaded PLGA-poloxamer blend nanoparticles induce cell cycle arrest in mesothelioma cells. *Eur J Pharm Biopharm*, 93:37-45; Giarra S, Serri C, Russo L, Zeppetelli S, De Rosa G, Borzacchiello A, Biondi M, Ambrosio L, Mayol L (2016). Spontaneous arrangement of a tumor targeting HA shell on irinotecan loaded PLGA NPs. *Carbohydr Polim*, 140: 400-407; Serri C, Argirò M, Piras L, Mita D.G., Saija A, Mita L, Forte M, Giarra S, Biondi M, Crispi S, Mayol L (2017). Nano-precipitated curcumin loaded particles: effect of carrier size and drug complexation with (2-hydroxypropyl)-b-cyclodextrin on their biological performances. *Int J Pharm*, 520:21-28].

In the chapter 5, sterically stabilized enoxaparin coated self-emulsifying drug delivery systems for tumor targeting were successfully prepared with an easily up-scalable method. The study demonstrated that the enoxaparin-coated self-emulsifying drug delivery systems are suitable to be administered by intravenous route. The *in vitro* cell uptake studies showed that the decoration of self-emulsifying drug delivery systems with enoxaparin increases the uptake both on human breast adenocarcinoma and on human epithelial colorectal adenocarcinoma cell lines, when compared with uncoated formulation. The results of this study are reported in one research article submitted for publication in an international scientific journal [Giarra S, Lupo N, Mayol L, De Rosa G, Bernkop-Schnürch

A. In vitro evaluation of tumor targeting ability of enoxaparin-coated self-emulsifying drug delivery systems for parenteral administration. *Nanomedicine (Lond): submitted*].

All together, the results of this thesis support the use of polysaccharides-based polymeric systems for different applications in tumor treatment although further investigation is required in order to optimize, clarify and support the advantages of these formulations. More in detail, in the chapter 3, hyaluronic acid-coated polyelectrolyte complexes for $CD44^+$ cells targeting were developed. Despite hyaluronic acid-coated polyelectrolyte complexes were able to increase the drugs cytotoxicity compared to free drugs, they were no more potent compared with uncoated polyelectrolyte complexes, also in MCF7 cell lines overexpressing CD44 receptor. In this context, it would be important to quantify the amount of targeting hyaluronic acid moieties on polyelectrolyte complexes, available for the interaction with CD44 receptor. Moreover, taking into account that in many cases MCF7 cells do not overexpress CD44 receptor, further *in vitro* studies on different $CD44^+$ cancer cells will be needed to confirm their efficacy by means of validated *in vitro* assay, able to evaluate also the degree of CD44 expression. In the chapter 5, enoxaparin coated self-emulsifying drug delivery systems for tumor targeting were successfully prepared. The potential usefulness of self-emulsifying drug delivery systems is well known for oral administration of lipophilic drugs. In this work we demonstrated the potential application of self-emulsifying drug delivery systems through parenteral route of administration. Future perspectives in this field, include the use of suitable excipients for loading of drugs with antitumor activity, with particular attention on their solvent capacity, miscibility and chemical stability, in order to obtain multifunctional drug delivery systems.

Despite the large number of research work dealing with polysaccharide drug delivery systems for tumor treatment, there is an imbalance between the number of scientific publications and the number of marketed products. This could be related to the fact that, unfortunately, little is known about their safety on patients. After administration into the body, the fate of these polymeric systems could be different from what is expected since they may accumulate into non-target tissues, such as liver, spleen and bone marrow with toxic effects. To this end, studies on *in vitro/in vivo* tumor models are needed for evaluating their absorption, distribution, metabolism and excretion (ADME) after their administration into the body. Moreover, *in silico* modeling approaches able to mimic the interactions between drug delivery systems and the surface of living systems, will be needed for predicting their toxicity in human body.